

**School of Civil and Mechanical Engineering**

**A Model of Granular Materials Cemented by Bacterial Calcite**

**Ella Kashi**

**This thesis is presented for the Degree of**

**Doctor of Philosophy**

**of**

**Curtin University**

**December 2019**

## **Declaration**

This thesis contains no material previously published by any other person except where due acknowledgment has been made to the best of my knowledge and belief.

This thesis contains no material which has been accepted for the award of any other degree or diploma in any university.

Signature: .....Ella Kashi..... Date: .....25/12/2019.....

## **Authorship**

I hereby certify that the work embodied in this thesis contains published paperwork of which I am a joint author. As part of the thesis, I have included a written statement, endorsed by my supervisor, attesting to my contribution to the collaborative publication/s/scholarly work.

## **Acknowledgments**

I thank my supervisors, Professor Abhijit Mukherjee and Professor Antoinette Tordesillas, for their guidance. Special thanks to my life-coach, Professor Abhijit Mukherjee: because I owe it all to you. Many Thanks!

## **Dedication**

To my parents for their endless love and support.

## Co-Authored Publications

This thesis contains the following work that has been published and/or prepared for publication: Journal Papers

- ElahehKashizadeh, AbhijitMukherjee, AntoinetteTordesillas, 2019, Experimental and numerical investigation on heap formation of granular soil sparsely cemented by bacterial calcification - **Published**
- ElahehKashizadeh, AbhijitMukherjee, AntoinetteTordesillas, 2019, Experimental and Numerical Investigations on Confined Granular Systems Stabilized by Bacterial Cementation - **Published**
- ElahehKashizadeh, AbhijitMukherjee, AntoinetteTordesillas, 2019, Experimental Studies and Numerical Models for Granular Columns with Progressive Biocementation – **submitted for publication**

### Conference Paper:

Kashizadeh, E., A. Mukherjee, et al. "Numerical Model of Granular Materials Partially Cemented by Bacterial Calcite." V International Conference on Particle-Based Methods - Fundamentals and Applications (PARTICLES 2017), 552-563, In Center Numerical Methods Engineering, 201. **Published**

# Table of Contents

<b>DECLARATION.....</b>	<b>2</b>
<b>AUTHORSHIP .....</b>	<b>3</b>
<b>ACKNOWLEDGMENTS .....</b>	<b>4</b>
<b>DEDICATION .....</b>	<b>5</b>
<b>CO-AUTHORED PUBLICATIONS .....</b>	<b>6</b>
<b>TABLE OF CONTENTS .....</b>	<b>7</b>
<b>LIST OF FIGURES .....</b>	<b>10</b>
<b>LIST OF TABLES .....</b>	<b>13</b>
<b>ABSTRACT.....</b>	<b>14</b>
<b>CHAPTER 1: INTRODUCTION.....</b>	<b>16</b>
1.1. BACKGROUND .....	16
1.2. AIMS, OBJECTIVES AND RESEARCH QUESTION .....	18
1.3. LIMITATIONS AND ISSUES.....	20
1.4. SIGNIFICANCE.....	21
<b>CHAPTER 2: LITERATURE REVIEW .....</b>	<b>23</b>
2.1. MICROBIAL INDUCED CALCITE PRECIPITATION .....	24
2.2. FACTORS AFFECTING THE MICP PROCESS .....	28
2.2.1 <i>The Effects of Temperature on the MICP Process.....</i>	28
2.2.2 <i>The Effects of Bacteria Types on the MICP Process .....</i>	29
2.2.3 <i>The Effects of the Degree of Saturation on the MICP Process .....</i>	29
2.3. APPLICATIONS OF MICP .....	29
2.3.1 <i>Semi-aggregated sand grains: Aggregated heaps .....</i>	30
• GAPS AND OPPORTUNITIES.....	32
2.3.2 <i>Stabilised granular system with confinement .....</i>	33
• GAPS AND OPPORTUNITIES.....	36
2.3.3 <i>Stabilised granular system without confinement .....</i>	36
• GAPS AND OPPORTUNITIES.....	38
<b>CHAPTER 3: LOOSE AND SEMI-AGGREGATED SAND GRAINS .....</b>	<b>39</b>
<b>EXPERIMENTAL AND NUMERICAL INVESTIGATION ON HEAP FORMATION OF GRANULAR SOIL SPARSELY CEMENTED BY BACTERIAL CALCIFICATION .....</b>	<b>39</b>
ABSTRACT.....	39
3.1. INTRODUCTION .....	45
3.2. EXPERIMENTAL METHODOLOGY .....	48
3.2.1 <i>Materials .....</i>	48
3.2.2 <i>Methods.....</i>	51
3.2.3 <i>Estimation of cementation.....</i>	52

3.2.4. <i>Heap formation</i> .....	53
3.3. NUMERICAL MODEL .....	54
3.3.1. <i>Sparsely Aggregated Grains</i> .....	56
3.3.2. <i>Shape of the heap</i> .....	56
3.3.3. <i>Numerical results</i> .....	58
<i>i. Loose Spherical Glass Beads</i> .....	58
<i>ii. Validation</i> .....	59
3.4. PARAMETRIC STUDY.....	61
3.4.1. <i>Damping</i> .....	62
3.4.2. <i>Internal Friction Angle</i> .....	63
3.4.3. <i>Grain Size</i> .....	63
3.4.4. <i>Grain size distribution</i> .....	64
3.4.5. <i>Cementation</i> .....	65
3.5. CONCLUSION .....	66
3.6. REFERENCES.....	67
<b>CHAPTER 4: A MICP STABILISED CONFINED GRANULAR SYSTEM.....</b>	<b>71</b>
<b>EXPERIMENTAL AND NUMERICAL INVESTIGATIONS ON CONFINED GRANULAR SYSTEMS</b>	
<b>STABILISED BY BACTERIAL CEMENTATION .....</b>	<b>71</b>
ABSTRACT.....	71
4.1. INTRODUCTION .....	72
4.2. EXPERIMENTAL INVESTIGATION .....	74
4.2.1. <i>Cementation System</i> .....	75
4.2.2. <i>Method</i> .....	75
4.2.3. <i>Estimation of Calcium carbonate deposition</i> .....	76
4.2.4. <i>Test Matrix</i> .....	77
4.2.5. <i>Triaxial Tests</i> .....	77
4.2.6. <i>Microstructural Analysis</i> .....	78
4.2.7. <i>Scanning Electron Microscopy (SEM)</i> .....	78
4.2.8. <i>Energy Dispersive X-Ray Spectroscopy (EDS)</i> .....	79
4.2.9. <i>Quantitative EDS</i> .....	80
4.2.10. <i>Mechanical performance</i> .....	80
4.3. NUMERICAL MODEL .....	84
4.3.1. <i>Unit cell model</i> .....	84
4.3.2. <i>Global Model</i> .....	88
4.3.3. <i>Model Validation</i> .....	90
<i>i. Loose sand</i> .....	90
<i>ii. Biocemented sand</i> .....	92
<i>iii. Sparsely cemented sand</i> .....	94
4.4. PRESENT MODELS .....	96
4.4.1 <i>Comparison of models</i> .....	96
4.4.2 <i>Varying cementation and confining pressure</i> .....	98
4.5. CONCLUDING REMARKS .....	100
4.6. DATA AVAILABILITY .....	101
4.7. REFERENCES.....	101
<b>CHAPTER 5: A MICP STABILISED UNCONFINED GRANULAR SYSTEM.....</b>	<b>105</b>
ABSTRACT.....	105



5.1. INTRODUCTION .....	106
5.2. EXPERIMENTAL INVESTIGATION .....	108
5.2.1. <i>Materials</i> .....	108
5.2.2. <i>Sample preparation</i> .....	108
5.2.3. <i>Cementation levels</i> .....	109
5.2.4. <i>Uniaxial Compressive Strength Test</i> .....	110
5.2.5. <i>Mechanical performance</i> .....	111
5.3. NUMERICAL MODELLING.....	112
5.3.1. <i>Global Model</i> .....	113
5.4. NUMERICAL RESULTS AND VALIDATION.....	115
5.5. EVOLUTION OF DAMAGE.....	117
5.6. CONCLUDING REMARKS.....	122
5.7. REFERENCES.....	124
<b>CHAPTER 6: CONCLUSIONS AND RECOMMENDATIONS.....</b>	<b>127</b>
6.1 CONCLUSION .....	127
6.2 RECOMMENDATIONS.....	133
<b>CHAPTER 7: REFERENCES .....</b>	<b>134</b>
<b>CHAPTER 8: APPENDIX - CONFERENCE PAPER .....</b>	<b>142</b>
<b>A MODEL OF GRANULAR MATERIALS PARTIALLY CEMENTED BY BACTERIAL CALCITE .....</b>	<b>142</b>
ABSTRACT.....	142
8.1. INTRODUCTION.....	143
8.2. DEM MODELLING .....	145
8.3. METHODOLOGY.....	147
8.3.1. <i>Loose and Semi-aggregated Grains</i> .....	148
8.3.2. <i>Aggregated Grains</i> .....	149
8.4. RESULTS.....	149
8.4.1. <i>Loose spherical glass beads</i> .....	149
8.4.2. <i>Semi-aggregated granules</i> .....	150
8.4.3. <i>Aggregated cylinders</i> .....	153
8.5. CONCLUSION.....	157
8.6. REFERENCES .....	157

## List of Figures

<b>Figure 2.1:</b> Embodied energy and emissions of building materials.....	23
<b>Figure 2.2:</b> Framework for a generalised approach to soil engineering.....	24
<b>Figure 2.3:</b> Convert loose sand to free-standing sand columns through the MICP process.....	25
<b>Figure 2.4:</b> Overview of bio-mediated calcite precipitation using ureolysis .....	26
<b>Figure 2.5:</b> Our observation on the stages of biocementation: (a) Bacterial cells secure themselves within the grooves of sand grains; (b) The crystals grow to form mesocrystals; (c) The crystals bridge the neighbouring sand grains to cement them together; and (d) Quantitative EDS can scan the various stages of biocementation. ....	32
<b>Figure 3.1:</b> Heaps of sand dumped on the beach at Half Moon Bay, Melbourne, Australia .....	45
<b>Figure 3.2:</b> Our observation on the stages of biocementation: (a) Bacterial cells secure themselves within the grooves of sand grains; (b) The crystals grow to form mesocrystals; (c) The crystals bridge the neighbouring sand grains to cement them together, and (d) Quantitative EDS can scan the various stages of biocementation.....	46
<b>Figure 3.3:</b> Grain Frequency Histogram: (a) Sphericity; (b) Roundness .....	49
<b>Figure 3.4:</b> Definition of particle shape according to (Cho et al., 2006) .....	50
<b>Figure 3.5.:</b> Sand grains graduation curve ( $D_{50} = 0.425$ ) .....	51
<b>Figure 3.6:</b> Proctor compaction curve.....	52
<b>Figure 3.7:</b> Microscopic pictures of cemented sand under the effects of the MICP process.....	53
<b>Figure 3.8:</b> The contact models for grains with rolling resistance by Cundall .....	54
<b>Figure 3.9:</b> Mechanical stiffness of normal, tangential and rolling contact models .....	55
<b>Figure 3.10:</b> Numerical models for shape of heap study, (a), (b) and (c) represent different stage.....	56
<b>Figure 3.11:</b> The proposed model for the analytical model.....	57
<b>Figure 3.12:</b> Comparison of the analytical (white curve) and the DEM heap model.....	58
<b>Figure 3.13:</b> Shape of the heap of mono-sized glass beads (a) present numerical model, (b) experimental result.....	59
<b>Figure 3.14:</b> (a) Shape of the accumulated grains loose sand (a) Shape of the accumulated grains of the four days treated experimental sample (c) Shape of the accumulated grains of the eight days treated experimental sample.....	59
<b>Figure 3.15:</b> (a) Shape of the heap after four days treatment (b) Shape of the heap modelled by the DEM.....	60
<b>Figure 3.16:</b> (a) Shape of the heap after eight days of treatment, (b) Shape of the heap modelled by the DEM.....	61
<b>Figure 3.17:</b> Effect of damping ratio on $\theta$ and $\eta$ .....	62
<b>Figure 3.18:</b> Effect of internal friction angle on $\theta$ and $\eta$ .....	63
<b>Figure 3.19:</b> Effect of particle size on $\theta$ and $\eta$ .....	64
<b>Figure 3.20:</b> Particle size distribution curves for four different sand particle size distributions.....	65
<b>Figure 3.21:</b> Effect of particle size distribution on $\theta$ and $\eta$ .....	65
<b>Figure 3.22:</b> Modelling cemented grains by triads (a) No clumping, (b) Clumping 50%, (c) Clumping 75%.....	66
<b>Figure 3.23:</b> Effect of clumping ratio on $\theta$ and $\eta$ .....	66
<b>Figure 4.1.</b> Sand grains graduation curve ( $D_{50} = 0.425$ ).....	77
<b>Figure 4.2.</b> Proctor compaction curve .....	78
<b>Figure 4.3.</b> SEM image of the cement treatment sand sample (55% cementation through MICP process treatment).....	81
<b>Figure 4.4.</b> Energy-dispersive X-ray spectrum of cement samples that treated for 12 days (20% cementation) .....	81
<b>Figure 4.5.</b> SEM image of the sand sample after (a) 20%, (b) 35%, (c) 55%, (d) 70% days cement treatment.....	82

<b>Figure 4.6.</b> MICP samples with different level of cementation after applying triaxial test conditions - confining pressure of 100kPa.....	83
<b>Figure 4.7.</b> Stress-strain curves under triaxial test - confining pressure 100kPa.....	85
<b>Figure 4.8.</b> Stress-strain curves under triaxial test - confining pressure 200kPa.....	85
<b>Figure 4.9.</b> The unit cell model.....	87
<b>Figure 4.10.</b> A constitutive model for plastic behaviours of cement material.....	88
<b>Figure 4.11.</b> Different levels of cementation (a) 20%, (b) 40%, (c) 60%, (d) 80%, (d) 100% cementation.....	88
<b>Figure 4.12.</b> Load-deflection curves of the cemented samples in tension.....	89
<b>Figure 4.13.</b> Load-deflection curves of cemented samples in compression .....	89
<b>Figure 4.14.</b> Numerical models showing levels of cementation in colour codes (a) Homogenous, (b) Binary, (c) Spatio-temporal samples.....	92
<b>Figure 4.15.</b> Stress-strain plot for triaxial compression (a) experimental (Li 1985) and numerical (Wang and Li 2014), (b) present and (Li1985).....	94
<b>Figure 4.16:</b> Stress-strain plots for loose and cemented sand columns at 50 kPa confining pressure.....	95
<b>Figure 4.17:</b> Stress-strain plots for loose and cemented sand columns at 150 kPa confining pressure.....	96
<b>Figure 4.18.</b> Stress-strain curves for sparsely cemented columns in 100 kPa triaxial compression (a) Yang, O'Donnell et al. 2017 (b) present binary model .....	97
<b>Figure 4.19.</b> Stress-strain plots for Homogenous, Binary and Spatio-temporal models .....	99
<b>Figure 4.20.</b> A numerical approach to predict the failure mode – Confining pressure 100kPa For (a) Exp. 100-70, (b) Uniform, (c) Binary, (d) Spatio-temporal.....	100
<b>Figure 4.21.</b> A numerical approach to predict the failure mode – Confining pressure 100kPa For (a) Exp. 100-35, (b) Uniform, (c) Binary, (d) Spatio-temporal.....	100
<b>Figure 4.22.</b> Stress-strain plots for a confining pressure of 100kPa.....	101
<b>Figure 4.23.</b> Stress-strain plots for a confining pressure of 200kPa.....	102
<b>Figure 5.1.</b> Cement Capped MICP samples for the UCS test .....	114
<b>Figure 5.2.</b> Experimental MICP samples under uniaxial compression test .....	114
<b>Figure 5.3.</b> Stress-strain curves with varying cementation.....	116
<b>Figure 5.4.</b> A numerical model for sand column .....	117
<b>Figure 5.5.</b> Initial and final states of a cylindrical sample under uniaxial compression .....	118
<b>Figure 5.6.</b> Inter-grain distances at different stages of the compression test – unit is mm.....	119
<b>Figure 5.7.</b> Comparison of the failure modes obtained through the experiment and the DEM simulation – unit is mm.....	119
<b>Figure 5.8.</b> Comparison of experimental and numerical stress-strain plots .....	120
<b>Figure 5.9.</b> Damage evolution at 35% cementation.....	122
<b>Figure 5.10.</b> Damage evolution at 55% cementation.....	124
<b>Figure 5.11.</b> Damage evolution at 70% cementation.....	126
<b>Figure 8.1.</b> The relation between a granular material and a highly complex structural frame .....	151
<b>Figure 8.2.</b> The contact models for grains with rolling resistance .....	151
<b>Figure 8.3.</b> Mechanical stiffness of normal, tangential and rolling contact models .....	153
<b>Figure 8.4.</b> (a) The proposed numerical model in this study, (b) The experimental study by Zhou <i>et al.</i> [18], the angle of repose in both study is 37 degree.....	156
<b>Figure 8.5.</b> The angle of repose study with pop-corn (a) pop-cons in a container (b) accumulated shape of pop-corns after removing the container.....	157
<b>Figure 8.6.</b> Comparison of Numerical model – the coloured grains have used to make clumps distinguishable (a) and Experimental study (b) for semi-aggregated heaps, where the shape of the pop-corn grain simulated as three spheres clumped.....	158
<b>Figure 8.7.</b> Sand grain distribution to study Jawad <i>et al.</i> , Porter <i>et al.</i> .....	160
<b>Figure 8.8.</b> The stress-strain of the proposed numerical and experimental study .....	160
<b>Figure 8.9.</b> The stress-strain of the proposed numerical in the current study and experimental study by Porter <i>et al.</i> .....	161
<b>Figure 8.10.</b> Inter-grain distances at different stages of the compression test on a highly complex structural frame where different colours are representing the distance between grains, the blue is the smallest and red is the largest distance– unit is mm.....	162

**Figure 8.11.** Comparison of failure modes obtained through the experiment and DEM simulation –unit is mm.....162

## List of Tables

<b>Table 3.1:</b> Particle Size Distributions for Sand Mix.....	50
<b>Table 3.2:</b> Weight of precipitated calcium carbonate in one cycle of feeding.....	52
<b>Table 3.3:</b> Adopted numerical parameters to validate the proposed model(Zhou et al., 2002).....	59
<b>Table 3.4:</b> Relation between the percentage of clumping and weight of calcium carbonate precipitation.....	60
<b>Table 3.5:</b> The variables which considered for parametric study.....	62
<b>Table 3.6:</b> Grain size distribution groups .....	64
<b>Table 4.1.</b> Weight of precipitated calcium carbonate in one cycle of feeding.....	79
<b>Table 4.2.</b> Nomenclature of samples for the experimental tests.....	79
<b>Table 4.3:</b> The effects of the cement process on the main mechanical properties of the aggregated grains (x: value could not be measured).....	86
<b>Table 4.4.</b> Properties of grains and cement materials.....	87
<b>Table 4.5.</b> Relationships between the level of aggregation of the cement samples and the cohesion between grains.....	90
<b>Table 4.6:</b> Distribution of % cementation for different bond types.....	92
<b>Table 4.7.</b> Optimum values of the micro parameters to model the experimental results.....	93
<b>Table 4.8.</b> Input parameters for the numerical model .....	94
<b>Table 5.1:</b> Test matrix for the physical uniaxial test models.....	113
<b>Table 5.2.</b> The strength parameters with varying cementation.....	116
<b>Table 5.3.</b> Parameters for the experimental models.....	120
<b>Table 1.8.</b> The variables which considered for validation.....	156
<b>Table 8.2.</b> Optimum values of micro parameters to model Jawad experimental results.....	160
<b>Table 8.3.</b> Optimum values of micro parameters to model Porter <i>et al.</i> experimental results.....	161

## **Abstract**

Granular materials such as sand, silt, and clay are aggregated in nature into forms such as beach rocks, anthills, and other forms of microbialites. Microbial Induced Calcium Carbonate Precipitation (MICP) is common bio-geo-chemical cementation. MICP process occurs due to the mineralisation of calcium through bacterial enzymatic action. Unlike engineered cement, which consumes very high amounts of energy and emits large quantities of CO<sub>2</sub>, this natural cementation occurs in ambient conditions, with negligible energy consumption. Hence, it is a sustainable construction method. Natural cementation is a gradual process, where grains are initially bonded to form clumps. The clumps grow in size to form aggregates, finally creating free-standing samples. This process of natural cementation can be useful in a host of engineering constructions. Prominent uses in geotechnical engineering are improving mechanical properties of foundations, soil stabilisation, and reducing permeability. However, it is imperative to develop numerical tools to predict the biocemented materials' properties accurately for field application of the technology. Like other natural systems, MICP is a complex process with many controlling factors. The present numerical tools neglect the inherent inhomogeneity of the growth process and include the effect of MICP as a smeared uniform cohesion between all grains.

In this research, we perform controlled experiments on MICP and utilise the experimental results to model the different aggregation phases through MICP numerically. A series of experimental studies have been conducted at different levels of sand aggregation (lightly aggregated to free-standing columns) to achieve a thorough understanding of the essential parameters. The results have been utilised to validate the numerical models. The discrete element method (DEM) has been employed to model the aggregated granular materials formed due to MICP. The model is applied to study different sand aggregation levels, from sand heaps involving unbonded and bonded grains to free-standing columns. A micro-scale Finite Element Model (FEM) has been developed to study the intergranular properties due to different levels of MICP, and the results are plugged into the macro-scale DEM model. The novelty of the present numerical model is that it captures the MICP process's inhomogeneity and estimates its effect on the mechanical properties of aggregated grains.

Chapter 1 introduces the background and current research outlines. Chapter 2, followed by, provides a literature review of the critical physical and numerical studies on the MICP processes.

Chapter 3 studies the loose and semi-aggregated sand grains via MICP treating process. This chapter presents a numerical framework to model the sparsely cemented granular heaps. A rigorous experimental program has been offered to observe the relationship between the level of cementation and heap shapes. A discrete element unit model for sparsely cemented grains has been developed. The extent of cementation is modelled through the clumping of grains. A parametric study of the grain size distribution, internal friction angle, shape of clumps, and the extent of cementation has been performed. A polynomial for defining the form of the heap has been developed. The results will be useful for predicting the profile of a sparsely cemented granular heap

Chapter 4 discusses the effect of the MICP process. Focusing on the aggregated samples where they are not strong enough to use for overground applications, they could be used for stabilisation and underground applications when there is confining pressure around the samples. Cylindrical samples were prepared with a specified grain size distribution. The samples were then subjected to an Unconsolidated Undrained Triaxial Test at a constant rate until they collapsed. Experimental and Numerical investigations are conducted to understand the mechanical behaviour of aggregated samples under confined stress.

Chapter 5 describes the high levels of aggregation of sand grains through using the MICP process. In this case, not only can the specimen retain its shape under the action of gravity, but the aggregation is also strong enough to tolerate external loads without any need for confining pressure. This level of aggregation of the MICP samples has several overground applications like foundation settlement reduction (Martinez & DeJong, 2009), improving engineering properties, e.g. the durability and strength of mortar of concrete, healing building cracks (Achal et al., 2013a; Achal et al., 2013b; Qian et al., 2010; Reddy, 2013). Unconfined compressive strength tests were conducted to study the mechanical properties of well-aggregated MICP samples, on high-level MICP cemented stands, simulated by developing the numerical model using a discrete element model (DEM) approach. To understand the materials' mechanical behaviours, an insight into the micromechanics of the material was essential. There are a series of

experimental investigations which have taken place at the microscale level, such as resin impregnation, solidifying-sectioning using digital image analysis (Kuo et al., 1996), imaging through magnetic impregnation (Ng & Wang, 2001), X-ray tomography (Wang et al., 2004).

Digital Image Correlation (DIC) analysis was conducted on the physical samples to demonstrate the numerical model's capability to capture the failure paths of the MICP samples under the effects of uniaxial compressive testing. The results were compared with the numerical models.

Finally, Chapter 6 presents the significant findings of the study and discusses possible future work.

The appendix illustrates the overall content of the thesis, focusing on how physical and numerical methods are developed to study the effect of different levels of sand grains aggregation through MICP treatments, at micro and macro levels.

## **Glossary of Terms**

MICP	Microbially Induced Calcium Carbonate Precipitation
DEM	Discrete Element Model
FEM	Finite Element Method
DIC	Digital Image Correlation
EDS	Energy Dispersive X-Ray Spectroscopy
SEM	Scanning Electron Microscope
UCS	Unconfined Compressive Strength



# Chapter 1: Introduction

## 1.1. Background

Earth's supply of quality granular materials is limited and used at an ever-increasing rate for the sake of infrastructural development. Granular materials are often stabilised with a small quantity of binder (<10%) to limit their use. This stabilisation process causes some grains to bond together and interlock with other grains. Thus, it increases the effective angle of friction and increases the angle of the stable slope of embankments. However, binders commonly used in the industry, such as cement, use a large energy quantity. Cement manufacturing is known to emit large amounts of greenhouse gases (nearly one tonne of greenhouse gas per tonne of cement). Thus the world faces the dichotomy of maintaining infrastructural growth while protecting the environment.

Many roads, bridges, and building have been built in the last hundred years, and they play a big part in the world's economic wealth. In the developed world, many face a need to maintain and renew the existing constructed structures. Building constructions consume most natural resources and lead to a significant portion of greenhouse gas emissions (Achal & Mukherjee, 2015). Australia is a continent with sparse population density. Connecting remote locations with road networks has resulted in the country having the highest road length per capita. Australian road network comprises 873,573 km of roads, 83% can be classified as rural roads (DoIRD, 2015). Such a vast and remote road network creates a challenging problem in monitoring deterioration in pavement structures and the identification and prioritisation of maintenance and rehabilitation works. In 2005 to 2015, Australia has spent \$21 billion on road and bridge maintenance works (DoIRD, 2015). Understandably, a durable road base system that would minimise the need for frequent inspection and maintenance has been opted for. Cement stabilisation is a practice commonly used in the Australian road industry for ensuring adequate strength and stiffness of a granular road base material. According to Austroads (2006), it is common for the cost of the binder material (cement) in stabilisation works to be approximately

40% or greater of the total cost of the works. Typical energy consumption rates for cement stabilised materials have been estimated to be around 5,000 mJ/tonne while the actual placement and construction of the stabilised road base is estimated to consume only 50mJ/tonne (Austroads, 2007). Although the present road base has proved to be very functional, the mandate on developing sustainable technologies necessitates drastically limiting its energy consumption and emission. A sustainable binder for road base material with dramatically lower embodied energy and emission must be designed.

Ordinary Portland Cement (OPC) is widely used in the construction of building structures. 3.5 billion tonnes of cement produced per year worldwide and 57.3% consumed by China alone. OPC is responsible for 6% global carbon dioxide emission, and 50% of all carbon dioxide emission worldwide come from building construction and operation (Achal & Mukherjee, 2015). With high-energy consumption, construction industry today lead to hazardous waste disposal, water contaminant and global warming, which impact on earth are complicated to be solved. Unfortunately, the world population keep increasing, and the pace of consumption continues to grow (DeJong et al., 2010a). Therefore, the cement industry needs a solution to counter the depletion of raw materials and fuel and also environmental degradation.

Soil improvement methods such as chemical admixture, grouting stabilisation, soil replacement and preloading for achieving consolidation are not economical and time-consuming. Grouting and admixture stabilisation can cause environmental impact due to acrylamide grout seeping into the waterways and cause poisoning. Thus, the use of chemical grouts is restricted due to the hazard of leaching. Therefore, adopting other options for soil improvements are essential to managing economic viability, optimum performance and environmental sustainability (Cheng et al., 2013).

Nature has been building materials in a sustainable way for millions of years. Biological materials are all composites like bones made of high modulus crystalline calcium carbonate and ant hills form by cementation of sand similar to cement mortar. Due to advancement of technology, understanding of natural materials could help with improving the manufactured ones. Abundant calcium compounds in the form of phosphates, carbonates, and sulphates are used for manufacturing materials of

construction. Low consumption amount of energy for the production of a natural compound can have enormous potential for developing sustainable construction materials (Achal & Mukherjee, 2015).

(DeJong et al., 2010a; Whiffin, 2004) developed bio-mediated methods for soil improvement. One of these developed technologies is microbial induced calcium carbonate precipitation (MICP), which precipitation takes place in soil matrix by introducing calcium carbonate through ureolysis activated by the bacterium *Sporosarcina pasteurii* and other ureolytic bacteria. Main reactions related to calcite precipitation occur given with a solution of urea and calcium chloride. Oxidation of ammonium could dissolve the calcite precipitation during an acidifying process. Ammonium chloride produced should be removed during the cementation process because it can cause geological effects on the environment. Calcite will be stabilised if underground water pH is greater or equal to 6.3. The calcite cementation produced by bacteria depends on the amount of urea and calcium given. Therefore, the number of injections of urea and calcium requires gaining a sufficient level of cementation. The set times for microbial reaction in the MICP process can be controlled to be slower than chemical grouts which will allow the MICP reaction to spreading more through a greater volume of soil (Feng & Montoya, 2015).

As mentioned, soil properties improvement is a time-consuming process. Also, there is a limitation to model MICP samples in large scales and different level of aggregation through cementation process; numerical models could be a reliable substitute by having the capability to model complex networks like porous media.

## **1.2. Aims, Objectives and Research Question**

The proposed research is a comprehensive study to capture the behaviour of granular particles stabilised using MICP. This report analyses the impact of microbially induced calcium carbonate precipitation cemented sand on the mechanical behaviour of the material with parameters such as strength and stiffness. The research scope includes

developing a unified numerical model for all stages of cementation. All the stages of aggregation due to the MICP process have been studied in the following steps:

- 1- Aggregated heaps: At this stage of aggregation, a sand column is unable to stand freely and collapses into a heap. However, the shape of the heap is influenced by the extent of aggregation. Numerical models for the heap formation are reported with experimental validation.
- 2- A stabilised granular system with confinement: At this stage, a sand column is confined and subjected to external pressure, as experienced in the underground condition. Numerical models for the stress-strain behaviour of confined stabilised columns is developed and validated through experiments.
- 3- A stabilised unconfined granular system: At this stage, the cementation is progressed to a stage that the sand columns can freely support the load, as experienced in overground condition. Numerical models for the stress-strain behaviour of unconfined stabilised columns is developed and validated through experiments.

The steps adopted in this study are as follows:

- Design and conduct experimental studies conducted to study different levels of aggregation due to the MICP process.
- Finite element numerical modelling (FEM) to investigate the material property of MICP samples
- Discrete element numerical modelling (DEM) of the unbounded sand particles– Validate the numerical model with existing studies.
- Discrete element numerical modelling (DEM) of the bonded sand particles: Semi and fully aggregated sand grains validate the numerical model with existing studies. Three scenarios will be considered to model the aggregated sand grains,
  - 1- Homogenous aggregation: when the cohesion value between all grains is the same.
  - 2- Non-homogenous: when there are two types of cohesion between sand grains to illustrate the aggregated and non-aggregated grains
  - 3- Graded aggregation: when the cohesion type between grains will be more than two.
    - Comparing numerical and experimental results.

As mentioned earlier, this study will develop discrete element models (DEM), whose bulk mechanical can faithfully simulate the experimental counterparts. To achieve these results at the macroscopic scale, the DEM models will be closely calibrated to the initial configuration and packing density of the experimental systems, as well as the contact and particle size distribution of the constituent particles. Open source code simulation software "YADE" is used as a DEM modelling tool. The bonded grains are known to change the load resistance path. The responses of the clumped grains are modelled by employing a constitutive model which is driven by a combination of Hook's and Coulomb's laws. The results of the model will be compared with experimental observations. The effect of different levels of clumping on the stress-strain response will be demonstrated through a parametric study. It is appropriate that the results are utilised to determine the optimum level of calcium carbonate precipitation for achieving the desired engineering properties of the material.

- The expected outcomes of this research are:
  - Develop a robust numerical and experimental framework to design the MICP samples with an optimum level of aggregation.
  - Investigate the effect of MICP phenomenon on the mechanical behaviour of aggregated sand grains at various stages of cementation.
- The research question of this report is:

If Microbial Induced Calcite Precipitation (MICP) cemented, sands could be a reliable substitute of traditionally cemented sands in future by investigating the mechanical behaviour of MICP samples.

### **1.3. Limitations and issues**

The microbial cementation method is more complex as the microbial activity depends on many environmental factors which are temperature, pH, the concentration of donors and acceptors of electrons, concentration and diffusion rates of nutrients and metabolites. Economic limitation of the use of laboratory-grade nutrient sources as medium ingredients cost much higher than operating cost. Production of ammonia during ureolysis cause toxic effect in different aspects such as human health, eutrophication and acidification of ecosystems. But little works give the understanding of the formation and

development of the bond and de-bond behaviour of bio-cemented sand. Also, the current existing numerical models are limited to homogenous studies which do not capture what it happens in reality through the MICP process.

#### **1.4. Significance**

Achieving environmental sustainability is one of the eight millennium development goals of the United Nations, which emphasises on the principles of sustainable policies of member countries, minimising the loss of environmental resources (United Nations, 2014). Current construction technologies need to reduce their use of materials and energy considerably to approach this goal. Buildings in the European Union consume approximately 50% of the total European Union's energy usage over their life cycle (construction, operation, rehabilitation and demolition). Buildings contribute almost 50% of the released CO<sub>2</sub> to the atmosphere (Dimoudi & Tompa, 2008). The National Sustainability Council of Australia states that "While our cities are among the most liveable in the world, they lag on some aspects of sustainability" and asks, "How can we create more sustainable and affordable buildings?" (Sustainable Australia Report, 2013). To achieve sustainable construction, we must first identify the components of the building industry that contribute significantly to environmental degradation. Greater than 60% of the solid waste from inner Sydney can be attributed to construction and demolition (Year Book Australia, 2003). A study in Hong Kong finds that 82–87% of the total GHG emission from building construction is from the embodied emission of their materials. The results also indicate the embodied GHG emission of concrete and reinforced steel account for 94–95% of those building materials, (Yan et al., 2010). Considerable research has been undertaken to produce green concrete, including partial replacement of the cement with industrial by-products such as fly ash, (Mehta, 2004). However, transformational changes are essential for achieving sustainability.

When the microbial fluid is passed through granular (sand) or porous (brick, concrete) materials, the microbes catalyse the chemical process of deposition of crystals of calcium carbonate, (some other forms are also possible) in the vacant spaces. This precipitation enhances the substrate in two ways,

1. It decreases the permeability of the material by creating a barrier for ingress of moisture and other deleterious materials,
2. It binds the grains of the substrate together.

Both the above processes significantly improve the engineering properties of the substrate, preventing deterioration and increasing durability. The improved bond between particles increases the strength of the material and reduces material consumption. The efficiency of MICP depends on several factors such as the microbial strain, environmental conditions, the concentration of the constituents in the fluid and grain sizes and pores. Only a few specialised research laboratories in the world have demonstrated MICP, and its emergence as a potential construction material requires several critical breakthroughs. A fresh approach going beyond the traditional moorings of engineering disciplines is essential for exploring this exciting prospect.

The present study caters to the strategic goal of the design of sustainable construction materials by developing a numerical model which simulates how the granular particles precipitate together in order to accurately predict the MICP process. The results will be supported by physical models that are developed in this study.

## Chapter 2: Literature Review

Presently, 3.6 billion tonnes per annum of Portland cement is produced worldwide, contributing approximately 6% of all anthropogenic greenhouse gases (Imbabi et al., 2012). Technologies that can dramatically reduce or possibly eliminate Portland cement must be explored to improve the sustainability quotient of civil infrastructure. Existing building materials use high amounts of energy and produce high volumes of carbon dioxide gases, as shown in Figure 2.1. Consequently, one of the critical requirements to change building materials has to do with their sustainability.

Although cement has less embodied energy compared to other building materials, due to the enormous quantities of cement being produced, it contributes 6% of global carbon dioxide emissions and 50% of the carbon dioxide emissions from building construction and operation worldwide.

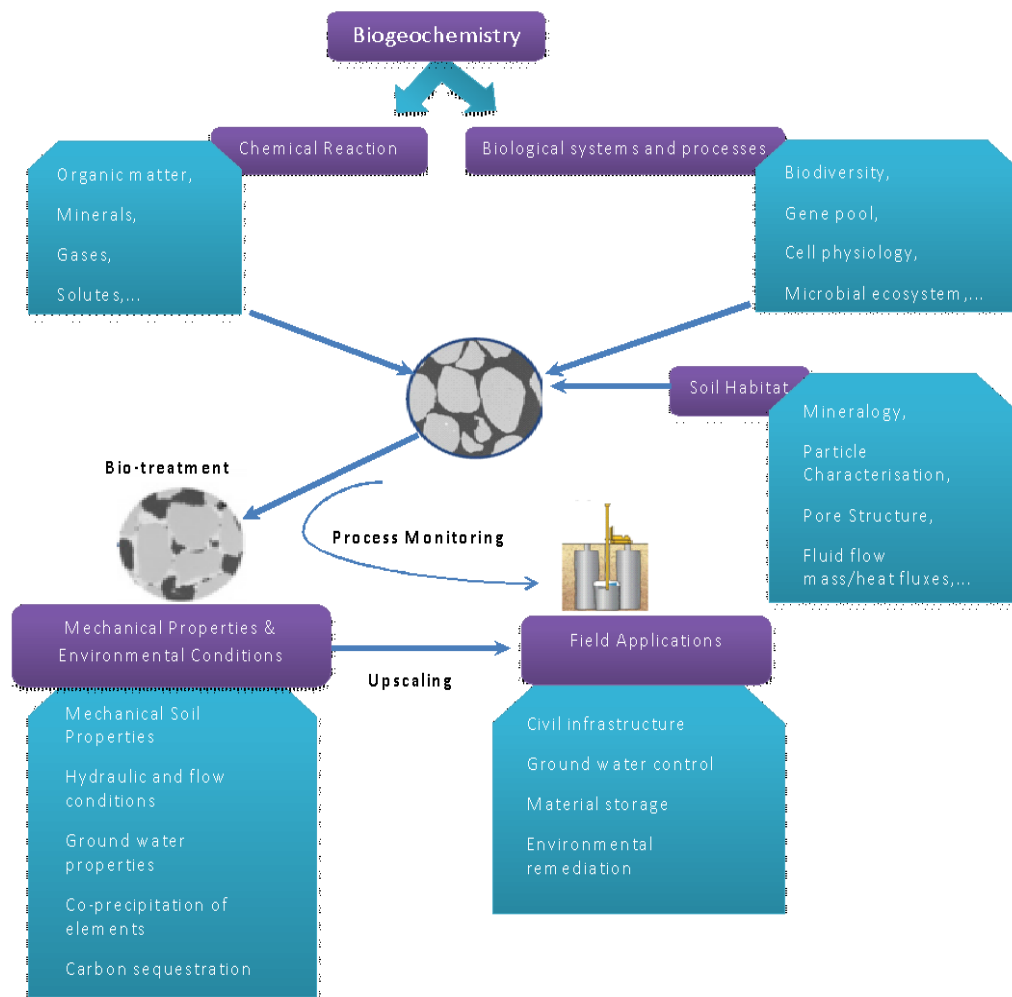
Material	Energy (MJ/kg)	Carbon (kg CO <sub>2</sub> /kg)	Density (kg /m <sup>3</sup> )
Aggregate	0.083	0.0048	2240
Concrete (1:1.5:3 eg in-situ floor slabs, structure)	1.11	0.159	2400
Concrete (eg in-situ floor slabs) with 25% PFA RC40	0.97	0.132	
Concrete (eg in-situ floor slabs) with 50% GGBS RC40	0.88	0.101	
Bricks (common)	3.0	0.24	1700
Concrete block (Medium density 10 N/mm <sup>2</sup> )	0.67	0.073	1450
Aerated block	3.50	0.30	750
Limestone block	0.85		2180
Cement mortar (1:3)	1.33	0.208	
Steel (general - average recycled content)	20.10	1.37	7800
Steel (section - average recycled content)	21.50	1.42	7800

**Figure 2.1:** Embodied energy and emissions of building materials (Greenspec research 2015-Greenspec.co.uk)

One-quarter of the world's landmass, which is home to more than one billion people, is threatened by desertification. In the denitrification process the fertile land changes to desert due to drought and deforestation. The capital of Mauritania, Nouakchott, has been suffering from desert encroachment.

A bio-mediated calcification process derived from a framework for a generalised approach to soil engineering is shown in Figure 2.2 (DeJong et al., 2010a).



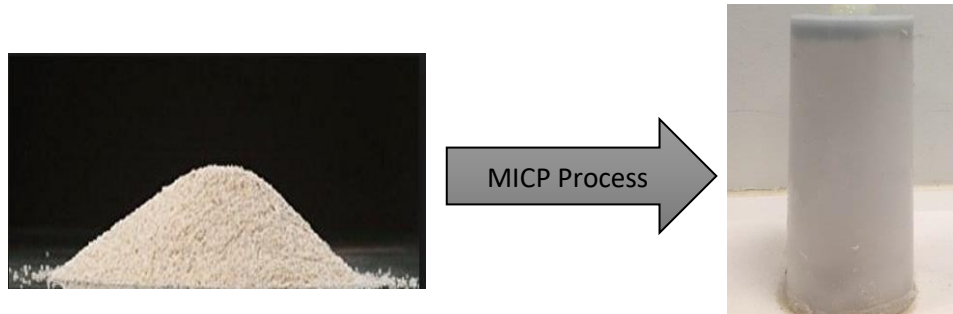


**Figure 2.2:** Framework for a generalised approach to soil engineering (DeJong et al., 2010a)

## 2.1. Microbial Induced Calcite Precipitation

Recently, natural cementation, Microbial Induced Calcite Precipitation (MICP), has been introduced as an alternative to cement binder (Achal & Mukherjee, 2015). In this process, the bacterial enzymes catalyse a hydrolysis reaction, which eventually leads to nucleation in the presence of calcium ions at an appropriate pH. (Achal & Mukherjee, 2015). Several critical applications of the process have been reported (Achal et al., 2011). MICP is a bio-geo-chemical process that is performed to synthesise granular materials for a designed mechanical performance (Achal et al., 2011; Achal et al., 2010; Achal et al., 2012b; Ramachandran et al., 2001b; Whiffin et al., 2007). The key achievements of the MICP process have been decreasing the permeability of samples and the compressibility behaviours of porous media in

granular samples, increasing the stiffness and shear strength of samples and it helps to control the volumetric response of a soil mass.



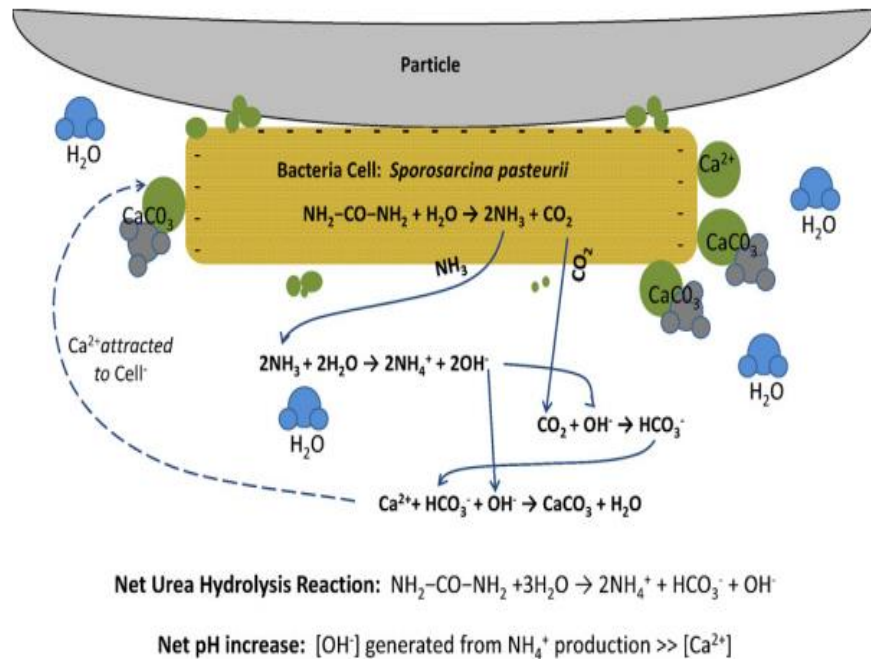
**Figure 2.3:** Convert loose sand to free-standing sand columns through the MICP process

In this process, microorganisms develop calcium carbonate precipitation by metabolic processes that increase the alkalinity of the soil in the natural environment. In the MICP process, bacteria containing a urease enzyme which can consume urea ((NH<sub>2</sub>)<sub>2</sub>CO) as a source of energy to produce ammonium (NH<sub>4</sub><sup>+</sup>) through ureolysis. Urea hydrolysis is triggered by urease to produce ammonium and carbonate ions (CO<sub>3</sub><sup>2-</sup>). Then, ammonium breaks off into ammonia NH<sub>3</sub> and causes the pH to increase to 9.3 until equilibrium between the NH<sub>4</sub><sup>+</sup> / NH<sub>3</sub> and HCO<sub>3</sub><sup>-</sup> / CO<sub>3</sub><sup>2-</sup> can be achieved.



The products in Equation (2.1) include carbonate, bicarbonate (HCO<sub>3</sub><sup>-</sup>), carbonic acid (H<sub>2</sub>CO<sub>3</sub>), hydroxide ions (OH<sup>-</sup>) and protons (H<sup>+</sup>) which react with the calcium ions (Ca<sup>2+</sup>) to form calcium carbonate because of the attraction of the anions and cations. Lastly, several phases of the mineralisation process take place: nucleation, crystal formation and crystal growth. Calcium carbonate can precipitate more and add mass in a soil matrix if the produced carbonate is sufficient (Fauriel & Laloui, 2012).





**Figure 2.4:** Overview of bio-mediated calcite precipitation using ureolysis (Dejong et al. 2010)

One of the limitations of the MICP process is its dependency on the material's pore size. The minimum pore size must range between 0.5 and 5 micrometres for the bacteria to move freely to have the optimum results. The MICP is assumed to be efficient in silts, fine sands and coarser materials under particular conditions.

A series of experimental studies on the MICP phenomenon has been performed during the last decade (Al Qabany et al., 2011; Stocks-Fischer et al., 1999; van Paassen et al., 2008; Whiffin, 2004).

Along with an increase in the binding due to calcium carbonate, the presence of bacterial biomass is envisaged to reinforce the concrete increasing strength (Achal et al., 2013b). In the case of cracked samples remediated by microbial precipitation, up to a 60% increase in strength has been reported (Ramachandran et al., 2001a), (Achal et al., 2010).

An essential benefit of MICP is that it reduces the permeability of construction materials. In (Achal & Mukherjee, 2015), and references therein, it has been observed that researchers have reported 40-90% reductions in water absorption in concrete due to MICP (De Muynck et al., 2008), (Achal et al., 2011). MICP process dramatically improves the durability of the materials as a reduction in the water permeability also impedes the ingress of other deleterious substances. It has also been found that there

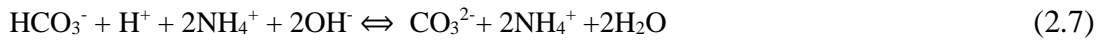
were reduced chloride diffusion and a consequent decrease in reinforcement corrosion due to MICP (Achal et al., 2012a), (Jonkers & Schlangen, 2008).

MICP has been found to consolidate loose particles in soil, sand and dust (De Jong et al., 2013). Microbial calcite crystals form "cohesive bridges" between the sand grains, thereby leading to an increase in the stiffness of the sand, with a corresponding decrease in permeability (DeJong et al., 2006), (De Jong et al., 2013). It has also been found that MICP caused a 23% increase in the strength and a 30% decrease in the porosity of unfired blocks made of sand and clay (Dhami et al., 2012). Such blocks also sequester atmospheric carbon by utilising another microbial enzyme, carbonic anhydrase (Shaffer, 2010),(Sharma & Bhattacharya, 2010).

MICP involves complicated biochemical reactions controlled by two enzymes, urea and carbonic anhydrase, which are produced by bacteria and utilise urea as a substrate. It supplies calcium for mineralisation. Due to urease activity, one mole of the consumed urea produces 1 mole of ammonia and 1 mole of carbonate ion (carbamate) (Eq. 2.2), which hydrolyses to make one mole of ammonia and carbonic acid (Eq. 2.4), called ureolytic activity. Bicarbonate is made of two moles of ammonium and one mole of hydroxide ion (Eqs. 2.5 and 2.6). The changes in water equilibrium increase the pH level, that causes the formation of carbonate ions (Eq. 2.7). Increasing the alkalinity in the cell creates the high extracellular calcium ion concentration and low extracellular proton concentration required to produce carbonate ions. The formation of  $\text{CO}_3^{2-}$  from the  $\text{HCO}_3^-$  occurs due to the alkalinity conditions. Lastly, increasing the carbonate concentration raises the supersaturation level governing the  $\text{CaCO}_3$  precipitation around the cell in the presence of soluble calcium ions (Eqs. 2.8 and 2.9).

Another enzyme that promotes the inter-conversion of  $\text{CO}_2$  and  $\text{HCO}_3^-$  and builds up the precipitation of  $\text{CaCO}_3$  is carbonic anhydrase.  $\text{HCO}_3^-$  is the source of the dissolved organic carbon and the carbonate anhydrase triggers its conversion into  $\text{CO}_2$  and the overall reaction shown in Eqs. 2.10 and 2.11 (Achal & Mukherjee, 2015).





## 2.2. Factors Affecting the MICP Process

MICP is a natural process which depends on the metabolic activities of microorganisms and the chemical reactions under the effects of environmental conditions. Many factors affect the ureolysis of the bacteria and the formation of calcium carbonate precipitates, including the bacteria concentration, bacteria type, medium pH value, temperature, calcium ion concentrations, availability of nucleation sites, mineralogy and the particle sizes of the soil, typically, coarse-grained sand.

(Mortensen et al., 2011) declared that the factors that affect the bacterial growth, metabolism and the precipitation induced by the bacterium *Sporosarcina pasteurii* are the concentration of the ammonium, oxygen quantities, mineralogy and soil particles and temperature which are the parameters that influence the ureolytic activity of the bacteria.

Many factors affect the ureolysis of the bacteria and the formation of calcium carbonate precipitates including the bacteria concentration, bacteria type, medium pH value, temperature, calcium ion concentration, availability of nucleation sites, mineralogy and particle sizes of the soil, soil types, pH range of salinity and the concentration of ammonium chloride (Umar et al., 2016a). Below are some of the crucial parameters that affect the MICP process.

### 2.2.1 The Effects of Temperature on the MICP Process

(Okwadha & Li, 2010) and (Mitchell and Ferris 2005) revealed that *Sporosarcina pasteurii*, at an optimum temperature (10°C), increases the rate of the urea hydrolysis with an increase in the concentration of the bacterium and leads to a massive increase of calcium carbonate precipitation. Increasing the rate of the urea hydrolysis caused

a ten times increase of calcium ions. (Okwadha & Li, 2010) and (Mitchell and Ferris 2005) also reported that breaking down the urea into ureolysis is a temperature-dependent process, like enzyme reactions. It was shown that when the temperature is between 20°C to 37°C, the efficiency of the MICP is optimum. (Nemati & Voordouw, 2003) and (Warren et al., 2001) have stated that the rate of urease activity increases two times by increasing the temperature from 10°C to 15°C, and five times more by increasing the temperature from 15°C to 20°C. In another study (Whiffin, 2004), it was reported that urease activity is proportional to temperature up to 70°C.

### **2.2.2 The Effects of Bacteria Types on the MICP Process**

(Ng et al., 2012) used *Bacillus megaterium* species to induce calcium carbonate precipitate in soil. The process has been done in a condition of using  $1 \times 10^8$  cfu/ml bacteria concentration and 0.5M cement reagents ( $\text{CaCl}_2$ ), that after 48 hours of treatment the shear strength increased by 69% also the treatments caused 90% reduction in hydraulic conductivity.

### **2.2.3 The Effects of the Degree of Saturation on the MICP Process**

(Cheng et al., 2013) illustrated the effects of different levels of saturation on bio-cemented sands. It was reported from a scanning electron microscope that the high degree of saturation samples formed scattered calcite crystals on the grains' surfaces. In contrast, the low degree of saturation samples developed strong calcite coatings on the sand grains which bonded together. They proved that high strength could be achieved in low saturation with fewer chemicals. It was also found that aerobic microbial activity performs best at a 60% to 80% level of saturation. Since the small quantity of cementation can be produced at a lower degree of saturation of samples (Umar et al., 2016b), it can be concluded that the MICP treatment has a great potential to move towards the eco-friendly and economical process.

## **2.3. Applications of MICP**

Different stages of grains aggregation through MICP process have specific applications. As mentioned in Chapter one in this thesis, the applications are categorised in three main stages:

### **2.3.1. Semi-aggregated sand grains: Aggregated heaps**

Dust suppression is one of the use-cases for poorly aggregated sand grains by increasing the interlocking between grains. Construction equipment is damaged under the effect of the building materials' (concrete, sand,...) dust, other than that dust normally causes health issues. To address this issue; chemicals, salts, petroleum products or water have been used for dust suppression, traditionally.(Bolander & Yamada, 1999; Lohnes & Coree, 2002; Rushing et al, 2006).

Loosely aggregated sand grains as a result of the MICP treatment are one of the environmentally friendly solutions for dusty environments (Benini et al., 1996), (Braissant et al., 2003),(Stocks-Fischer et al., 1999), (Warren et al., 2001), (Chu et al., 2012), (Bang & Bang, 2011), (Van Paassen et al., 2010), (Dhami et al., 2016b), (Porter et al., 2017a).

Frequency of extreme weather events such as storms and floods is on the rise, due to climate changes (Steffen et al., 2014). It poses new engineering challenges to the countries like Australia, where 80% of the population lives within 50 km from the coastline (2006). Protection coasts against waves, river banks against currents, embankments against soil liquefaction pressure are some of the examples that study of heaps of natural granular materials such as sand, silt and clay, plays an important role (Eric & Nick 2015). The aesthetic acceptability and minimal effect on the native flora and fauna of the soil mound make it more popular in comparison with other invasive forms of protection such as groynes or rock armours in renourishing the beaches and river banks(Williams et al., 2018). The optimum model is required to design the mounds to achieve the best performance against destabilising forces such as waves, currents and hydrostatic pressures. The loose grains form a heap characterised by their grain size distribution and internal angles of friction (Herrmann, 1998).

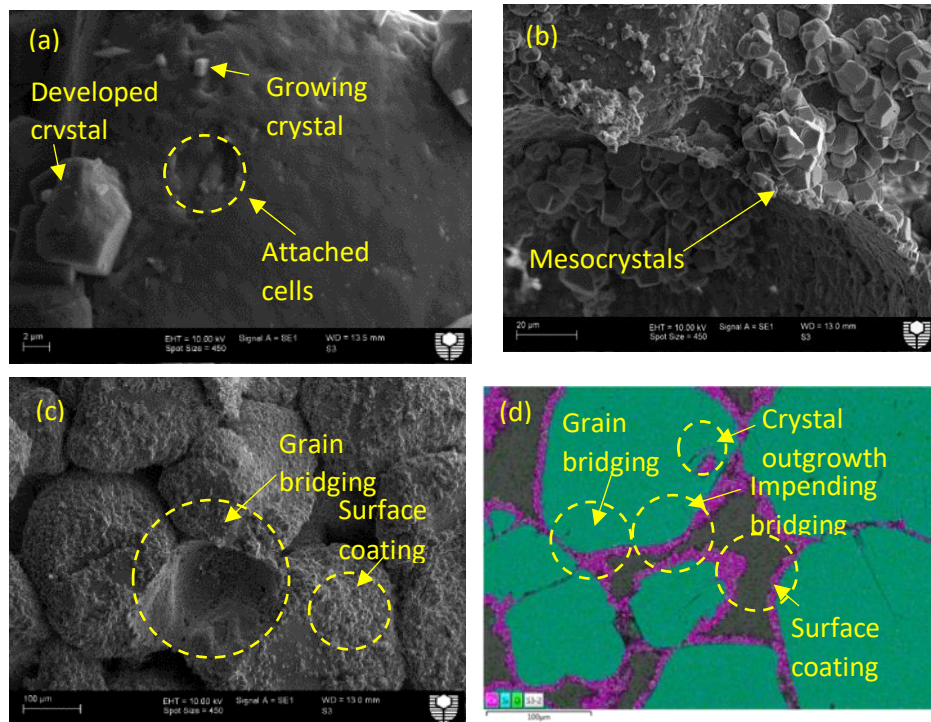
Loosely packed granular heaps have long been studied through experimental and theoretical approaches (Train, 1958). It is observed that grain properties such as inter-granular friction (Carstensen & Chan, 1976), (Zhou & Ooi, 2009; Zhou et al., 2001) grain shape (Friedman & Robinson, 2002; Kozicki & Tejchman, 2011; Wensrich & Katterfeld, 2012), and grain size distribution (Derakhshani et al., 2015; Matuttis, 1998; Miller & Byrne, 1966; Robinson & Friedman, 2002) influence the shape of the heap. Additional resistance against motion must be created, when the frictional resistance is

not sufficient to resist the destabilising forces. Often, a small dose of cement is added to the granular media resulting in some grains clumping together. There are two main factors to increase the clumping increases resistance to motion by 1) grain interlocking and 2) inter-grain cohesion. However, the addition of cement can be toxic to the native flora and fauna.

Engineered cement emits large quantities of CO<sub>2</sub> by consuming vast amounts of energy (Gielen et al., 2008). Annual production of Portland Cement makes up around 6% of all anthropogenic greenhouse gas emissions (Imbabi et al., 2012). On the other hand, nature clumps grains due to bio-geo-chemical processes in sand heaps, especially when it is moist for a substantial period (Polat Pelin et al., 2018). Natural clumping is non-toxic and devoid of environmental hazards. Nature might therefore offer clues towards sustainable stabilisation of sand heaps.

Recently, a natural cementation technology through microbially induced calcium carbonate precipitation (MICP) has been developed. Despite some challenges like energy consumption, and cost, MICP can be a potential alternative to cement binders (Achal & Mukherjee, 2015; Achal et al., 2015). Due to this process, bacterial enzymes are utilised to nucleate calcium carbonate as the cementing material (Achal & Mukherjee, 2015). A series of lab studies are conducted to apply the technology in a number of engineering problems such as stabilisation of road bases (Porter et al., 2016a), fortification of rammed earth (Porter et al., 2018a) and sustainable bricks (Dhami et al., 2013). Dhami et al. showed a significant advancement in the process in 2016 (Dhami et al., 2016a). There is a fundamental difference between soil biostabilisation process and the engineered cement binders. Our team research proved that biocementation is initiated when bacterial cells secure themselves in the grooves of the substrate, such as sand (Porter et al., 2017b). They act as nucleation sites for the growth of calcium carbonate crystals (Fig. 2.5a). The crystals grow to form mesocrystals (Fig. 2.5b), and then the mesocrystals grow to bridge neighbouring particles, thus achieving cementation (Fig. 2.5c). The quantitative energy dispersive X-ray scanning method is used in this thesis, to estimate the degree of sands' aggregation due to MICP process (Fig. 2.5d). Thus, biocementation grows in layers with initiating from a plethora of nucleation sites dictated by the concentration of microbial cells (Achal & Mukherjee, 2015).





**Figure 2.5:** Our observation on the stages of biocementation: (a) Bacterial cells secure themselves within the grooves of sand grains; (b) The crystals grow to form mesocrystals; (c) The crystals bridge the neighbouring sand grains to cement them together; and (d) Quantitative EDS can scan the various stages of biocementation.(Achal & Mukherjee, 2015)

- **Gaps and opportunities**

Literature reviews in this area highlight the need for pressing research to achieve detailed knowledge of granular materials behaviour under varying degrees of partial cementation. In particular, a model is needed to predict: (i) the location and degree of cementation, and (ii) the consequent influence of varying partial degrees of cementation on the mechanical response of the material.

The capability of the discrete element method (DEM) to model complex networks can facilitate simulating the inter-granular interactions. (Cundall & Strack, 1979) reported that a minimum number of grains must be used for the DEM to capture the desired phenomenon. The limitation of DEM in modelling non-spherical grains is overcome through the imposition of rigidity condition among a group of spheres arranged in the desired shape (Thomas & Bray, 1999). Using DEM, particle shape (Ting et al., 1995), size (Jacobson et al., 2007) and frictional behaviour (Suiker & Fleck, 2004) of

granular assemblages have been investigated. Development of public domain codes for DEM, such as YADE, has made the technique freely available to researchers (Kozicki & Donzé, 2008).

Cohesive bond defined between the grains to model the granular cementation systems (Estrada et al., 2010; Utili & Nova, 2008). Some reports demonstrate using of DEM for modelling bio-cemented samples; in all these studies, an average homogenous inter-grain cohesive strength has been assumed to represent the degree of cementation (Khoubani & Evans, 2018; Yang et al., 2019). The averaged cohesive strength is adjusted through trial and error to achieve results close to that obtained from experiments. In these cases, the stress-strain behaviour of sand columns is predicted through DEM. Use of DEM for prediction of the shape of the heap for sparsely cemented material is not reported hitherto.

DEM is specially equipped to model the formation of a heap as it can incorporate inter-granular friction, sliding, rolling and movements of grains that are several orders of magnitude higher than the grain sizes. Moreover, cementation can be introduced through clumping of grains. Considering these capabilities, in this thesis, we report an experimental and numerical investigation on sparsely cemented sand grains. To bind the grains partially, MICP has been performed on loose sand; only a small fraction of grains are bonded forming clumps. Due to the low level of cementation, the grains can still move freely to create a heap. For the first time, the process of formation of the heap, especially with partial grain bonding, has been numerically modelled. The experimental results are used to validate the accuracy of the numerical model, Both the experimental and numerical results have been utilised in developing a polynomial fit for the shapes of the heaps based on the basic geometric parameters. The expression is useful to determine the degree of cementation required to obtain the target shape of the heap.

### **2.3.2. Stabilised granular system with confinement**

Fully aggregated grains which result from the MICP process, where the grains reach to free-standing columns, do not fall under the effects of gravity. Although the samples may not have a high level of strength, they are appropriate for underground and stabilisation applications when they can tolerate the loads under confined pressures (DeJong et al., 2010a; Ferris et al., 1996; Le Metayer-Level et al., 1999; Van Paassen et al., 2009; Whiffin et al., 2007). In Australia, a large proportion of OPC

is used in stabilisation of granular materials such as road bases and mine backfills (Porter et al., 2016b). Eliminate the usage of industrial cement is one of the main focused technology areas to improve sustainable construction. Beach rocks, stromatolites and sandstones are some examples of sustainable bio cementation process in nature. In last decades researchers have been successful in emulating the bacterial cementation in the laboratory (DeJong et al., 2010a; Montoya et al., 2013). Pieces of literature show the bio-cementation process increases strength and stiffness of granular materials (Chou, 2011; DeJong et al., 2006; Montoya et al., 2013; Mortensen & DeJong, 2011; Van Paassen et al., 2010; Whiffin, 2004). Scientists show, MICP process increases the relative density and water resistance of granular samples (DeJong et al., 2006; DeJong et al., 2010a; Van Paassen et al., 2010); and prevents soil liquefaction (Montoya et al., 2012; Mortensen & DeJong, 2011; O'Donnell et al., 2017). The probability of cost efficiency and sustainability of the process has been examined (Achal & Mukherjee, 2015; Cheng et al., 2014). The technology has been developed as stand-alone as well as in conjunction with industrial binders (Porter et al., 2017b). Series of applications of the bio-cementation process have been designed such as road bases (Porter et al., 2016b); rammed earth (Porter et al., 2018a) and self-healing systems (Kaur et al., 2018).

It is essential to determine the mechanical properties of the stabilised granular system in realistic conditions, including confinement and partial cementation. Experimental investigations on traditional cemented granular media to assess its static such as (Schnaid et al., 2001) and dynamic such as (Díaz-Rodríguez & López-Molina, 2008); (Saxena et al., 1988) properties have been reported. It has been understood that the inter-particle interaction has a vital role in the macro mechanical behaviour of the material (Oda et al., 1982). Also, the effect of types of cement (Ismail et al., 2002) and injection methods (Karol, 2003) in cemented systems, has been investigated. There are too many parameters that affect the mechanical behaviour of confined and cemented granular media which can be mapped through experiments alone. Thus, numerical models have been developed. It is imperative to capture inter-grain interaction at the microscopic level (at submillimeter scale) to realistically predict the behaviour at macroscopic level (at 10 cm scale). Thus, the size of the numerical model can be intractably large to achieve realistic length scales. Moreover, the surface boundary conditions need a realistic representation. Around four decades ago, the initial models

were developed in 2D with simple inter-grain interaction and rigid surface boundary (Oda et al, 1982). Models became more advanced with the inclusion of particle rotation (Bardet, 1994) and later with rolling resistance and flexible surface boundary (Jiang et al., 2005). The initial models with identical spheres (Dvorkin et al., 1994) have been refined with the inclusion of grain size distribution (Estrada et al., 2010) and packing densities (Masson & Martinez, 2001). (Bardet & Proubet, 1991) reported the development of shear band due to the microstructural variation. The emergence of the discrete element method (DEM) helped to make a significant step-change towards realistic modelling of the granular media (Sitharam & Nimbkar, 1997). The development of public domain codes for DEM, such as YADE, has made the technique freely available to researchers (Kozicki & Donzé, 2008). By using the Discrete Element Method, a realistic representation of the confinement condition has been possible through the introduction of flexible boundary conditions (Belheine et al., 2009); (Iwashita & Oda, 1998); (Wang & Li, 2014); (Zhao & Evans, 2009). All these models are for conventional cement.

There is a fundamental difference between stabilisation with biocement and conventional cement. Gradual aggregation happens due to biocementation process. Consequently, cementation density is varied in different degree of cementation (Huang & Airey, 1998). Thus, the numerical model becomes further complicated involving a coupled analysis of two phenomena: 1. a reactive transport process to determine the rate and distribution of cementation; 2. a load-resistance model to assess the mechanical properties of the cemented media. There are a few attempts to develop a coupled model. In reported finite element model by (Fauriel & Laloui, 2012) a homogenised property of the grains and the cement were studied, which ignores inter-grain interactions. A stand-alone reactive fluid transport model has been developed to determine the flow characteristics of the cementation process (Martinez et al., 2014); (Barkouki et al., 2011b). Several load-resistance models following the traditional DEM techniques;(Khoubani et al., 2016), (Jiang et al., 2015) have also been reported. The degree of cementation has been included as inter-grain cohesive strength (Yang et al., 2016). In general, an equivalent homogenised cohesive strength is assumed for the entire domain. In another variation, separate spheres as cement elements have been introduced (Khoubani et al., 2016). However, the increased computation does not improve the corresponding accuracy of the solution. In all these models, the stress-strain behaviour of columns as observed in experiments is matched in the

computational model by adjusting the homogenised cohesive strength by trial and error (Evans et al., 2015).

- **Gaps and opportunities**

The gradual growth with repeated cycles is an essential feature of bio-cementation (Huang & Airey, 1998). As a result, the Spatio-temporal variations of cementation throughout cementation action, need careful consideration. This microstructural parameter would have a significant effect in terms of damage initiation, its progression and failure modes. No attempt has been made hitherto to incorporate Spatio-temporal variations in case of bio-cementation. This thesis studies experimental and numerical approaches to investigate the biocemented sand columns over an extended range of degree of cementation. A controlled experiment for the degree of cementation from 0 to 88% has been conducted. To assess the degree of cementation Scanning Electron Microscopy (SEM) and Energy Dispersive X-ray Spectroscopy (EDS) have been performed. A unit cell analysis has been conducted to determine the inter-grain cohesion for varying degrees of cementation. These properties are used in the development of a macro model for different stages of cementation. Mechanical behaviour of the experimental and numerical samples is modelled through modelling the triaxial test condition. In DEM Triaxial test condition has been simulated through the imposition of pressure boundary conditions (Belheine, Plassiard, Donzé, Darve, & Seridi, 2009). The stress-strain relationship and damage progression process are studied with numerical and experimental models to evaluate the mechanical behaviour of MICP samples.

### **2.3.3. Stabilised granular system without confinement**

Highly aggregated sand grains can tolerate loads without any confining pressure. This level of aggregated sand grains is applicable for overground applications. Some of the MICP applications are used in structural engineering and Biogenic Mineral Plugging (Ferris et al., 1996) (Ramachandran et al., 2001a), as well as in Bio-Bricks, which is one of the products of the bioMASON company, where microorganisms are aroused to grow the cement (bioMASON.com).

Granular materials' cementation is a fundamental requirement in construction technologies. The industrial cementing process has been evolved by understanding the

natural process of cementitious binding in nature, e.g. in mud to lime. Due to understanding the bio-cementation, the strength of cemented materials has improved phenomenally. With the advent of cement, concrete has dominated as the preferred material for construction. More recently, the environmental penalty of industrial cement has been unravelled, and the need for a sustainable cementing material has been felt. Cement not only is used in concrete but also, in a large quantity in other applications such as soil stabilisation, mine backfills. Traditional soil improvement methods like cement or chemical treatment and soil replacement are costly, time-consuming and may present a severe threat to the environment (DeJong et al., 2010a; Karol & Berardinelli, 2003). In the last decade, researchers have focused on finding an alternative method for improving the soil properties in a cost-effective and environmentally sustainable manner (DeJong et al., 2006; Van Paassen et al., 2010; Whiffin et al., 2007). By learning from nature, Microbially Induced Calcium Carbonate Precipitation (MICP), can potentially be a method of sustainable cementation of granular media (Madigan et al., 1997; Tiano et al., 2006; Whiffin, 2004). Biocement has been used in the restoration of stone monuments (Castanier et al., 2000; Rodriguez-Navarro et al., 2003), rammed earth construction (Porter et al., 2018a), soil improvement (Whiffin et al., 2007) as well as in concrete (Ramachandran et al., 2001a). There are different use-cases for different stages of sand grains cementation under the effect of the MICP process. By clumping the sand grains due to lightly cementation, the shape of soil's heap can be controlled (Kashizadeh et al., 2020). An intermediate stage of cementation is required for underground applications such as soil stabilisation, where the sand grains are subjected to confining stress ((Kashizadeh et al., 2019), (Harkes., 2010)).

MICP samples with a high level of aggregation can bear load without confinement. There are numbers of overground applications for highly aggregated MICP samples. They improve engineering properties such as durability and strength (Achal et al., 2013a; Achal et al., 2013b; Qian et al., 2010; Reddy, 2013; Yang et al., 2011; Zhao et al., 2014). The unconfined compression strength of biocemented granular sand columns have been observed to have increased in some recorded experiments (Jiang et al., 2011; Oda et al., 1982; Porter et al., 2018b; Zhao et al., 2014).

- **Gaps and opportunities**

As discussed earlier, understanding the mechanical behaviour of cemented sand requires insight into its inter-granular interactions. This thesis proposes the novel experimental and numerical models to study the mechanical properties of biocemented sand columns for a wide range of cementation. The models simulate the unconfined compressive strength tests. The numerical model studied the inter-grain mechanical properties for an extensive range of cementation, carefully. Trial and error approach is adopted to match inter-grain mechanical properties. A comprehensive experimental test matrix has been designed to validate the numerical results. Then, a comparison study on the damage mechanism is conducted between the experiments and predicted numerical results. Same as confined test samples, bio-cemented samples were prepared in various level of aggregation (0 to 88%). Also, Scanning Electron Microscopy (SEM) and Energy Dispersive X-ray Spectroscopy (EDS) were adopted to assess the level of cemented grains aggregation.

Finite Element and Discrete Element models are developed to study the intergranular behaviour of cemented grains at micro and macro levels via respectively. As a result, stress-strain behaviour and failure mechanisms of highly aggregated columns are simulated and compared with experimental test outcomes Digital Image Correlation (DIC) is adopted to study the failure paths of experimental samples. Results illustrated the capability of the model to predict both stress-strain and the failure paths of aggregated granular systems.

## Chapter 3: Loose and Semi-aggregated Sand Grains

### Experimental and Numerical Investigation on Heap Formation of Granular Soil Sparsely Cemented by Bacterial Calcification

Author 1

Elaheh Kashizadeh, Postgraduate Student

Department of Civil Engineering, Curtin University, Bentley, Perth, WA 6102 Australia

[Elaheh.kashizadeh1@postgrad.curtin.edu.au](mailto:Elaheh.kashizadeh1@postgrad.curtin.edu.au)

0000-0003-1529-2125

Author 2

Abhijit Mukherjee, Professor

Department of Civil Engineering, Curtin University, Bentley, Perth, WA 6102 Australia

[Abhijit.mukherjee@curtin.edu.au](mailto:Abhijit.mukherjee@curtin.edu.au)

0000-0002-3042-6454

Author 3

Antoinette Tordesillas, Professor

Department of Mathematics & Statistics, The University of Melbourne, Melbourne, Victoria 3010  
Australia

[Atordes@unimelb.edu.au](mailto:Atordes@unimelb.edu.au)

#### Abstract

Bacterial cementation can be a pathway to sustainable cementation in soil mounds. It consumes a minuscule amount of energy in comparison to engineered cement. Bacteria cement grains through progressive formation of inter-granular bridges of precipitated minerals. This study presents a numerical framework to model the sparsely cemented granular heaps. A rigorous experimental program has been given to observe the relationship between different stages of cementation and shapes of the heap. A discrete element model (DEM) for sparsely cemented grains has been developed. The extent of cementation is modelled through random clumping of



grains. It is observed that DEM is capable of capturing the effect of cementation through grain clumping. A parametric study of the grain size distribution, internal friction angle, shape of clumps and the extent of cementation has been performed. The results show that friction angle, grain size distribution and grain clumping have a considerable effect on the shape of heap. A cubic polynomial is able to capture the shape of heap reasonably well. The results will be useful for predicting the profile of sparsely cemented granular heaps.

### **Keywords**

Granular materials; bicementation; Mechanical properties; Discrete Element method; shape of heap

### **List of notations**

$f^n$	is the normal force component
$f$	is the tangential force component
$k^n$ & $k^s$	are the normal and shear spring stiffness coefficients
$b^n$ & $b^s$	are the normal and shear viscous damping coefficients
$\mu$	is the coulomb friction coefficient
$\Delta u^n$ & $\Delta u^t$	are the relative normal and tangential displacements
$\Delta \dot{u}^n$ & $\Delta \dot{u}^t$	are the relative normal and tangential translational velocities
$R_1, R_2$	are the radii of the two interacting particles
$R_{min}$	is the minimum radii of the two interacting particles
$k^r$	is the rolling stiffness coefficients
$k^s$	is the shear stiffness coefficients
$\mu^r$	is the friction coefficient
$\Delta \alpha$	is the relative rotation
$\Delta \alpha^\circ$	is the relative rotational velocities
$E_c$	is the young modulus

$v_c$	is the Poisson ratio,
$\beta$	is the rolling stiffness coefficient
$I^c$	is the rolling resistance
$h$	is the height of the heap
$l$	is the base of the heap
$\xi$	is the normalised x coordinate
$\zeta$	is the normalised y coordinate
$ \mu_h$	is the base angle of heap
$\eta_h$	is the height-to-base ratio of heap
$\theta$	is the maximum angle of heap

### 3.1. Introduction

With climate change, the frequency of extreme weather events such as storms and floods is on the rise (Steffen et al., 2014). It poses new engineering challenges to the countries like Australia, where 80% of the population lives within 50 km from the coastline (2006). Study of heaps of natural granular materials such as sand, silt and clay is essential for the solution of problems such as protection coasts against waves, river banks against currents, embankments against soil liquefaction pressure (Eric & Nick 2015; Mujah et al., 2017). These mounds need to be designed for optimal performance against destabilising forces such as waves, currents and hydrostatic pressures. The loose grains form a heap characterized by their grain size distribution and internal angles of friction (Herrmann, 1998).

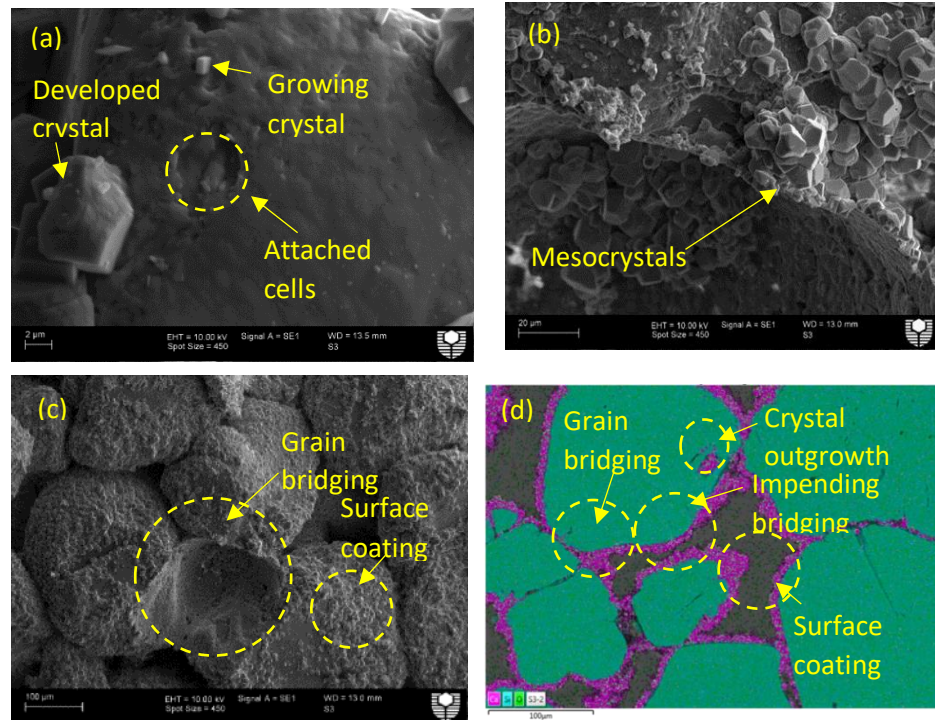


**Figure 3.1:** Heaps of sand dumped on the beach at Half Moon Bay, Melbourne, Australia [3]

Granular heaps comprising loosely packed grains have long been studied through experimental and theoretical approaches (Train, 1958). It is observed that grain properties such as inter-granular friction (Carstensen & Chan, 1976), (Zhou & Ooi, 2009; Zhou et al., 2001) grain shape (Friedman & Robinson, 2002; Kozicki & Tejchman, 2011; Wensrich & Katterfeld, 2012), and grain size distribution (Derakhshani et al., 2015; Matuttis, 1998; Miller & Byrne, 1966; Robinson & Friedman, 2002) influence the shape of the heap. When the frictional resistance is not sufficient to resist the destabilising forces, additional resistance against motion must be created. Often, a small dose of cement is added to the granular media resulting in some grains clumping together. The clumping increases resistance to motion by 1) grain interlocking and 2) inter-grain cohesion. However, the addition of cement can be toxic to the native flora and fauna. Moreover, engineered cement consumes vast

amounts of energy and emits large quantities of CO<sub>2</sub> (Gielen et al., 2008). Annual production of Portland Cement makes up around 6% of all anthropogenic greenhouse gas emissions (Imbabi et al., 2012). In nature, on the other hand, clumping of grains is observed due to bio-geo-chemical processes in sand heaps, especially when it is moist for a substantial period (Polat Pelin et al., 2018). In contrast to the engineered clumping, natural clumping is non-toxic and devoid of environmental hazards. Nature might therefore offer clues towards sustainable stabilisation of sand heaps.

Recently, Microbially Induced Calcium Carbonate Precipitation (MICP) process has been introduced as an alternative to other industrial cementation approaches (Achal & Mukherjee, 2015; Achal et al., 2015). In this process, bacterial enzymes are utilised to nucleate calcium carbonate as the cementing material (Achal & Mukherjee, 2015). The technology has been applied in several engineering problems such as stabilisation of road bases (Porter et al., 2016a), fortification of rammed earth (Porter et al., 2018a) and sustainable bricks (Dhami et al., 2013). Significant advancement in the process has been made, which has been discussed elsewhere (Dhami et al., 2016a). However, the process of biostabilisation of soil is fundamentally different from that of the engineered cement binders. Our research proved that biocementation is initiated when bacterial cells secure themselves in the grooves of the substrate, such as sand (Porter et al., 2017b). They act as nucleation sites for the growth of calcium carbonate crystals (Fig. 3.2a). The crystals grow to form mesocrystals (Fig. 3.2b), and then the mesocrystals grow to bridge neighbouring particles, thus achieving cementation (Fig. 3.2c). Quantitative energy dispersive X-ray scanning method (Fig. 3.2d) is used to estimate the degree of sands' aggregation. Thus, biocementation grows in layers with initiating from a plethora of nucleation sites dictated by the concentration of microbial cells.



**Figure 3.2:** Our observation on the stages of biocementation: (a) Bacterial cells secure themselves within the grooves of sand grains; (b) The crystals grow to form mesocrystals; (c) The crystals bridge the neighbouring sand grains to cement them together; and (d) Quantitative EDS can scan the various stages of biocementation.[25]

Pressing research need in the advancement of biocementation is detailed knowledge of granular media behaviour under varying degrees of partial cementation. In particular, a model is needed to predict: (i) the location and degree of cementation; also, (ii) the consequent influence of varying partial degrees of cementation on the mechanical behaviour of the granular materials. The emergence of the discrete element method (DEM) has facilitated the numerical modelling of inter-granular interactions. It is noted that a minimum number of grains must be used for the DEM to capture the desired phenomenon (Cundall & Strack, 1979). The limitation of DEM in modelling non-spherical grains is overcome through the imposition of rigidity condition among a group of spheres arranged in the desired shape (Thomas & Bray, 1999). Using DEM, particle shape (Ting et al., 1995), size (Jacobson et al., 2007) and frictional behaviour (Suiker & Fleck, 2004) of granular assemblages have been investigated. Development of public domain codes for DEM, such as YADE, has made the technique freely available to researchers (Kozicki & Donzé, 2008). Triaxial test condition has been

simulated through the imposition of pressure boundary conditions (Belheine et al., 2009). The bonded granular systems have been modelled by introducing a cohesive bond between the grains.(Estrada et al, 2010; Utili & Nova, 2008) Some reports on using DEM for modelling bio-cemented samples are available.(Khoubani & Evans, 2018; Yang et al, 2019) In all these investigations, an average homogenous inter-grain cohesive strength has been assumed to represent the degree of cementation. The averaged cohesive strength is adjusted through trial and error to achieve results close to that obtained from experiments. In these cases, the stress-strain behaviour of sand columns is predicted through DEM. Use of DEM for prediction of the shape of the heap for sparsely cemented material is not reported hitherto. DEM is specially equipped to model the formation of a heap as it is able to incorporate inter-granular friction, sliding, rolling and movements of grains that are several orders of magnitude higher than the grain sizes. Moreover, cementation can be introduced through clumping of grains.

In this paper, we report an experimental and numerical investigation on sand that is sparsely cemented. MICP has been performed on loose sand to bind the grains partially; only a small fraction grain is bonded forming clumps. Consequently, the grains can still move freely to create a heap. The process of formation of the heap, especially with partial grain bonding, has been numerically modelled for the first time. The experimental and numerical results have been compared. Both the experimental and numerical results have been utilised in developing a polynomial fit for the shapes of the heaps based on the basic geometric parameters. The expression is useful to determine the degree of cementation required to obtain the target shape of the heap.

## **3.2. Experimental Methodology**

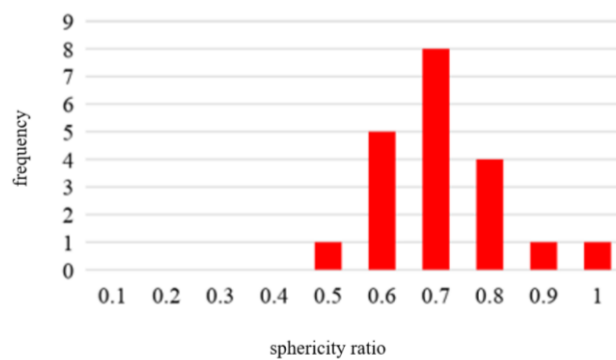
A series of experimental studies were conducted to understand how the MICP process affects the aggregation of the sand grains and causes changes in the shape of a sand heap. The experimental results have been used for validation of the numerical model.

### **3.2.1 Materials**

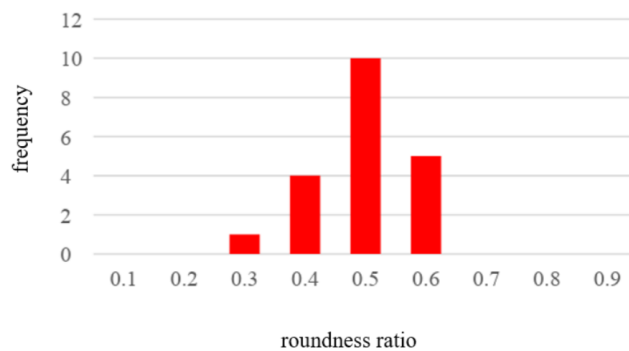
- **Sand**

Manufactured silica sand was sourced from Cook Industrial Minerals. The sphericity

and roundness of the sand mix were determined in accordance with the methodology presented by Cho et al. (Cho et al., 2006). The sphericity was defined as the overall equality between the length, width and height of the particle. In contrast, the roundness was defined as the radius of surface curvature; which demonstrates the size ratio of the particle. For this purpose, images of sample sand grains have been recorded and analysed. The process has been repeated, and the average standard deviation has been determined. The frequency histograms of the sphericity and roundness are shown in Figures 3.3. The average particle shape, according to the categories developed by (Cho et al., 2006), is shown in Figure 3.4.

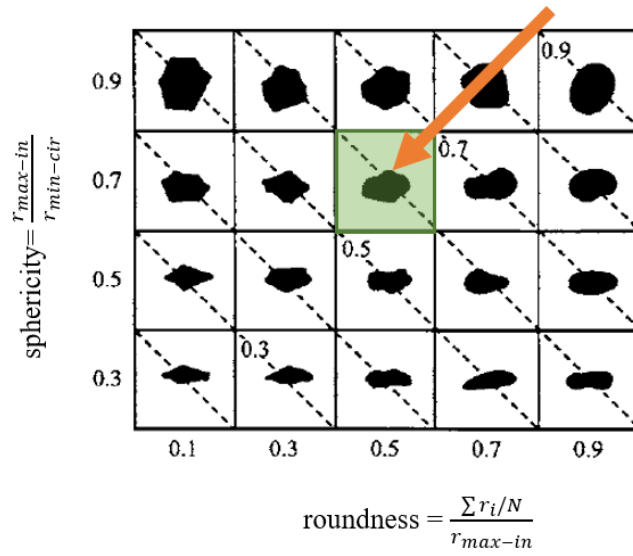


(a)



(b)

**Figure 3.3:** Grain Frequency Histogram: (a) Sphericity; (b) Roundness



**Figure 3.4:** Definition of particle shape according to (Cho et al., 2006)

The particle size distribution for the chosen sand in this research was  $D_{50}:0.425\text{mm}$  (shown in Table 3.1). This grain size distribution is used in the numerical model.

**Table 3.1:** Particle Size Distributions for Sand Mix

Sieve Size (mm)	Cumulative % Passing	Cumulative % Retained on Sieve
1	1	100
0.85	0.85	100
0.71	0.71	100
0.6	0.6	100
0.5	0.5	99.93
<b>0.425</b>	<b>0.425</b>	<b>99.71</b>
0.3	0.425	99.71
0.212	0.3	52.14
0.15	0.212	14.36
0.106	0.2	1.79
0.075	0.106	0
0.053	0.075	0
PAN	0.053	0

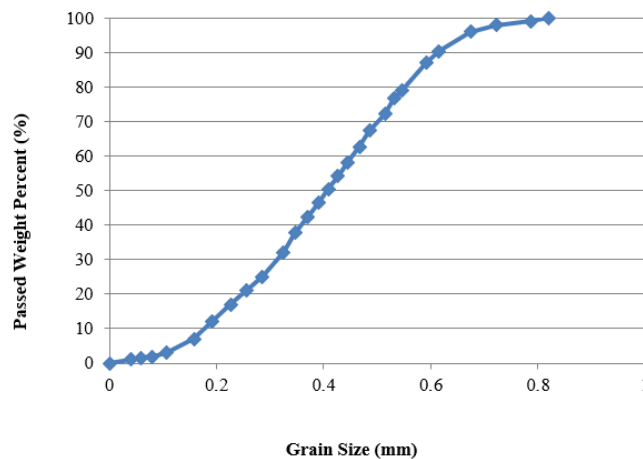


- **Cementation System**

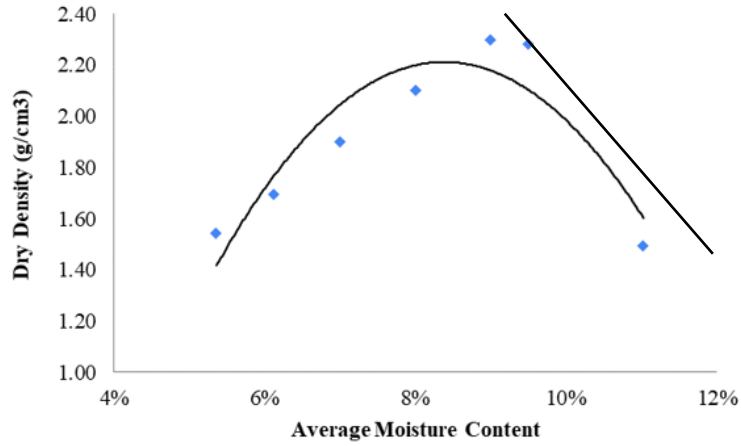
The cementation system consists of bacterial and cementation fluids. As described in earlier studies (DeJong et al., 2010b) the ureolytic bacterial isolate *Sporosarcina pasteurii* (ATCC 11859) was used in the cementation system. The culture was grown in an Ammonium Yeast extract media. It was cultivated under aerobics condition by incubating at 37°C at 200 rpm for 24-36 hours until the optical density (OD) at 600nm, measured using a spectrophotometer, reached 2. The cementation fluid consisted of 0.5M urea, 0.5M calcium chloride and 1g/L of nutrient broth powder.

### 3.2.2. Methods

The grain size distribution of the sand used is presented in Fig. 3.5. It had a D50 of 0.425mm. The Proctor density test results are shown in Fig. 3.6. The optimum moisture content of 9% by mass was observed. The sand was hand mixed and compacted into PVC moulds of 50 mm diameter by 100 mm height in three layers. Each layer was thoroughly compacted to ensure tight packing. All the samples were prepared in triplicates for cementation treatment. The top of the layer was scarified before placing the next layer.



**Figure 3.5.:** Sand grains gradation curve (D50 = 0.425)



**Figure 3.6:** Proctor compaction curve

three sets of samples with 0, 4 and 8 days of treatment were prepared. The treatment was started by rinsing the samples with 50mm calcium chloride solution in accordance with (Harkes et al., 2010). After one hour, one pore volume of the bacterial solution up flushed and retained for 24 hours as described in (Porter et al., 2017a). The process was followed by periodic pumping one pore volume of the cementation fluid (40ml) containing urea and calcium chloride at an interval of 12 hours. At the end of the treatment, all the samples were placed in a humidity-controlled chamber at 70°C over a period of 7 days to dry. The temperature and number of days have been based on previous experience.

### 3.2.3. Estimation of cementation

To estimate the amount of calcium chloride deposited in the column, we perform a chemical mass balance of the reactants. In each sample, 40 mL volume of the cementation fluid was injected two times a day; the amount of precipitated calcium carbonate in each time feeding the samples is calculated as per Table 3.2.

**Table 3.2:** Weight of precipitated calcium carbonate in one cycle of feeding

Volume of Solution (mL)	Molecular Weight of CaCl <sub>2</sub> (gr/mol)	Molecular Weight of CaCO <sub>3</sub> (gr/mol)	Concentration of CaCl <sub>2</sub> (mol)	Mass of CaCO <sub>3</sub> (gr)
40	110.98	100.086	0.5	2.53

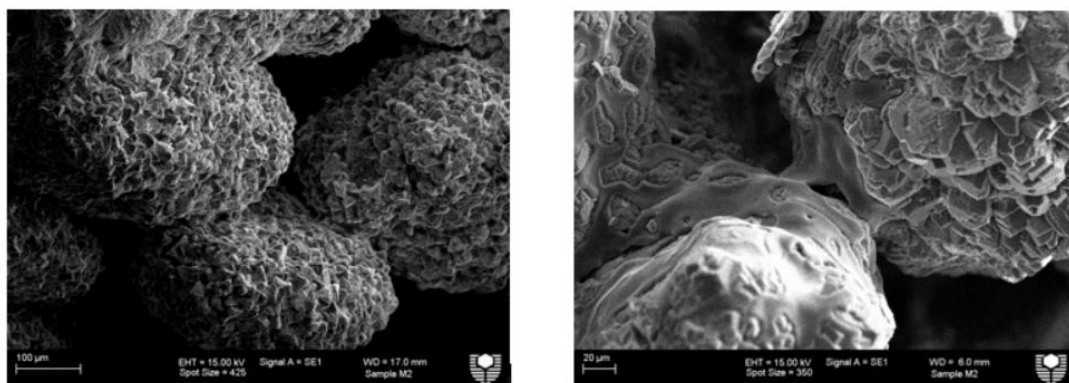
The prior research that claims 95% conversion to calcite is expected under the present conditions (Hannah Porter, 2016). The total mass of precipitated calcium carbonate in each cycle of feeding is 2.53 gram. The size of the samples is  $\varnothing 50*100\text{mm}$ . Sixty days of feeding are required to achieve the full aggregation of samples where the initial dry density of the sample ( $\rho$ ) is  $1.9 \text{ g/cm}^3$ , and the pore volume is 40% the samples were fed, at the rate described above.

### 3.2.4. Heap formation

After the samples were treated and dried, they were carefully placed at the centre of a flat surface with concentric rings drawn on it, with the open face of the samples facing down. The cylinder mould was carefully removed. The sand formed heap was photographed from the side. The base diameter, the height and the heap angle were measured.

#### Microscopic Investigation

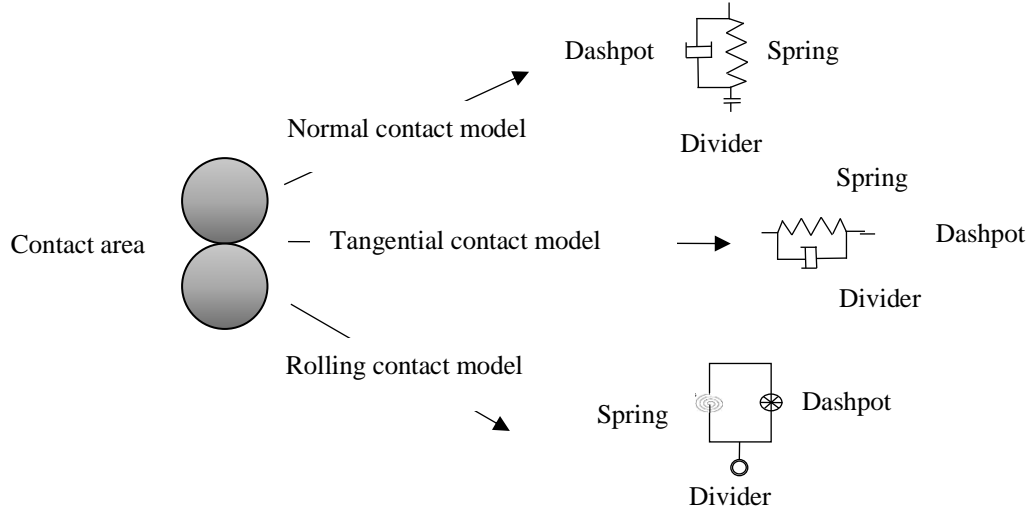
Microscopic analysis was performed on the cemented samples to record inter-granular cementation. For this purpose, a scoop of about one cubic centimetre was collected from the central region of the heap. All of the samples were flushed with tap water and dried at  $60^\circ\text{C}$  temperature for 24 hours before microscopic investigation. Scanning electron microscopy (SEM) was performed according to DeJong et al. 2010. Fig. 3.7 presents a few sample images of intergranular bonding. It can be seen that calcium carbonate has coated some parts or the whole surface of the grains before bridging to the neighbouring grains. Thus, only a fraction of the calcium carbonate is deposited at the inter-grain boundary. Our previous research shows that about 30% of the calcium carbonate deposit would participate in grain bridging (Hannah Porter, 2016).



**Figure 3.7:** Microscopic pictures of cemented sand under the effects of the MICP process

### 3.3. Numerical Model

A DEM model of the granular heap is developed using the open-source software YADE (Kozicki & Donze, 2008). A spring–dashpot system is used to model the contact interaction between the particles, as summarised in Figure 3.8.



**Figure 3.8:** The contact models for grains with rolling resistance by Cundall (Cundall, 1971)

The contact forces are given by a combination of Hooke's and Coulomb's laws:

$$f^n = k^n \Delta u^n + b^n \dot{\Delta u}^n \quad (3.1)$$

$$f^s = k^s \Delta u^s + b^s \dot{\Delta u}^s, \text{ for } |\Delta u^s| < \mu |f^n| / k^s \quad (3.2)$$

The normal stiffness,  $k_n$  shear stiffness,  $k_s$  and rolling stiffness,  $k_r$  parameters were calculated, as follows. (Figure 3.9)

$$k^n = E_c \frac{2R_1 R_2}{R_1 + R_2} \quad (3.3)$$

$$k^s = E_c \nu_c \frac{2R_1 R_2}{R_1 + R_2} \quad (3.4)$$

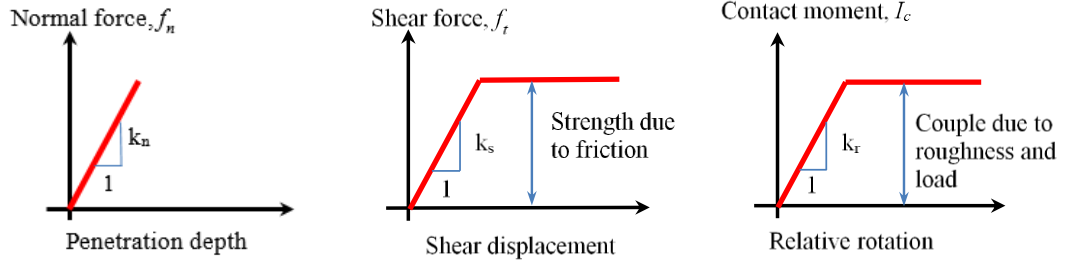
$$k^r = \beta k^s R_1 R_2 \quad (3.5)$$

The rolling resistance or contact moment, defined in an analogous fashion to

Coulomb's law, is expressed as:

$$I^c = k^r \Delta\alpha + b^r \dot{\Delta\alpha}, \text{ for } |\Delta\alpha| < \mu^r R_{\min} |f^n| / k^r \quad (3.6)$$

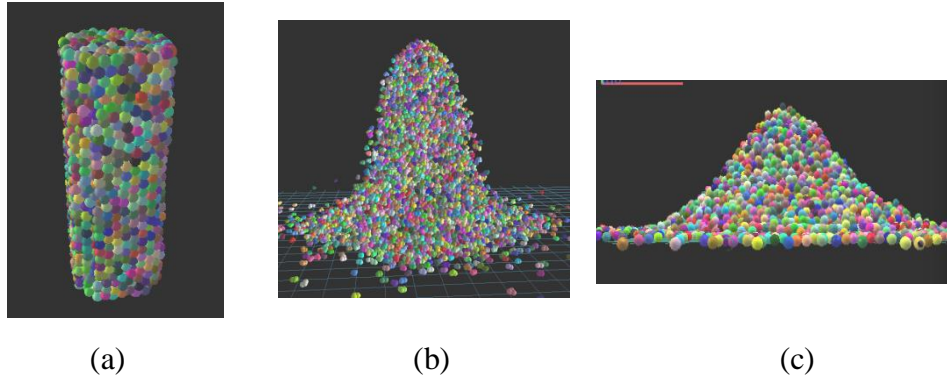
$$I^c = \mu^r R_{\min} |f^n|, \text{ for } |\Delta\alpha| \geq \mu^r R_{\min} |f^n| / k^r \quad (3.7)$$



**Figure 3.9:** Mechanical stiffness of normal, tangential and rolling contact models (Kozicki & Teichman, 2011)

The material parameters such as friction, elastic modulus and Poisson's ratio are initially selected based on the previous investigations. The cementation is introduced through clumping of grains as described in the next section. At first, the experimental results have been used to fine-tune the parameters. The shapes of the heaps have been determined based on the initial parameter settings. They are compared with the experimentally obtained shapes. The parameters are adjusted to minimise the errors between the experimental shape and numerical prediction. Based on these parameters, new numerical predictions have been made for cases where experimental results were not available.

We form various granular heaps by first filling a cylindrical domain with spheres of a specified number and grain size distribution (Fig. 3.10a). The boundary constraints of the cylinder are removed to simulate the heap formation, thereby allowing the grains to move freely under gravity and the resistance to motion due to inter-granular sliding and rolling friction. The movement of each sphere is tracked at fixed time intervals. The process is terminated when the shape of the heap no longer changes in time. Fig. 3.10b shows the intermediate stage, and Fig. 3.10c shows the final heap obtained.



**Figure 3.10:** Numerical models for shape of heap study, (a), (b) and (c) represent different stage

### 3.3.1. Sparsely Aggregated Grains

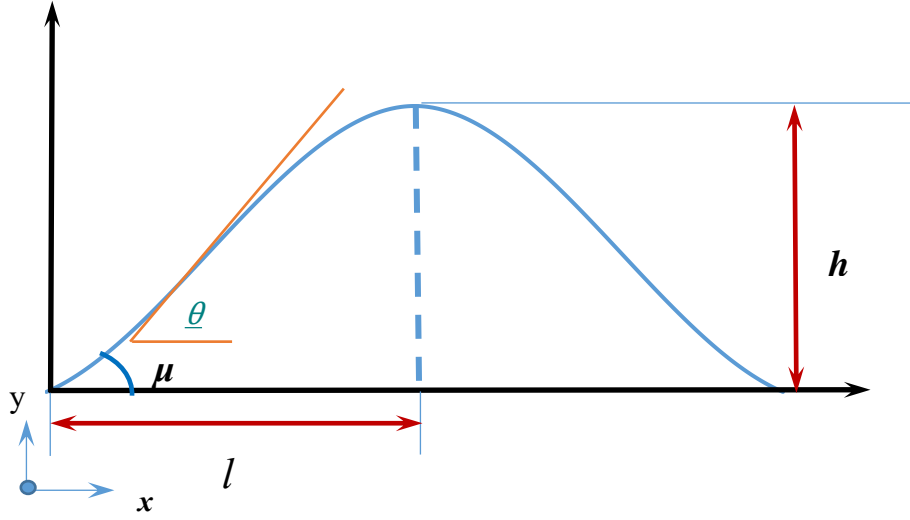
Similar to the loose grains, for the sparsely aggregated sand, the grains do not form a solid mass. They form a heap under the action of gravity. Cementing grains together to form a clump is called Sparse aggregation. Thus, in addition to the frictional resistance, additional resistance is generated due to the interlocking of the particles. Although the movement of the grains is prevented somewhat due to the formation of particle clumps, bonding is not widespread to avoid the failure of the form in the unconfined state. Therefore, the shape of the heap changes depending on the degree of cementation or aggregation. In this investigation, the sparsely aggregated state is modelled by rigidly connecting three grains to form mutually connected triads. Designed algorithms randomly bonded the grains. The fraction of the triads is proportional to the degree of the aggregation. A cylindrical assembly of grains, including clumped ones, is shown in Fig. 3a. The cylindrical confinement is removed instantaneously at the beginning of the simulation. The movement of the grains is calculated at a defined time step. The process is finished when the movement of the grains were smaller than a specified limit. The limit was lowered consecutively to make sure convergence of the shape and height of the heap.

### 3.3.2. Shape of the heap

A cubic polynomial is developed to define the shape of the heap. The expression is arrived at by choosing an algebraic name that closely follows the shapes obtained through the experiments and simulations (see Fig. 3.11). The shape is defined by two

parameters; the base angle ( $\mu$ ) and the height-to-base ratio ( $\eta$ ).

$$\xi = \frac{x}{l}; \zeta = \frac{y}{l}; \eta = \frac{h}{l} \quad (3.8)$$



**Figure 3.11:** The proposed model for the analytical model

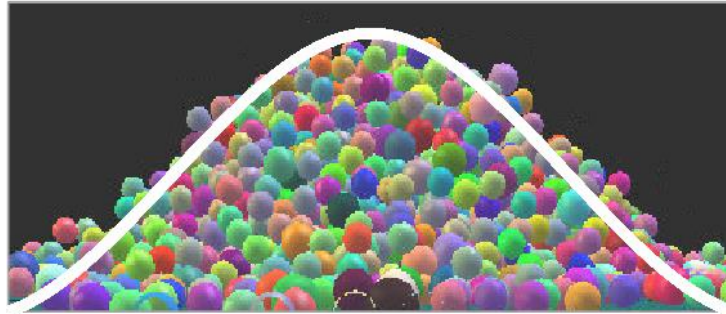
The shape is defined as:

$$\zeta = \mu\xi + (3\eta - 2\mu)\xi^2 + (\mu - 2\eta)\xi^3 \quad (3.9)$$

The maximum angle  $\theta$  is calculated at:

$$\theta = \frac{3\eta - 2\mu}{6(2\eta - \mu)} \quad (3.10)$$

It may be noted that the internal friction of the spheres governs the base angle. In the case of loose sand, a near conical shape is expected; thus, the lower bound of  $\eta$  is  $\tan^{-1}(\mu)$ . With increasing degree of cementation,  $\eta$  is likely to increase monotonically. Therefore,  $\eta$  can be calibrated with the degree of cementation. As shown in Fig. 3.12, there is good agreement between the analytical model and the DEM heap model.



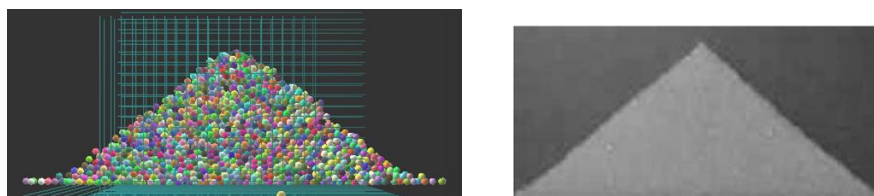
**Figure 3.12:** Comparison of the analytical (white curve) and the DEM heap model.

### 3.3.3. Numerical results

The numerical model is validated with available experimental and numerical results.

#### i. Loose Spherical Glass Beads

Zhou et al. (Zhou et al., 2002) studied the angle of the heap for mono-sized spheres with 2mm diameter glass beads constrained by two glass walls separated by 40mm. The numerical model was developed by developing a container consisting of four glass walls with 80×8mm in plan and 40mm in height. The box was filled with 2mm diameter glass beads. The two smaller walls were then removed to allow the flow of beads under the action of gravity. The parameters for the simulation are presented in Table 3.3. The shape converged at ten million-time steps, and the result is illustrated in Figure 3.13. The experimentally observed and numerically predicted shapes of the heaps agree well. As it is a heap of mono-sized spherical beads, it is expected to form a triangular heap of angle close of the internal friction. The base angle of heap reported by (Zhou et al., 2002) is  $37^\circ$ . The maximum inclination of the heap produced by the simulation is  $36.8^\circ$  in the simulation. However, in the simulation, the beads form a toe at the base. This local effect is not visible in the photograph obtained through the experiment.



**Figure 3.13:** Shape of the heap of mono-sized glass beads (a) present numerical model (b) experimental result (Zhou et al, 2002)



**Table 3.3:** Adopted numerical parameters to validate proposed model(Zhou et al, 2002)

Name of variable	Base value
Number of particles	2e3
Time step	5*10 <sup>-5</sup> s
Particle size	2 mm
Rolling friction coefficient	0.05
Sliding friction coefficient	0.4
Container thickness	40 mm
Density	2500 kNs <sup>2</sup> /m
Poisson ratio	0.3
Young's Modulus	2.16e6 Pa
Damping	0.4
Friction angle	22°

## ii. Validation

Fig. 3.14 presents the experimentally obtained heaps after different treatment durations. In the case of the untreated sample, the grains flowed freely, resulting in a heap close to the conical shape. For the treated samples, clumps of aggregated grains were visible. The clumps were a larger sample with a more extended treatment period. The clumps offered extra resistance in addition to the internal friction of the grains. As a result, the free flow of sand was restricted.



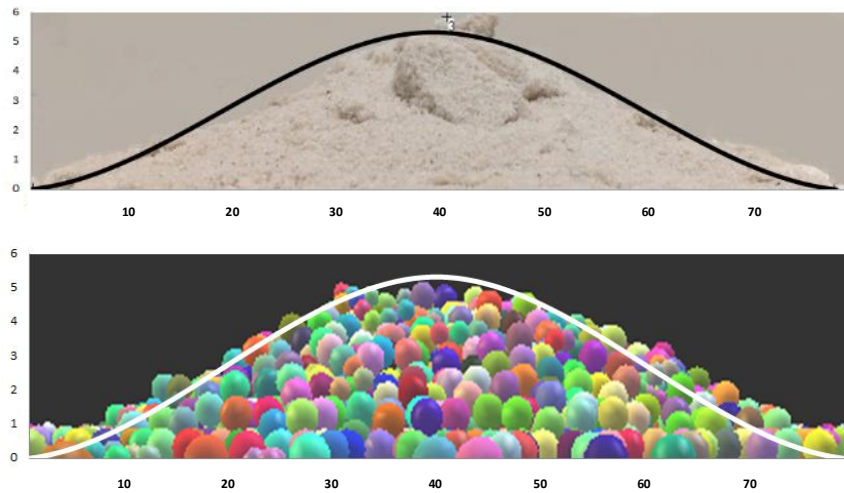
Figure 3.14: (a) Shape of the accumulated grains loose sand (a) Shape of the accumulated grains of the 4 days treated experimental sample (c) Shape of the accumulated grains of the eight days treated experimental sample

It was found that the heaps conform to the shape postulated in equation 9 (Fig. 3.15). The shape could be characterised by two parameters: the heap angle ( $\theta$ ) and the height-to-base ratio ( $\eta$ ). Both  $\theta$  and  $\eta$  increased with increasing time of treatment. The numerical model attempted to emulate the heap formation with treated samples. A fixed percentage of grains in a group of three were clumped at random locations to emulate aggregation. The rate of clumping would be in direct proportion with the

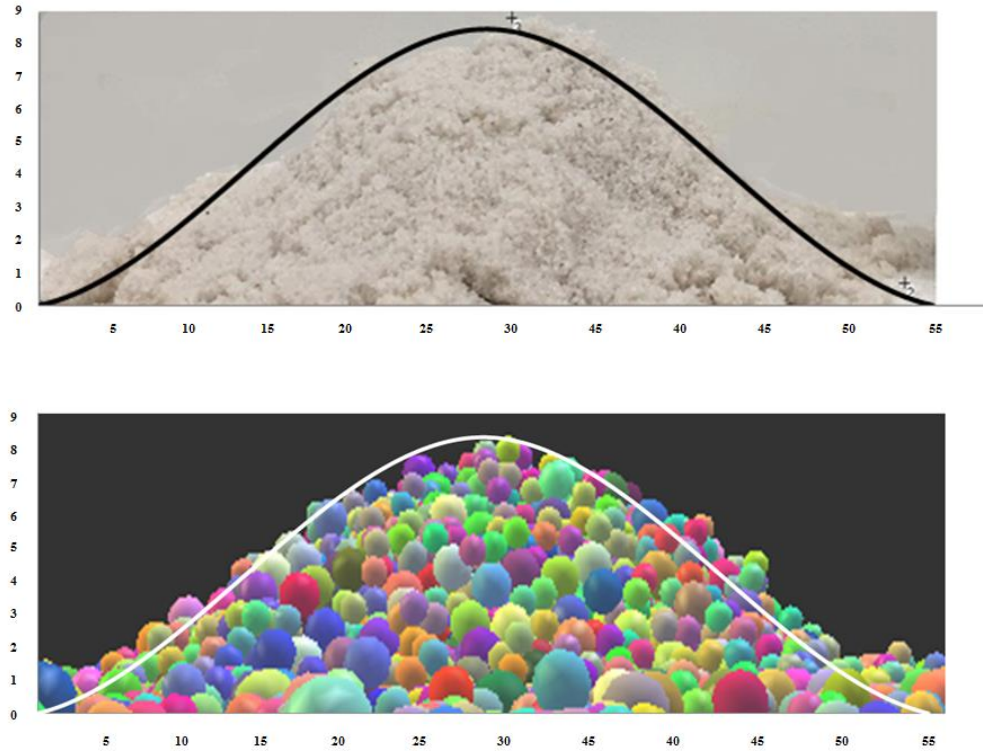
period of treatment. The best-fitting approach was used to compare the experimental and numerical results. A close match between the experimentally observed shape and the numerically obtained one could be achieved. Figures 3.15 and 3.16 show the shapes along with a fit with equation 3.9. Best fit for the 4day sample was obtained by clumping 13% of the grains; while the 17% clumped grains produced the best fit for the 8day. Table 3.4 summarises all the experimental and numerical results. The results show that the numerical model was able to match the experimental result closely.

**Table 3.4:** Relation between the percentage of clumping and weight of calcium carbonate precipitation

Treatment (days)	Numerical - Clumping (%)	Experimental - calcium carbonate precipitation (gr)	Experimental (3samples) - $\theta$ (°)	Experimental (3samples) - $\eta$	Numerical - $\theta$ (°)	Numerical - $\eta$
0	0	0	17±1	0.23±0.01	16	0.22
4	13	14.64	19.2±2	0.252±0.01	18	0.24
8	17	29.28	20.5±1	0.264±0.02	21	0.28



**Figure 3.15:** (a) Shape of the heap after four days treatment (b) Shape of the heap modelled by the DEM



**Figure 3.16:** (a) Shape of the heap after eight days of treatment, (b) Shape of the heap modelled by the DEM

### 3.4. Parametric Study

In the previous section, the present numerical model has been validated. In this section, the numerical model is used for an extensive parametric study. The base values of the variables are used in this study, listed in Table 3.5.

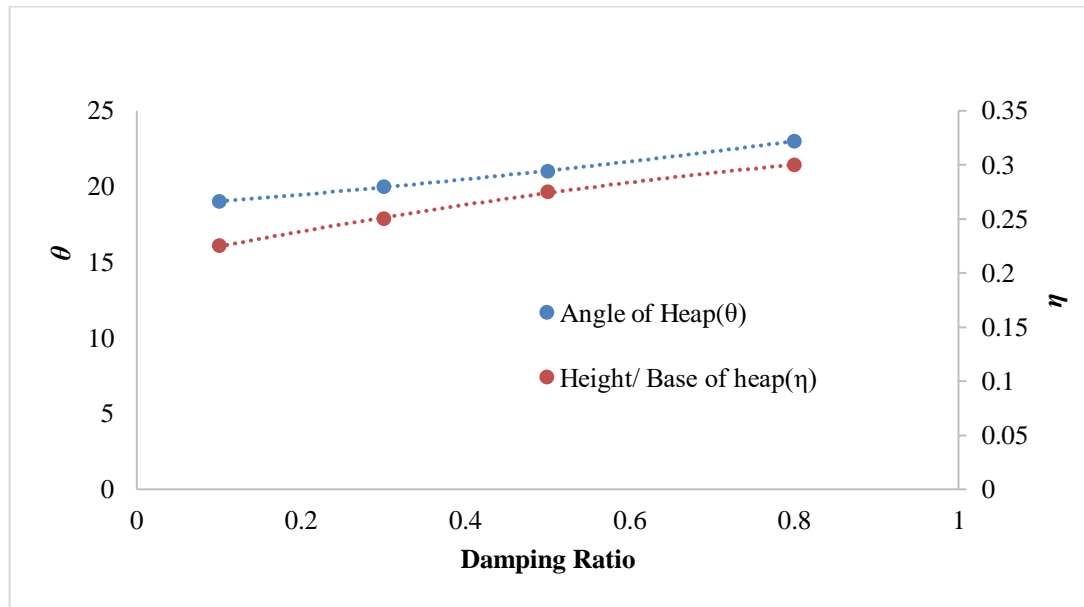
The numerical solution is also affected by the time step and the damping between the particles. A convergence study was conducted to obtain the optimal time step, and it was  $5 \times 10^{-5}$ s.

**Table 3.5:** The variables which have been considered for parametric study

Name of variable	Base value
Number of particles	2e4
Time step	5*10 <sup>-5</sup> s
Friction angle	30 degree
Particle size	0.2-0.8 mm (D <sub>50</sub> : 0.425mm)
Rolling friction coefficient	0.05 mm
Sliding friction coefficient	0.4
Density	2600 Kg/m <sup>3</sup>
Poisson ratio	0.3
Young's Modulus	2.16x10e6 Pa
Damping	0.3

### 3.4.1. Damping

The damping coefficient was varied in a range of 0.1 to 0.8 (Fig. 3.17). It is noticed that both  $\mu$  and  $\eta$  increase with increasing damping coefficient. Although by increasing the damping ratio, the angle of heap and height over the base of the heap ( $\eta$ ) increases slightly. This observation confirms the effect of this parameter is not significant in comparison to the effect of changing other parameters that have been studied in this paper.



**Figure 3.17:** Effect of damping ratio on  $\theta$  and  $\eta$

### 3.4.2. Internal Friction Angle

In this case, the unbonded grains with varying friction angle have been subjected to heap formation. The friction angle of the grains was varied from 15° to 40°. Both angles of the heap ( $\theta$ ) and height-to-base ratio ( $\eta$ ) went up with the increase in the angle of friction. At relatively low friction angles, the results showed that increasing the internal friction angle increased the  $\theta$  more rapidly than  $\eta$ . However, with the increase in the friction angle beyond 25°, even the rise in  $\eta$  was accelerated. The internal friction angle has a significant effect on the shape of the heap.

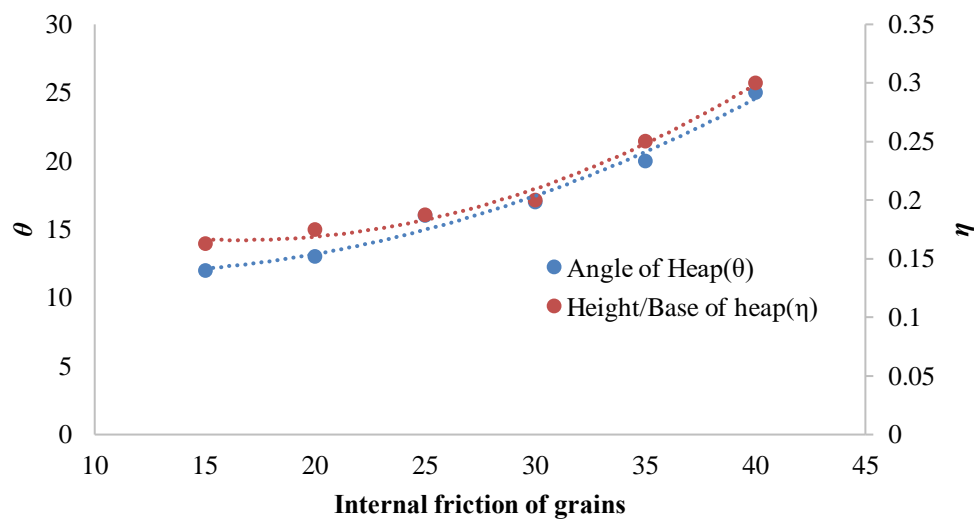


Figure 3.18: Effect of internal friction angle on  $\theta$  and  $\eta$

### 3.4.3. Grain Size

The size of the unbonded grains was varied in a range of 0.5 to 4 mm. The result showed the size of the grain affects the shape of the heap (Fig. 3.19). Both  $\theta$  and  $\eta$  reduce with the increase in the grain size. However, the rate of change is much less significant for the grain size than the friction angle. Similar observations have been reported by earlier researchers (Pilpel, 1970). It demonstrated that the rolling friction between the grains reduces by the grains size (Carstensen & Chan, 1976). Consequently, larger grains roll down the heap more efficiently, resulting in flatter heaps.

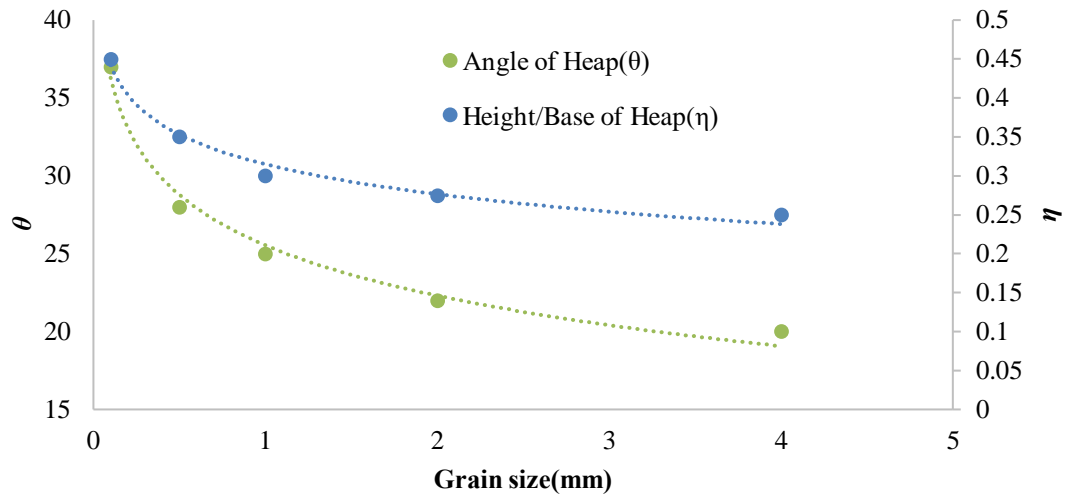


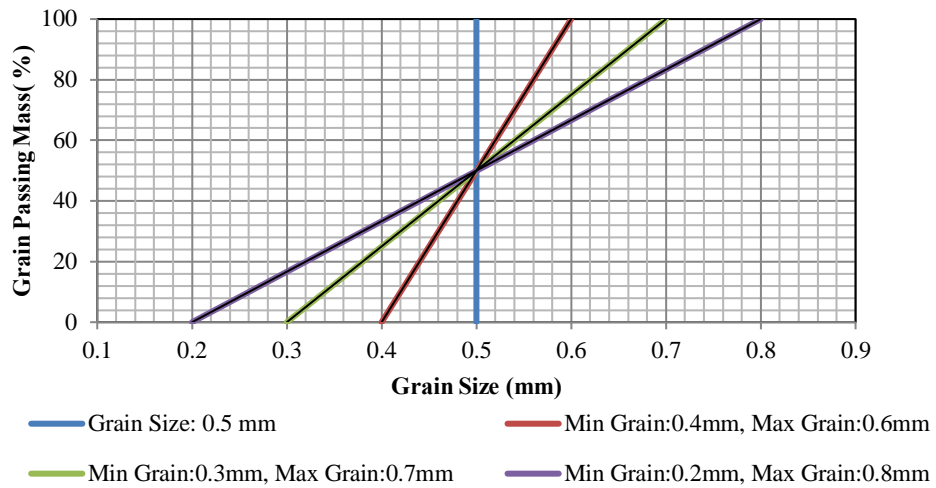
Figure 3.19: Effect of particle size on  $\theta$  and  $\eta$

### 3.4.4. Grain size distribution

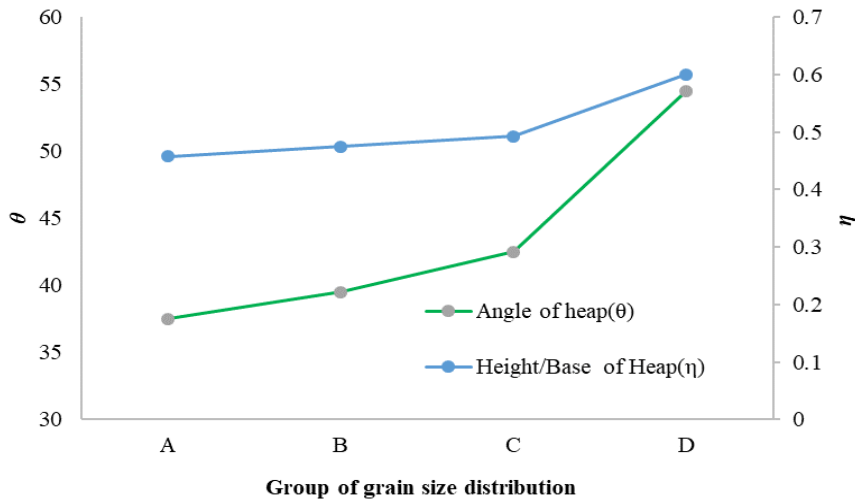
In reality, sand is composed of a range of grain sizes. The type of sand is characterised by its grain size distribution, as grains of different sizes are likely to interlock among one another developing resistance to sliding in addition to the internal friction. The uniform size distribution caused more interlocking among the grains. Increasing of interlocking phenomenon resulted in higher sliding resistance. In this study, four-grain size distribution curves have been adopted of the same average grain size (Table 3.6, Fig. 3.20). Group A has grains of one size only. The range of distribution gradually increases from Groups A to D. Figure 3.20 shows  $\theta$  and  $\eta$  for Groups A to D. As the grain size distribution gets wider, both  $\theta$  and  $\eta$  increase monotonically. A quantum jumps in  $\theta$  and  $\eta$  is noticed in the case of Group D. This result shows the utility of well-graded sand for making mounds. Prior research agrees with this observation (Derakhshani et al., 2015; Friedman & Robinson, 2002; Matuttis, 1998; Miller & Byrne, 1966).

Table 3.6: Grain size distribution groups

Group	Grain Size (mm)
A	0.5
B	0.4-0.6
C	0.3-0.7
D	0.2-0.8



**Figure 3.20:** Particle size distribution curves for four different sand particle size distributions

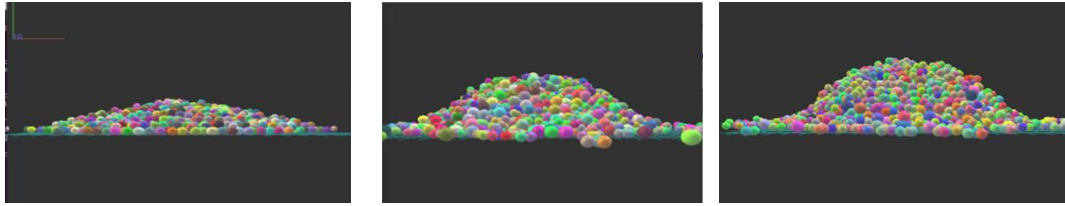


**Figure 3.21:** Effect of particle size distribution on  $\theta$  and  $\eta$

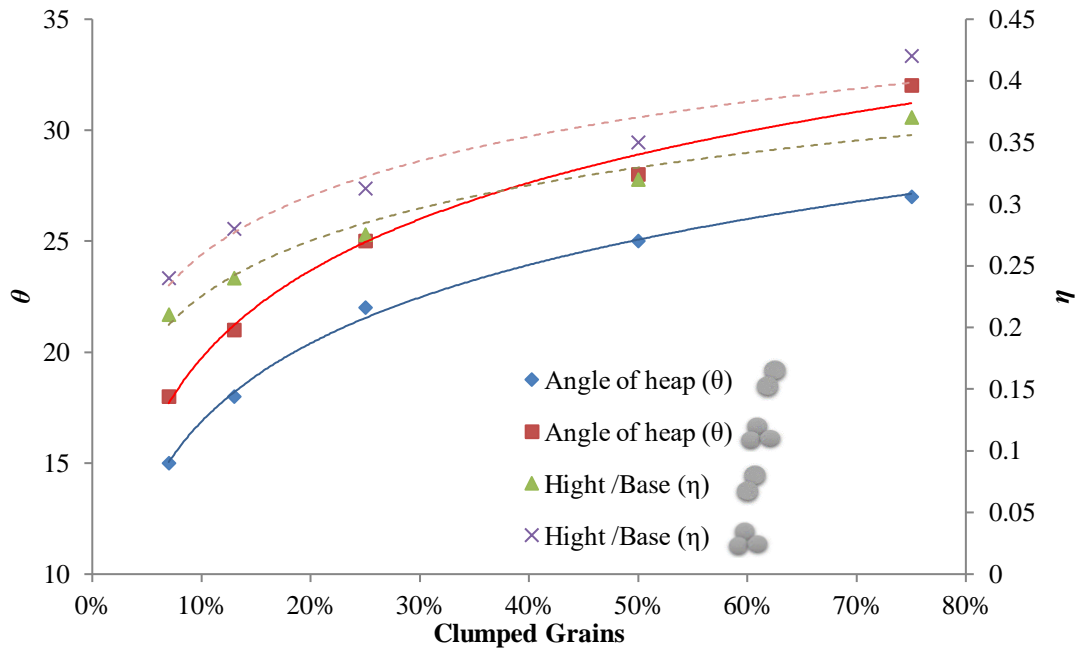
### 3.4.5. Cementation

Cementation is demonstrated in a column of sand of uniform grain diameter of 0.5mm. The cementation properties are presented in Table 3.5. Thus, it is modelled by clumping a fixed percentage of grains randomly. Figure 3.21 showed the shapes of heaps when the clumping was performed in the shape of triads. Clumping affects both  $\theta$  and  $\eta$  considerably. Due to clumping, the grains have a chance to interlock. Thus, there is a mechanical resistance to inter-granular sliding in addition to the friction. Thus, both  $\theta$  and  $\eta$  increase with the percentage of clumping. Figure 3.23 presents the

graphs for  $\theta$  and  $\eta$  for both diads and triads. Understandably, for the same portion of clumping, triads affect the shape of a heap more than the diads.



**Figure 3.22:** Modelling cemented grains by triads (a) No clumping, (b) Clumping 50%, (c) Clumping 75%



**Figure 3.23:** Effect of clumping ratio on  $\theta$  and  $\eta$

### 3.5. Conclusion

This paper demonstrates the shapes of heaps of grains that are sparsely cemented by MICP. A controlled experiment has been performed to record the shapes of heaps with sparse cementation. A polynomial expression for defining the shape of the heap has been developed. The shape of the heap is presented in two independent parameters: heap angle  $\theta$  and height-to-base ratio  $\eta$ . A discrete element model of the cemented system has been created. The DEM has been validated with present experimental results as well as the published ones. A parametric study for different material properties and level of cementation has been performed. Following conclusions can be made from the present study:

- The shape of a sand heap is altered significantly even at low levels of cementation.



- The shape of the heap can be defined by a 3rd degree polynomial. This expression has been validated through limited experimental studies conducted in this project. This expression may be refined when more results will be available in future.
- The polynomial has two independent parameters: heap angle  $\theta$  and height-to-base ratio  $\eta$ .
- Both  $\theta$  and  $\eta$  rise with the degree of cementation.
- A DEM model is capable of capturing the shapes of the heaps.
- Damping has a marginal effect on the shape of the heap, while friction angle and grain size distribution influence the shape considerably.
- Sparse cementation can be modelled in DEM using clumping.
- A convergence study was performed to determine the minimum number of grains to be representative of the experimental condition. It was noted that 10000 grains were sufficient in the present case.
- The degree of clumping can be calibrated with the amount of calcium carbonate deposited due to biocementation.

The present study is limited to the prediction of the shape of a sparsely cemented sand heap only. The effect of the destabilising forces will be reported in future. This work is part of a larger project of modelling bio-cemented granular materials at three stages of cementation: 1) sparsely cemented and unconfined, where the grains form a heap; 2) cemented and confined, where the columns retain their shape as long as confinement has been applied; and 3) heavily cemented and unconfined, where the columns are able to withstand external loading without and necessity of confinement. Stages 2 and 3 of the project are underway and will be reported shortly.

#### Acknowledgements

The first author would like to acknowledge fee scholarship and living stipend received from Curtin University for her doctoral work embodied in this project.

### 3.6. References

1. Steffen, W., J. Hunter, and I. Hughes, Counting the Costs: Climate Change and Coastal Flooding. 2014, Climate Council of Australia Limited.

2. Year Book Australia, 2004. 2006 07/02/2019]; Available from <http://www.abs.gov.au/ausstats/abs@.nsf/Previousproducts/1301.0Feature%20Article32004>.
3. Eric , B. and L. Nick Beach Renourishment. 2015.
4. Williams, A.T., et al., The management of coastal erosion. *Ocean & Coastal Management*, 2018. 156: p. 4-20.
5. Herrmann, H.J., On the Shape of a Sandpile, in *Physics of Dry Granular Media*, H. H.J., H. JP, and L. S., Editors. 1998, NATO ASI Series (Series E: Applied Sciences) . Springer, Dordrecht.
6. Train, D., Some aspects of the property of angle of repose of powders. *Journal of Pharmacy and Pharmacology*, 1958. 10(S1): p. 127T-135T.
7. Carstensen, J.T. and P.-C. Chan, Relation between particle size and repose angles of powders. *Powder Technology*, 1976. 15(1): p. 129-131.
8. Zhou, Y., et al., Numerical investigation of the angle of repose of monosized spheres. *Physical Review E*, 2001. 64(2): p. 021301.
9. Zhou, C. and J.Y. Ooi, Numerical investigation of progressive development of granular pile with spherical and non-spherical particles. *Mechanics of Materials*, 2009. 41(6): p. 707-714.
10. Friedman, S.P. and D.A. Robinson, Particle shape characterization using angle of repose measurements for predicting the effective permittivity and electrical conductivity of saturated granular media. *Water Resources Research*, 2002. 38(11).
11. Wensrich, C. and A. Katterfeld, Rolling friction as a technique for modelling particle shape in DEM. *Powder Technology*, 2012. 217: p. 409-417.
12. Kozicki, J. and J. Tejchman. Numerical simulations of sand behaviour using DEM with two different descriptions of grain roughness. in *II International Conference on Particle-based Methods–Fundamentals and Applications*. Particles. 2011.
13. Miller, R.L. and R.J. Byrne, The angle of repose for a single grain on a fixed rough bed. *Sedimentology*, 1966. 6(4): p. 303-314.
14. Matuttis, H.-G., Simulation of the pressure distribution under a two-dimensional heap of polygonal particles. *Granular Matter*, 1998. 1(2): p. 83-91.
15. Robinson, D. and S. Friedman, Observations of the effects of particle shape and particle size distribution on avalanching of granular media. *Physica A: Statistical Mechanics and its Applications*, 2002. 311(1): p. 97-110.

16. Derakhshani, S.M., D.L. Schott, and G. Lodewijks, Micro–macro properties of quartz sand: experimental investigation and DEM simulation. *Powder Technology*, 2015. 269: p. 127-138.
17. Gielen, D., J. Newman, and M.K. Patel, Reducing industrial energy use and CO 2 emissions: the role of materials science. *MRS bulletin*, 2008. 33(4): p. 471-477.
18. Imbabi, M.S., C. Carrigan, and S. McKenna, Trends and developments in green cement and concrete technology. *International Journal of Sustainable Built Environment*, 2012. 1(2): p. 194-216.
19. Polat Pelin , et al., Characterisation of beach rock biocementation in natural and in vitro conditions. *Frontiers of Microbiology*, 2018. Communicated.
20. Achal, V., et al., Biomineralization for sustainable construction - A review of processes and applications. *Earth-Science Reviews*, 2015. 148: p. 1-17.
21. Achal, V. and A. Mukherjee, A review of microbial precipitation for sustainable construction. *Construction and Building Materials*, 2015. 93: p. 1224-1235.
22. Porter, H., N. Dhami, and A. Mukherjee, Sustainable road bases with Microbial carbonate precipitation, in *Fourth International conference on Sustainable Construction Materials and Technologies*. 2016: Las Vegas, USA.
23. Porter, H., et al., Rammed earth blocks with improved multifunctional performance. *Cement & Concrete Composites*, 2018. 92: p. 36-46.
24. Dhami, N.K., A. Mukherjee, and M.S. Reddy, Viability of calcifying bacterial formulations in fly ash for applications in building materials. *Journal of Industrial Microbiology & Biotechnology*, 2013. 40(12): p. 1403-1413.
25. Dhami, N.K., A. Mukherjee, and M.S. Reddy, Micrographical, mineralogical and nano-mechanical characterisation of microbial carbonates from urease and carbonic anhydrase producing bacteria. *Ecological Engineering*, 2016. 94: p. 443-454.
26. Porter, H., N.K. Dhami, and A. Mukherjee, Synergistic chemical and microbial cementation for stabilization of aggregates. *Cement and Concrete Composites*, 2017.
27. Cho, G.-C., J. Dodds, and J.C. Santamarina, Particle Shape Effects on Packing Density, Stiffness, and Strength: Natural and Crushed Sands. *Journal of Geotechnical and Geoenvironmental Engineering*, 2006. 132(5): p. 591-602.
28. DeJong, J.T., et al., Soil engineering in vivo: harnessing natural biogeochemical systems for sustainable, multi-functional engineering solutions. *Journal of The Royal Society Interface*, 2010. 8(54): p. 1-15.

29. Harkes, M.P., et al., Fixation and distribution of bacterial activity in sand to induce carbonate precipitation for ground reinforcement. *Ecological Engineering*, 2010. 36(2): p. 112-117.
30. Porter, H., N.K. Dhimi, and A. Mukherjee, Sustainable road bases with microbial precipitation. *Proceedings of the Institution of Civil Engineers-Construction Materials*, 2017: p. 1-14.
31. Hannah Porter, N.K.D., Abhijit Mukherjee, Sustainable Road Bases with Microbial Carbonate Precipitation. SCMT4, Las Vegas, USA, August 7-11, 2016, 2016.
32. Kozicki, J. and F.V. Donze, A new open-source software developed for numerical simulations using discrete modeling methods. *Computer Methods in Applied Mechanics and Engineering*, 2008. 197(49-50): p. 4429-4443.
33. Cundall, P.A., The measurement and analysis of accelerations in rock slopes. 1971, University of London.
34. Zhou, Y., et al., An experimental and numerical study of the angle of repose of coarse spheres. *Powder Technology*, 2002. 125(1): p. 45-54.
35. Pilpel, N., Cohesive pharmaceutical powders. *Advances in pharmaceutical sciences*, 1970. 3: p. 173-219.

# Chapter 4: A MICP Stabilised Confined Granular System

## Experimental and Numerical Investigations on Confined Granular Systems Stabilised by Bacterial Cementation

Elaheh Kashizadeh<sup>1, a</sup>, Abhijit Mukherjee<sup>1, b</sup> and Antoinette Tordesillas<sup>2, c</sup>

<sup>1</sup> Department of Civil Engineering, Curtin University, Bentley WA 6102 Australia

<sup>2</sup> Department of Mathematics & Statistics, The University of Melbourne, Victoria 3010 Australia

<sup>a</sup>[Elaheh.kashizadeh1@postgrad.curtin.edu.au](mailto:Elaheh.kashizadeh1@postgrad.curtin.edu.au),

<sup>b</sup>[Abhijit.mukherjee@curtin.edu.au](mailto:Abhijit.mukherjee@curtin.edu.au),

<sup>c</sup>[Atordes@unimelb.edu.au](mailto:Atordes@unimelb.edu.au)

### Abstract

Bacterial cementation is a relatively new technology to stabilise granular systems. The cementation fluid causes gradual cementation in granular media. The mechanical performance of the bacterially cemented systems is critically dependent on the spatial and temporal variations of the precipitated cement. Numerical models proposed hitherto for mechanical behaviour of bacterial cementation have assumed simple homogenised cementation. This paper investigates the mechanical characteristics of bacterially cemented granular materials. The purpose is, developing reliable numerical models that incorporate the spatial and temporal variations in cementation. Controlled experiments validate the numerical models. Sand columns have been cemented to various degrees using a bacterial system. The degree of cementation was estimated by scanning electron microscopy. Triaxial compression tests have been conducted by varying the hydrostatic pressure. A multi-scale numerical model is developed to simulate the mechanical response of the cemented system. The numerical results show a good agreement with the experimental observations.

**Keywords:** bacterial cementation, granular materials, confinement, mechanical properties, finite element models, discrete element models, failure modes

#### **4.1. Introduction**

Worldwide, nearly 3.6 billion tonnes of Ordinary Portland Cement (OPC) is produced, which account for approximately 6% of anthropogenic greenhouse gas emission. In Australia, a large proportion of OPC is used in stabilisation of granular materials such as road bases and mine backfills (Porter, Dhami et al. 2016). Technologies to eliminate the usage of industrial cement for this purpose are paramount for sustainable construction. Nature has many examples of sustainable bacterial cementation such as beach rocks, stromatolites and sandstones. Recent research has been successful in emulating the bacterial cementation in the laboratory (DeJong, Mortensen et al. 2010, Montoya, DeJong et al. 2013). It has been demonstrated that bio-cementation improves stiffness and strength of granular materials (Whiffin 2004, DeJong, Fritzges et al. 2006, Van Paassen, Daza et al. 2010, Chou 2011, Mortensen and DeJong 2011, Montoya, DeJong et al. 2013). There are some researches that illustrate bio-cementation increases their relative density and water resistance (DeJong, Fritzges et al. 2006, DeJong, Mortensen et al. 2010, Van Paassen, Daza et al. 2010); and prevents soil liquefaction (Mortensen and DeJong 2011, Montoya, DeJong et al. 2012, O'Donnell, Kavazanjian Jr et al. 2017). The process has the potential of being cost-effective and sustainable (Cheng, Shahin et al. 2014, Achal and Mukherjee 2015). The technology has been developed as stand-alone as well as in conjunction with industrial binders (Porter, Dhami et al. 2017). Several applications have been developed such as road bases (Porter, Dhami et al. 2016); rammed earth (Porter, Blake et al. 2018) and self-healing systems (Kaur, Shah et al. 2018).

It is essential to determine the mechanical properties of the stabilised granular system in realistic conditions, including confinement and partial cementation. Experimental investigations on traditional cemented granular media to assess its static, e.g. (Schnaid, Prietto Pedro et al. 2001) and dynamic such as (Díaz-Rodríguez and López-Molina 2008); (Saxena, Avramidis et al. 1988) properties have been reported. It has been noted that the inter-particle interaction plays a vital role in the macro mechanical behaviour of the material (Oda, Konishi et al. 1982). In the case of cemented systems, the effect

of types of cement ((Ismail, Joer et al. 2002) and injection methods (Karol, 2003) has been investigated. Parameters that control the mechanical behaviour of confined and cemented granular media are too many to be mapped through experiments alone. It is imperative to capture inter-grain interaction at the microscopic level (at submillimeter scale) to realistically predict the behaviour at the macroscopic level (at 10 cm scale). Thus, the size of the numerical model can be intractably large to achieve realistic length scales.

Moreover, the surface boundary conditions need a realistic representation. The initial models were developed in 2D with simple inter-grain interaction and rigid surface boundary (Oda, Konishi et al. 1982). The 2D numerical model was advanced with the inclusion of particle rotation (Bardet 1994) and later with rolling resistance and flexible surface boundary (Jiang, Yu et al. 2005). The initial models with identical spheres (Dvorkin, Nur et al. 1994) have been refined with the inclusion of grain size distribution (Estrada, Lizcano et al. 2010) and packing densities (Masson and Martinez 2001). The development of shear band due to the microstructural variation have been reported (Bardet and Proubet 1991). The emergence of the discrete element method (DEM) facilitated the realistic modelling of the granular media (Sitharam and Nimbkar 1997). The development of public domain codes for DEM, such as YADE, has made the technique freely available to researchers (Kozicki and Donzé 2008). Using the method, a realistic representation of the confinement condition has been possible through the introduction of flexible boundary conditions (Belheine, Plassiard et al. 2009); (Iwashita and Oda 1998); (Wang and Li 2014); (Zhao and Evans 2009). All these models are for conventional cement. Thus, a 3D numerical models have been developed in YADE to fill the mentioned research gaps in this area.

Stabilisation with bio cement is fundamentally different from that with conventional cement. In biocementation, the aggregation builds up gradually with inherent variabilities in density and degree of cementation (Huang and Airey 1998). Thus, the numerical model becomes further complicated involving a coupled analysis of two phenomena: 1. a reactive transport process to determine the rate and distribution of cementation; 2. a load-resistance model to assess the mechanical properties of the cemented media. There are a few attempts to develop a coupled model. (Fauriel and Laloui 2012) have reported a coupled finite element model for this analysis where a homogenised property of the grains and the cement has been used, which ignores inter-

grain interactions. A stand-alone reactive fluid transport model has been developed to determine the flow characteristics due to cementation (Martinez, DeJong et al. 2014); (Barkouki, Martinez et al. 2011). Several load-resistance models following the traditional DEM techniques (Khoubani, Evans et al. 2016); (Jiang, Zhu et al. 2015) have also been reported. The degree of cementation has been included as inter-grain cohesive strength (Yang, O'Donnell et al. 2016). In general, an equivalent homogenised cohesive strength is assumed for the entire domain. In another variation, separate spheres as cement elements have been introduced (Khoubani, Evans et al. 2015). However, the increased computation does not improve the corresponding accuracy of the solution. In all these models, the stress-strain behaviour of columns as observed in experiments is matched in the computational model by adjusting the homogenised cohesive strength by trial and error (Evans, Khoubani et al. 2015).

An essential feature of biocementation is its gradual growth with repeated cycles (Huang and Airey 1998). As a result, the Spatio-temporal variations of cementation over the period of cementation action need careful consideration, because this microstructural parameter would have a significant effect in terms of damage initiation, its progression and failure modes. No attempt has been made hitherto to incorporate Spatio-temporal variations in case of biocementation. This paper reports an experimental and numerical investigation of biocemented sand columns over an extended range of degree of cementation. A controlled experiment for the degree of cementation from 0 to 88% has been conducted. Scanning Electron Microscopy (SEM) and Energy Dispersive X-ray Spectroscopy (EDS) has been performed for assessing the degree of cementation. Based on the experiment, a table for the Spatio-temporal variation of cementation has been prepared. A unit cell analysis has been performed to determine the inter-grain cohesion for varying degrees of cementation. These properties are used in the development of a macro model for different stages of cementation. The mechanical behaviour, including stress-strain relationship and damage progression, are studied through the experiment, and the numerical methods.

## **4.2. Experimental Investigation**

The experiment consisted of preparing bio-cemented sand columns with varying degrees of cementation and subjecting them to triaxial tests with varying hydrostatic pressure.

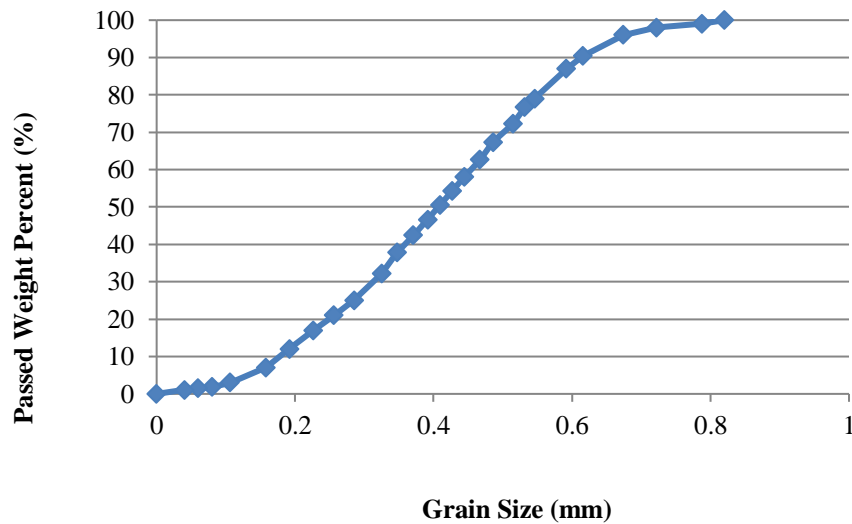


### 4.2.1. Cementation System

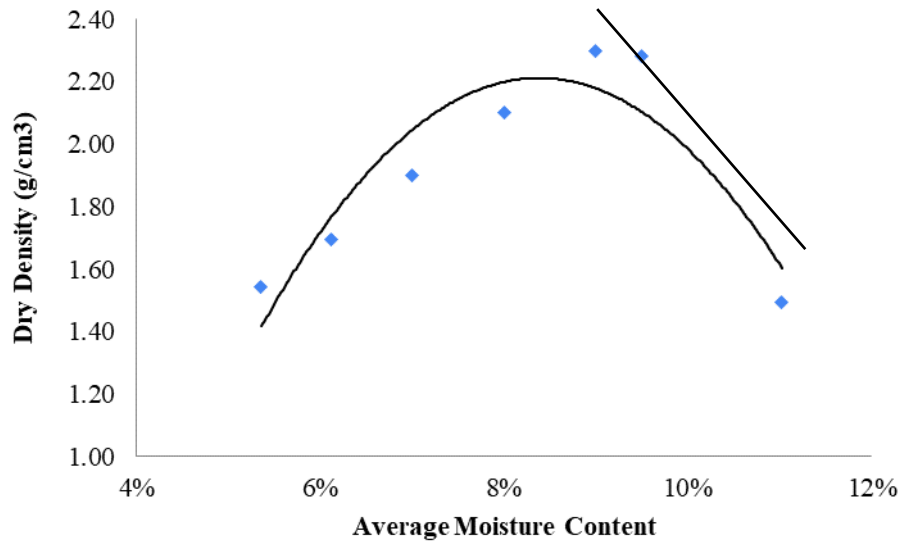
The cementation system consisted of a bacterial fluid and a cementation fluid. Ureolytic bacterial isolate *Sporosarcina pasteurii* (ATCC 11859) was used, and the culture was grown in an Ammonium Yeast extract media, as described in earlier studies (DeJong, Soga et al. 2010). The culture was cultivated in aerobic condition by incubating at 37°C at 200 rpm for 24-36 hours until the optical density (OD) at 600nm, measured using a spectrophotometer, reached 2. The cementation fluid consisted of 0.5M urea, 0.5M calcium chloride and 1g/L of nutrient broth powder.

### 4.2.2. Method

The grain size distribution of the sand used is presented in Fig. 4.1. It had a D<sub>50</sub> of 0.425mm. The Proctor density test results are shown in Fig. 4.2. The optimum moisture content of 9% by mass was observed. The sand was hand mixed and compacted into PVC moulds of 50 mm diameter by 100 mm height in three layers. Each layer was thoroughly compacted to ensure tight packing. All the samples were prepared in triplicates for cementation treatment.



**Figure 4.1.** Sand grains graduation curve (D<sub>50</sub> = 0.425)



**Figure 4.2.** Proctor compaction curve

Three sets of samples with 0, 4 and 8 days of treatment were prepared. The treatment started by, rinsing the samples with 30mM calcium chloride solution in accordance with Harkes, Van Paassen et al. 2010. After one hour, one pore volume of bacterial solution was up flushed and retained for 24 hours as described in Porter, Dhimi et al. 2017. The process was followed by periodic pumping of the one pore volume (40ml) cementation fluid containing urea and calcium chloride at an interval of 12 hours. Then all the samples were placed in a humidity-controlled chamber at 70°C over seven days to dry. The temperature and number of days have been based on previous experience.

### **4.2.3. Estimation of Calcium carbonate deposition**

To estimate the amount of calcium carbonate deposited in the column, we performed a chemical mass balance of the reactants. In each cycle, 40 mL of the cementation fluid with 0.5 molar calcium chloride was used. According to prior research, 90% conversion is expected under the present conditions (Hannah Porter 2016). Based on this information, the mass of deposited calcium carbonate in each feeding cycle has been estimated as in Table 1. Two cycles of feeding were performed each day. Total void space in the cylinder samples was estimated as 80 mL. It was estimated that 60 days of feeding is required to achieve 100% cementation.

**Table 4.1.** Weight of precipitated calcium carbonate in one cycle of feeding

Molar weight of CaCl <sub>2</sub> (g/mol)	Molar weight of CaCO <sub>3</sub> (g/mol)	Volume of Solution (mL)	Concentration of CaCl <sub>2</sub> (mol)	Mass of CaCO <sub>3</sub> (g)
110.98	100.086	40	0.5	1.75

#### 4.2.4. Test Matrix

A test matrix was designed to study the mechanical behaviour of samples subjected to a triaxial compression test. Samples were prepared in triplicate and treated with the cementation solution for 0, 12, 21, 33, 42, 53 days. After 53 days, it became too difficult to feed and up flush the samples due to the high levels of aggregation. The number of feeding days depends on some factors, e.g. the molarities of cementation media, bacterial concentration and environmental condition. Therefore, they are converted to % treatment based on estimated carbonate deposition. The nomenclature of the samples in different stages of treatments under two confining pressures is presented in Table 4.2.

**Table 4.2.** Nomenclature of samples for the experimental tests

Treatment		CaCO <sub>3</sub> (g)	Confining pressure	
Days	%		100 kPa	200 kPa
0	0	0	Exp. 0-100	Exp. 0-200
12	20	42	Exp. 20-100	Exp. 20-200
21	35	73.5	Exp. 35-100	Exp. 35-200
33	55	115.5	Exp. 55-100	Exp. 55-200
42	70	147	Exp. 70-100	Exp. 70-200
53	88	185.5	Exp. 88-100	Exp. 88-200

#### 4.2.5. Triaxial Tests

After the treatment, all the samples were placed in a humidity-controlled chamber at 70°C over seven days for drying. The samples were de-moulded by unzipping the PVC cylinder. The unevenness at the top of the samples was carefully smoothed. The samples were tested in a triaxial loading condition according to the Australian standard (AS 1289.6.4.1:2016). The load was applied at a displacement rate of 1 mm/min. The

force and displacement were recorded every 20 seconds. Tests were continued until failure of the specimen subjected to a maximum 15% axial strain. The stress-strain plot of each sample was generated.

#### **4.2.6. Microstructural Analysis**

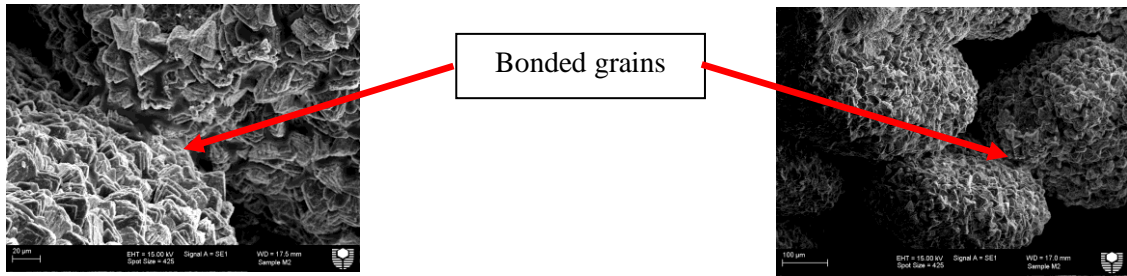
Microstructural analysis was undertaken on the samples to calculate the portion of the participation of calcium carbonate. Analysis has been done by using Scanning Electron Microscopy (SEM) and Energy Dispersive X-Ray Spectroscopy (EDS) in different stages of feeding the sand samples after undertaking triaxial tests.

Aluminium stubs were used to prepare samples for SEM images, where aluminium stubs mount the small portion of samples, treated by different stages of cementation. To have conductive samples, they have been coated by 10nm layer of carbon after mounting on aluminium.

For quantitative EDS small portions of the samples were coated with a 10 nm carbon coating and mounted in an epoxy resin. After mounting the surface of the sample was polished. Quantitative EDS mapping of the elements was done at points across the sample using a W-filament Zeiss EVO 40XVP. The elemental maps obtained across a matrix of 10x10 grains were plotted.

#### **4.2.7. Scanning Electron Microscopy (SEM)**

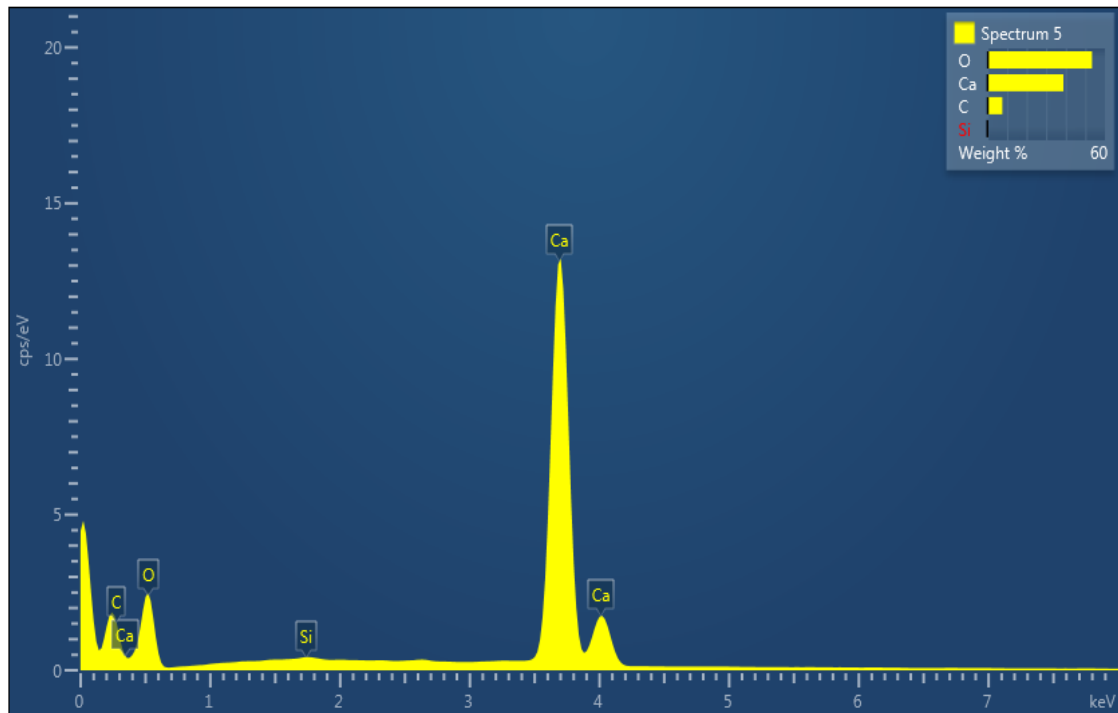
Representative samples were collected from the cylinders after the triaxial test was performed to conduct a scanning electron microscope (SEM). SEM is an electron microscopic that takes images by scanning the surface of samples. Figure 4.3. shows the samples after 55% of cementation due to MICP treatment. Extensive cementation has occurred that covered the grains. Grain bridging too is discernible.



**Figure 4.3.** SEM image of the cement treatment sand sample (55% cementation through MICP process treatment)

#### 4.2.8. Energy Dispersive X-Ray Spectroscopy (EDS)

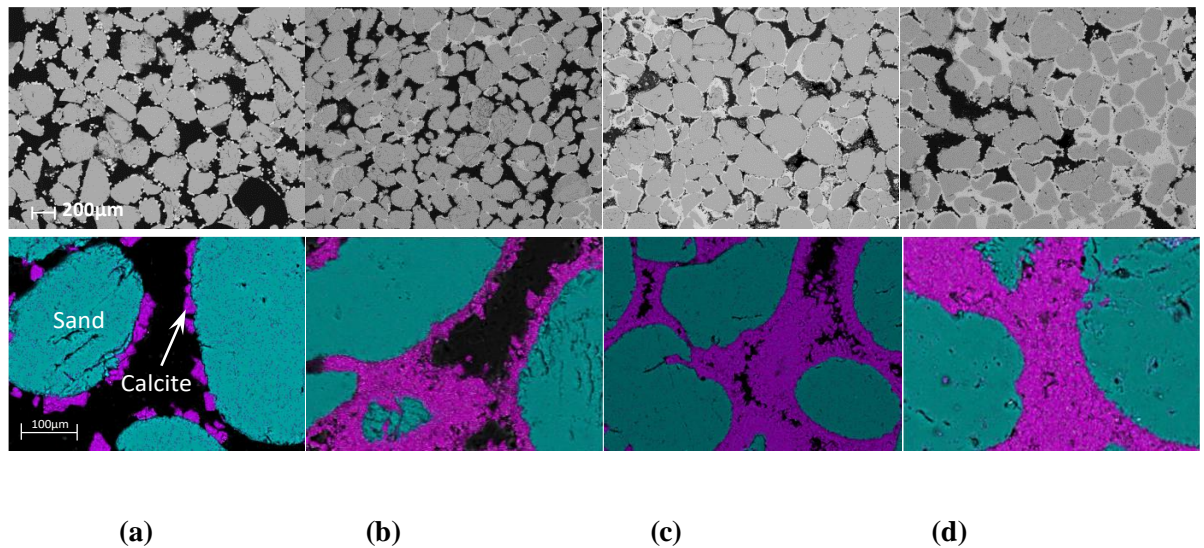
The results of EDS illustrate in all samples silicon and oxygen exist, where silicon representing the sand's material. Investigations shows, other main components are calcium and chloride. The main portion of calcium converted to carbonate form, and the observed chloride is the calcium chloride that remained in samples from the feeding process (Fig. 4.4).



**Figure 4.4.** Energy dispersive X-ray spectrum of cement samples that are treated for 12 days (20% cementation)

#### 4.2.9. Quantitative EDS

Figure 4.5 represents the quantitative energy dispersion spectra at different stages of aggregation after 20%, 35%, 55% and 70% cementation. It can be seen that the voids spaces have been filled gradually due to cementation. In the zoomed figures, purple indicates cement and cyan indicates sand. The figures have been analysed by an image analysis software ImageJ, to determine the proportions of sand, cement and void. There was a good agreement. It can be seen that at the initial stages, the cement is mostly attached to the sand but not thick enough to bridge the grains. Clear evidence of bridging is seen at 35% cementation where the gap between the grains is relatively small ( $<100\ \mu\text{m}$ ), although there are still areas where the cement has formed a coating on the sand grains but not bridged them. When 55% of sands in each sample are cemented, considerable bridging of grains is noticed. At 70% cementation level, there are just a few large voids are left to be filled. The proportion of cementation progresses roughly at the same rate as in theoretical calculations.



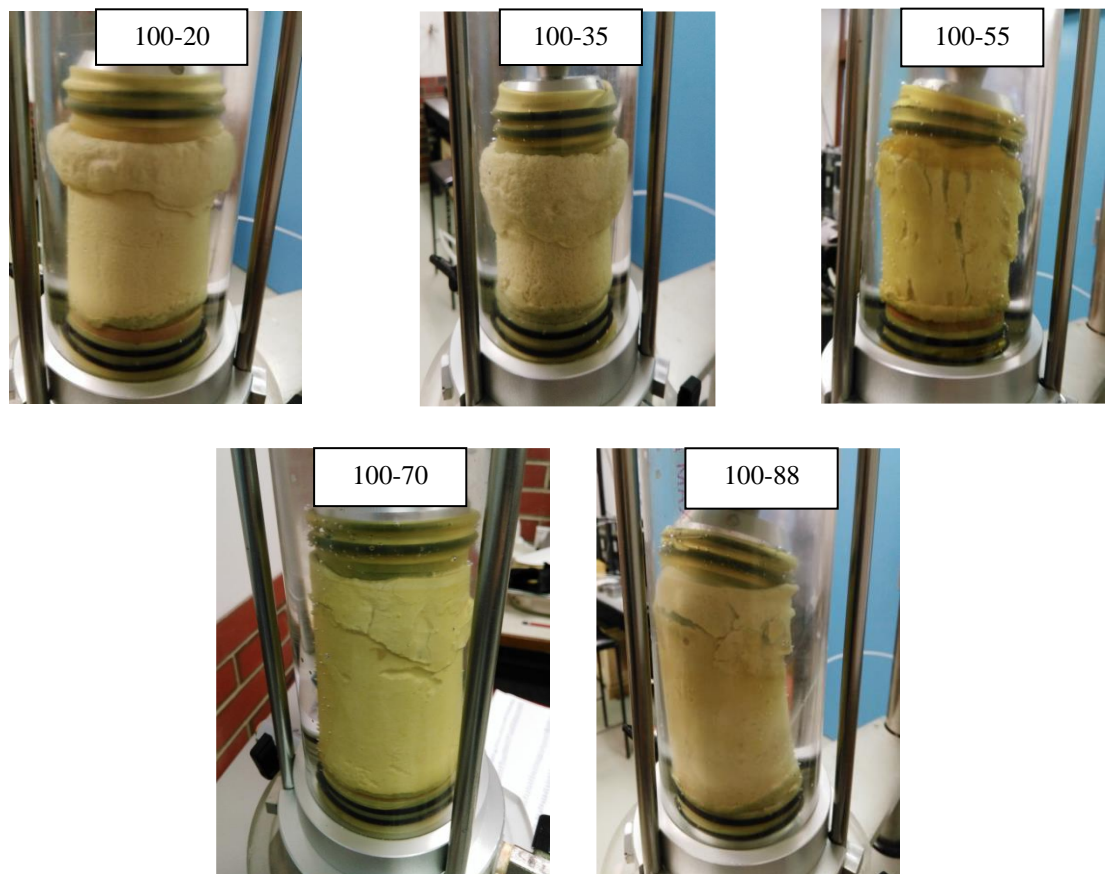
**Figure 4.5.** SEM image of the sand sample after (a) 20%, (b) 35%, (c) 55%, (d) 70% days cement treatment

#### 4.2.10. Mechanical performance

The undrained triaxial test was conducted on the loose and cemented sand samples. The control samples consisting of loose sand were tested under 100kPa and 200kPa confining pressure. The cemented samples were tested at the same confining pressures

after 20%, 35%, 55%, 70% and 88% cementation. Figure 6 illustrates the cemented samples under 100kPa confining pressure. At 20% cementation, the sample fails due to bulging at the head, as observed in untreated samples. At 35%, the bulging failure persists, although it is more spread in the sample. This suggests that intergranular cohesion is not strong enough to prevent the grains from slipping. At 55% cementation, the bulging is significantly reduced. Vertical cracks appeared on the samples indicating splitting at the centre due to tensile stresses. Thus, the effect of cementation manifests itself from this point onwards. The samples in 70% and 88% level of cementation pronounced diagonal cracking. Developed cracks indicate the development of shear slip planes, as observed in unconfined tests. Thus, they behave more like cemented columns than loose sand.

Samples at 88% of cementation, reached to the high level of the compressive strength.



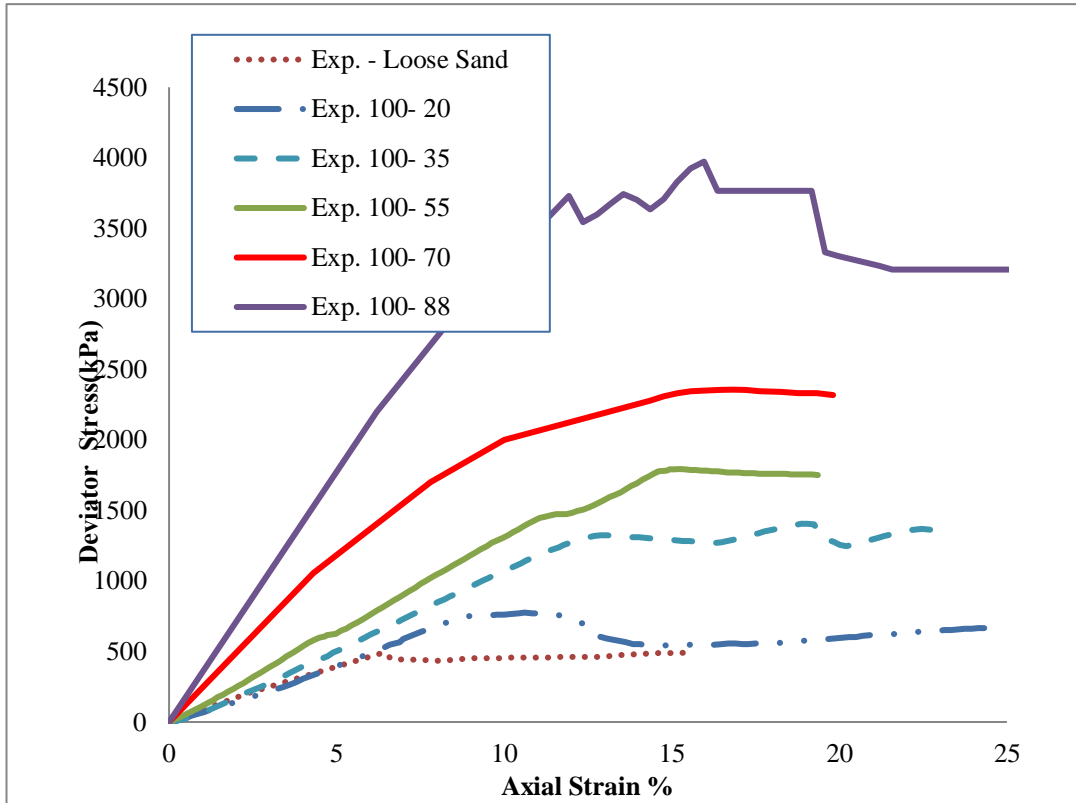
**Figure 4.6.** MICP samples with different level of cementation after applying triaxial test conditions - confining pressure of 100kPa

The stress-strain plots of the cemented samples along with that of loose sand are presented in Figures 4.7 and 4.8. They illustrate that the stiffness and strength of the samples increased dramatically with cementation. It was observed that at 20% cementation, the strength went up by at least 50% although the initial stiffness remained largely unaltered. At 35% cementation, the strength went up by more than three times, and the initial stiffness too started to rise. Beyond this point, both strength and stiffness had a quantum jump at every step. It may be recalled that beyond 35% cementation the failure mode changed from bulging to cracking. Its effect on the stress-strain behaviour is a significant jump in both stiffness and strength.

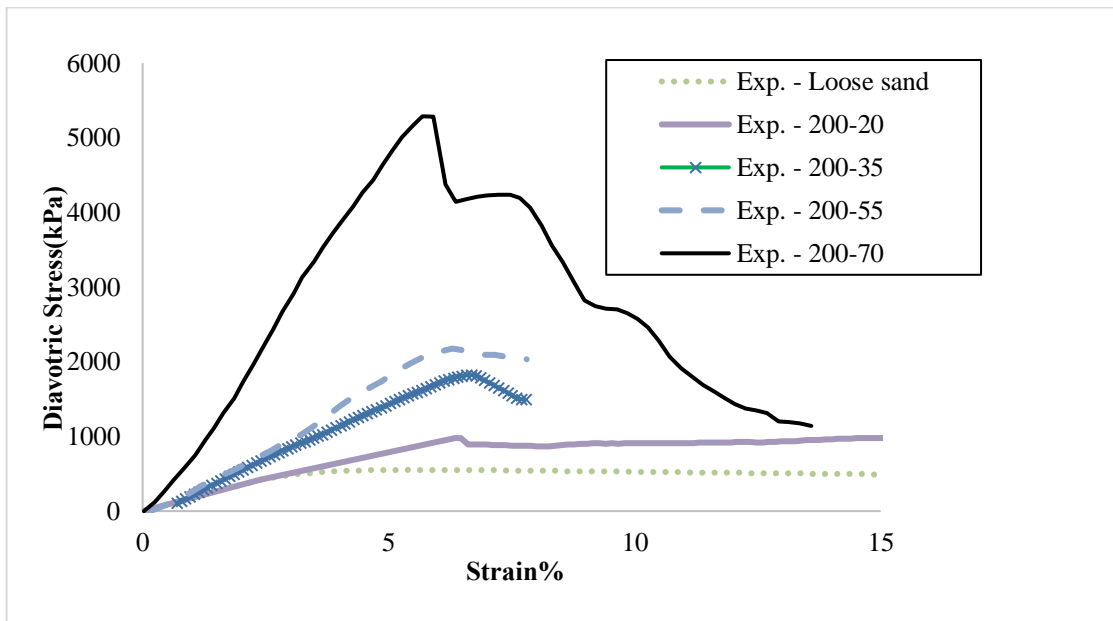
The samples with 200 kPa confinement generally show significantly higher stiffness and strength than those at 100 kPa confinement, especially at lower levels of cementation. This fact is expected as confinement pressure impedes bulging of the samples under compressive loading. At higher levels of cementation, however, the effect of confinement pressure is less predominant. At these levels, the samples develop significant, cohesive strength that prevents bulging.

The critical mechanical parameters altered due to cementation and confinement pressure are summarised in Table 4.3. These values have been used for validating the proposed numerical model.





**Figure 4.7.** Stress-strain curves under triaxial test - confining pressure 100kPa



**Figure 4.8.** Stress-strain curves under triaxial test - confining pressure 200kPa

**Table 4.3:** The effects of the cement process on the main mechanical properties of the aggregated grains (x: value could not be measured)

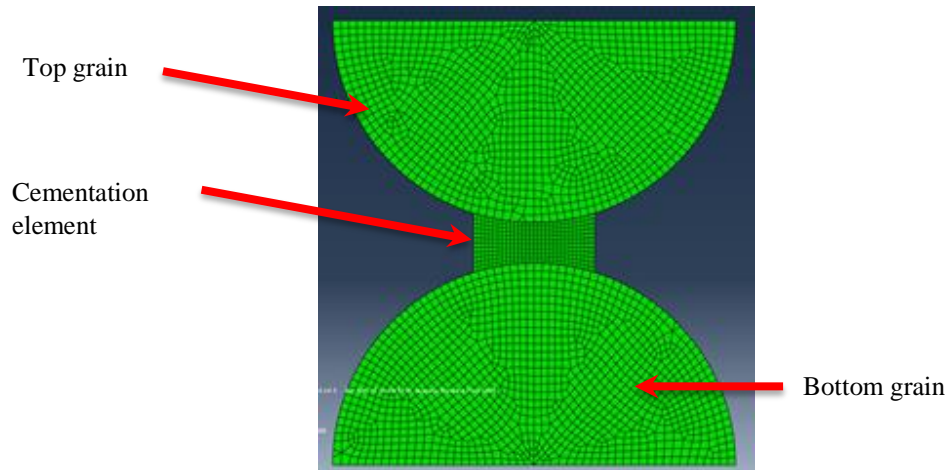
% of Cementation	Confinement pressure(kPa)					
	100			200		
	Initial stiffness (MPa)	Max stress (kPa)	Strain at maximum stress (%)	Initial stiffness (MPa)	Max stress (kPa)	Strain at maximum stress (%)
0%	2	487.8	6.5	2	525.6	3.7
20%	10	775.5	10.6	15	976.4	6.5
35%	16	1322.9	19	29	1823.2	6.7
55%	21	1793.4	15.3	35	2176.2	6.3
70%	29	2356.1	15.8	95	3171	5.7
88%	74	3973	16	x	x	x

### 4.3. Numerical Model

A numerical model is developed to simulate the MICP cementation process. The model presents the spatial variation of cementation levels within the sample. A unit cell model is coupled with the global model to perform this analysis. The unit cell model produces the inter-grain characteristics due to varying levels of cementation. The inter-grain properties, due to different levels of cementation, as obtained from the unit cell model, are plugged into the global model.

#### 4.3.1. Unit cell model

The unit cell model consists of two sand grains bonded by a cementation element (Figure 4.9). Several models with varying levels of cementation have been analysed. ABAQUS finite element software is employed to study the mechanical properties of the unit cell model.



**Figure 4.9.** The unit cell model

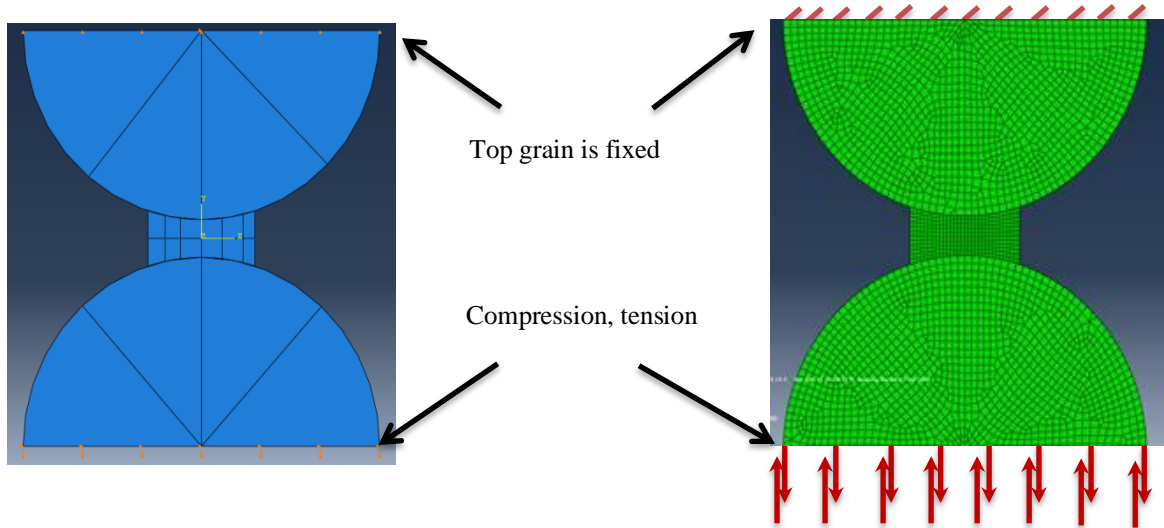
The constitutive material properties for the grain and cement elements are depicted in Table 4. The property values have been adapted from Kozicki and Donze 2008. As the failure is expected in the cement, elastic behaviour is considered for the sand grains, while the cement has a plastic limit. Moreover, the yield stress and ultimate strain for tension are considered 10% of that in compression.

**Table 4.4.** Properties of grains and cement materials

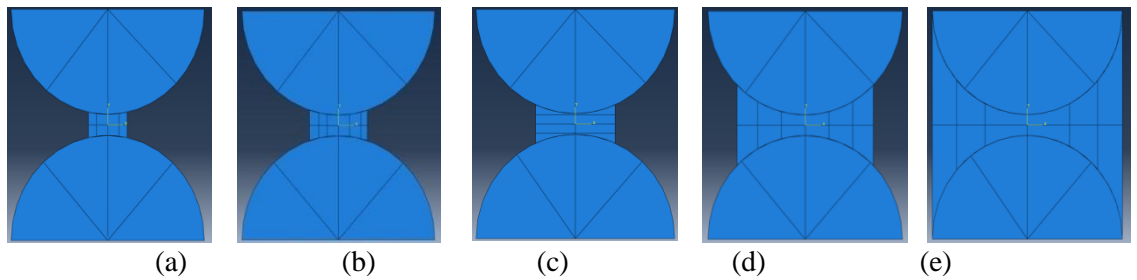
	Elastic properties			Plastic properties	
	Density (Kg/m <sup>3</sup> )	Young's Modulus (GPa)	Poisson's ratio	Yield Stress(MPa)	Yield Strain (10 <sup>-3</sup> )
Grain	2500	70	0.3	NA	NA
Cementation	2500	60	0.3	40	0.67

The unit cells were subjected to compression and tension, as shown in Figure 4.10. For this purpose, the top grain was fixed, and displacements were applied progressively on the bottom surface. A non-linear finite element analysis has been conducted. The load-displacement behaviour of the bottom surface is plotted. From the load-displacement plots in compression, the effective spring stiffness and the elastic limit of the cell for each load case were determined. The tensile load case was used to determine the cohesive strength between the grains. Different degrees of cementation is modelled by varying the width of the cementing element (see Fig 4. 11). Similarly, shear and a

couple were applied to the unit cell to determine the shear and rotation resistance. These parameters were used in the global model.

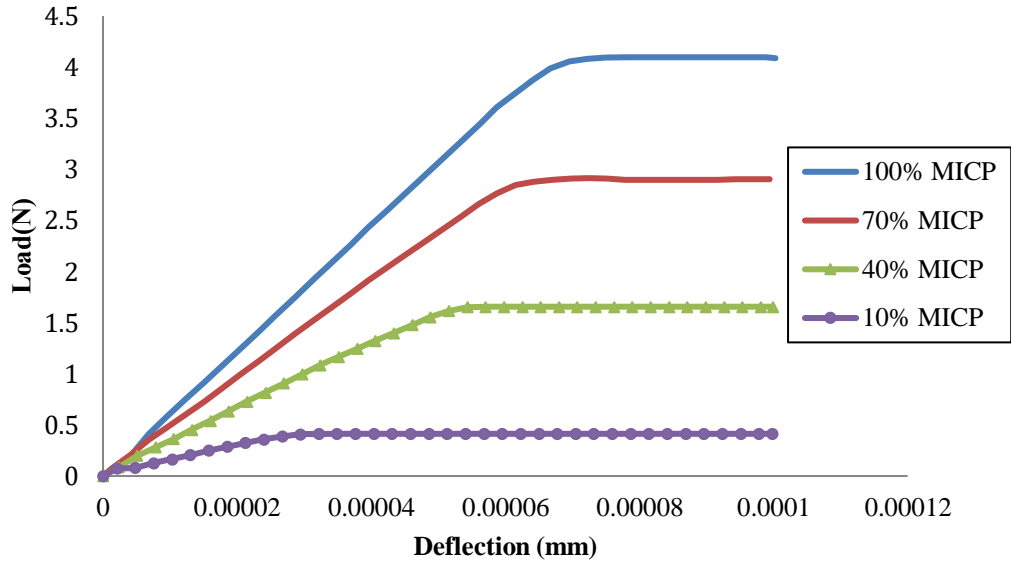


**Figure 4.10.** A constitutive model for plastic behaviours of cement material

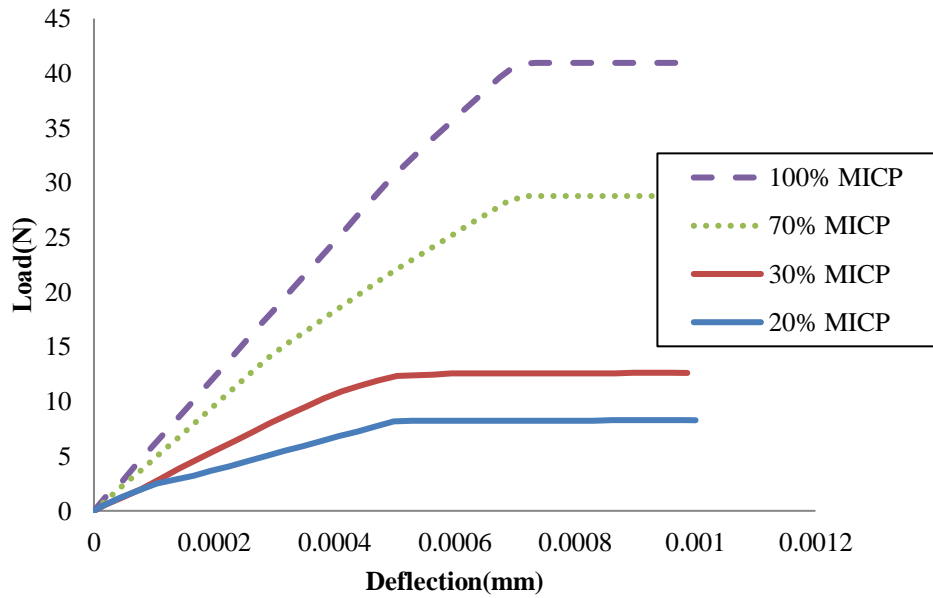


**Figure 4.11.** Different levels of cementation (a) 20%, (b) 40%, (c) 60%, (d) 80%, (d) 100% cementation

Different levels of cementation are shown in figures 4.12 and 4.13 by the load-deflection plots of the unit cell. The outputs are used as input to the global model. Table 4.5 presents the global parameters derived from the unit cell models.



**Figure 4.12.** Load-deflection curves of the cemented samples in tension



**Figure 4.13.** Load-deflection curves of cemented samples in compression

**Table 4.5.** Relationships between the level of aggregation of the cement samples and the cohesion between grains

Cementation (%)	Number of treatment days	Normal cohesion (Pa)	Shear cohesion (Pa)	Sliding friction coefficient	Friction angle (°)	Elastic Modulus (Pa)	Normal Stiffness (N.M <sup>-1</sup> )	Shear Stiffness (N.M <sup>-1</sup> )	Coefficient of Rolling Resistance
0	0	0.4e2	0.2e1	0.32	35	12e3	24e3	9.6e3	0.01
20	12	1.3e3	0.9e2	0.39	36	1.6e7	6e4	2.4e4	0.011
35	21	1.9e3	2.1e2	0.43	38.2	2.5e7	2e5	8e4	0.013
55	33	9e4	6.8e3	0.47	39.1	3.4e7	6e5	2.4e5	0.018
70	42	7.3e5	3.7e4	0.48	39.4	4e7	2e7	0.8e7	0.021
88	53	3e7	5e6	0.56	44	5.86e7	8e7	3.2e7	0.025

### 4.3.2. Global Model

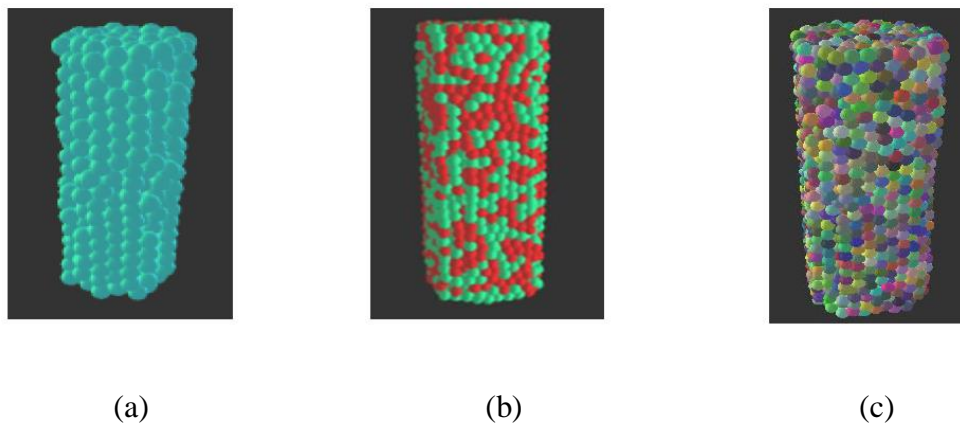
The global DEM model is developed in YADE as a column of grains with partial cementation. The sand of the given grain size distribution and intergranular properties is filled in a cylindrical container to build the model. The generated pack is compressed isotropically by squeezing the packing until a specified confining pressure, and void ratio is achieved. After application of the confining pressure, the top surface was given a gradual axial displacement while holding the bottom surface rigid to apply a compressive pressure along the axis of the cylinder while maintaining the specified confining pressure. The deformation of the cylinder is calculated at each load step. The stress-strain diagram of the cylinder was plotted. A convergence study was performed to determine the minimum number of grains to be representative of the experimental condition. It was noted that 10000 grains were sufficient in the present case.

Biocementation initiates at random locations of nucleation and grows gradually with time. Inclusion of this Spatio-temporal variation of cementation in the numerical model is attempted here. Fig. 4.14 represents the levels of cementation with different coloured grains. The simplest assumption is uniform cementation. In this case, the homogenous average cementation is assumed. Therefore, all intergranular material properties are identical. The intergranular material property is represented by the uniform colour of grains in Fig. 4.14a. This model has been used hitherto in numerical simulations. A more realistic case is binary cementation, where the grains are either loose or cemented to the same level. Grains of two different colours in Fig. 4.14b represent the spatial

distribution of the cemented and loose grains. In this case, the proportion of the cemented grains goes up in comparison to the loose grains with increasing level of cementation. In reality, the level of cementation between the grains can vary. The cementation gradually goes up with time. In this section, the graded cementation model has been used to model this situation (Fig. 4.14c). The unit cell models, as in Fig. 4.9, produced inter-grain properties for five levels of cementation varying from 20 to 100%. These characteristics are plugged into the global model through the random distribution of the bonded grains. The distribution with advancing levels of cementation is depicted in Table 4.6. table columns represent the percentage of grains, and each cell in the column is the corresponding percentage of cementation. Each row corresponds to a numerical model. Model 1 consists of loose grains with no bonding. Thus, all cells have 0% cementation. In Model 2, 20% grains (distributed randomly- the concept of the random distribution has been predefined in YADE software engines (Yade Manual)). In general, a range of grains size is defined in a specific size of samples) are bonded with at least 20% cementation, and rest are considered loose. Thus, the cell corresponding to 20% grains has a value of 20; the rest of the cells contain 0%. Likewise, in model 3, 20% of grains have achieved at least 40% cementation, while 40% of grains have at least 20% cementation. The cementation progresses with time as depicted in models up to 13. It may be noted that the range of cementation spreads until Model 5. In model 6, 100% cementation is reached for at least 20% grains, and all grains have at least 20% cementation. From model 6 onwards, the spread of cementation levels narrows down as more grains get 100% cementation. Thus, the variation of cementation through the entire process has been adequately captured in eleven numerical models. Fig. 4.14c depicts the spatial distribution of cementation by means of colour codes. The results of these numerical models have been compared with the stress-strain graphs obtained from the experimental investigation.

**Table 4.6:** Distribution of % cementation for different bond types

Numerical models	% Grains				
	20	40	60	80	100
1	0%	0%	0%	0%	0%
2	20%	0%	0%	0%	0%
3	40%	20%	0%	0%	0%
4	60%	40%	20%	0%	0%
5	80%	60%	40%	20%	0%
6	100%	80%	60%	40%	20%
7	100%	100%	80%	60%	40%
8	100%	100%	100%	80%	60%
9	100%	100%	100%	100%	90%
10	100%	100%	100%	100%	90%
11	100%	100%	100%	100%	100%



**Figure 4.14.** Numerical models showing levels of cementation in colour codes (a) Homogenous, (b) Binary, (c) Spatio-temporal samples

### 4.3.3. Model Validation

The results from the present model are compared with the prior experimental and numerical results for both loose and cemented sand.

#### i. Loose sand

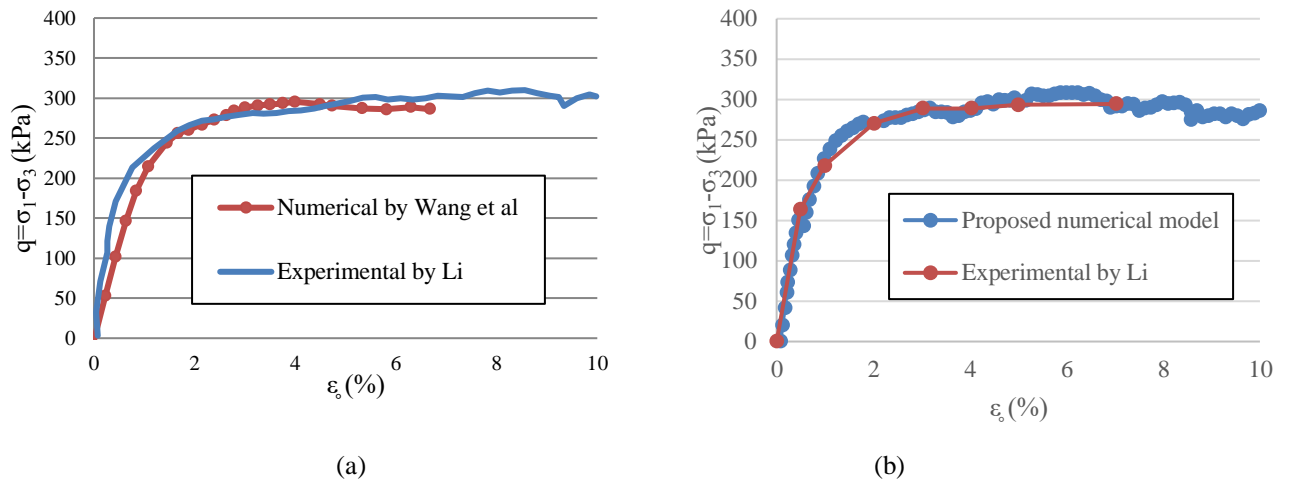
Loose sand in triaxial compression has been modelled according to experiments conducted by (Li 1985). Numerical prediction for the same sample is also available in (Wang and Li 2014). Table 4.7 presents the parameters used in the numerical model. Fig. 4.15 illustrates the prior results along with that from the present model. It can be



seen that the current numerical model accurately predicts the behaviour of loose sand in triaxial compression.

**Table 4.7.** Optimum values of the micro parameters to model the experimental results

Name of variable	Base value
Number of particles ( $n$ )	10000
Time step ( $t$ )	1.00E+07
Particle size ( $d$ )	0.2 -0.8 mm
Friction angle ( $\phi$ )	36.5°
Sliding friction coefficient ( $\mu_s$ )	0.4
Density( $\rho$ )	2500 Kg/m <sup>3</sup>
Poisson ratio ( $\nu$ )	0.4
Damping ( $\zeta$ )	0.4
Height of sample ( $h$ )	100mm
Diameter of sample( $D$ )	50mm
Porosity ( $\Phi$ )	40%
Rolling stiffness coefficient ( $\mu_r$ )	0.5
Contact Young's modulus ( $Y$ )	800 MPa
Stiffness ratio ( $\alpha$ )	0.1
Particle friction angle ( $\phi$ )	22
Coefficient of rolling stiffness ( $\alpha_r$ )	0.6
Lateral pressure ( $kPa$ )	100
Peak friction angle ( $\phi_p$ )	36°
Dilatancy angle ( $\psi$ )	12.8°



**Figure 4.15.** Stress-strain plot for triaxial compression (a) experimental (Li 1985) and numerical (Wang and Li 2014), (b) present and (Li 1985)

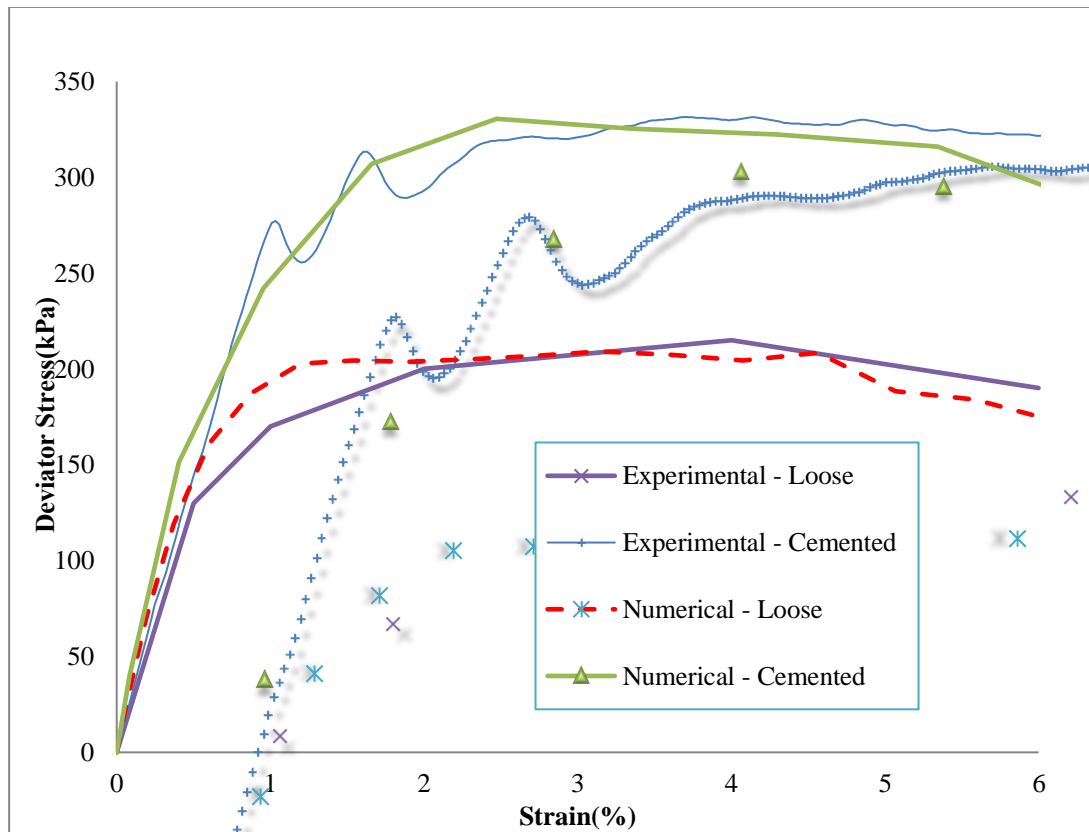
## ii. Biocemented sand

Loose and biocemented sand at varying triaxial compression have been investigated. Sand sourced from Cook Industrial Minerals were used to fill columns of 50 mm diameter and 100 mm height. They were treated to achieve a specific level of cementation. Treated samples subjected triaxial compression at confining pressures of 50 kPa and 150 kPa. The columns were modelled numerically with the presented parameters in Table 4.8. The homogeneous cementation model was assumed, and the cohesion strength was adjusted by trial and error. Figures 4.16 and 4.17 show the stress-strain plots from the experiment and the numerical model. It is evident that the present model has been successful in modelling the stress-strain behaviour.

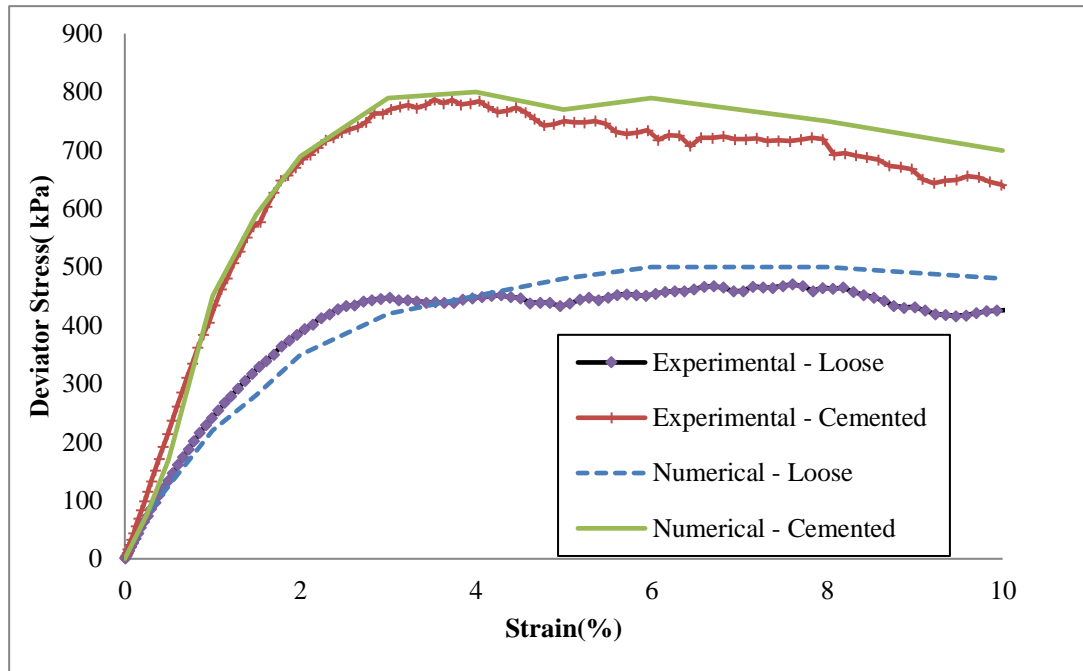
**Table 4.8.** Input parameters for the numerical model

Name of variable	Base value
Number of particles ( $n$ )	10000
Time step ( $t$ )	1.00E+07
Particle size ( $d$ )	0.15 mm and 0.5mm
Friction angle ( $\phi$ )	36.5°
Sliding friction coefficient ( $\mu_s$ )	0.4
Density ( $\rho$ )	2500 Kg/m <sup>3</sup>
Poisson ratio ( $\nu$ )	0.4
Damping ( $\zeta$ )	0.4

Height of sample ( $h$ )	100mm
The diameter of sample ( $D$ )	50mm
Porosity ( $\Phi$ )	40%
Young's module ( $E$ )	25e9 Pa
Normal cohesion ( $C_n$ )	2e3 Pa
Shear cohesion ( $C_s$ )	2e2 Pa



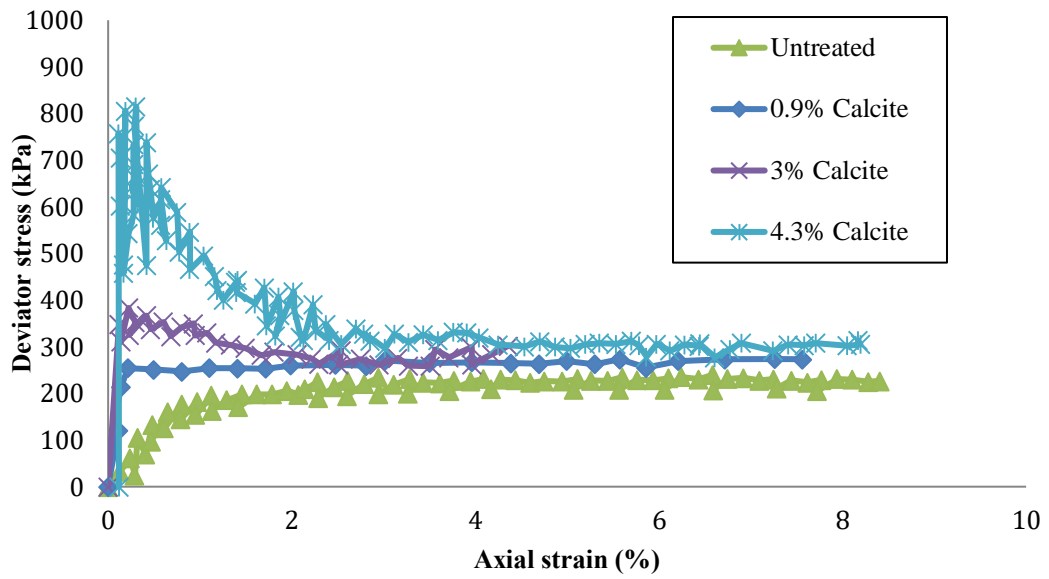
**Figure 4.16:** Stress-strain plots for loose and cemented sand columns at 50 kPa confining pressure



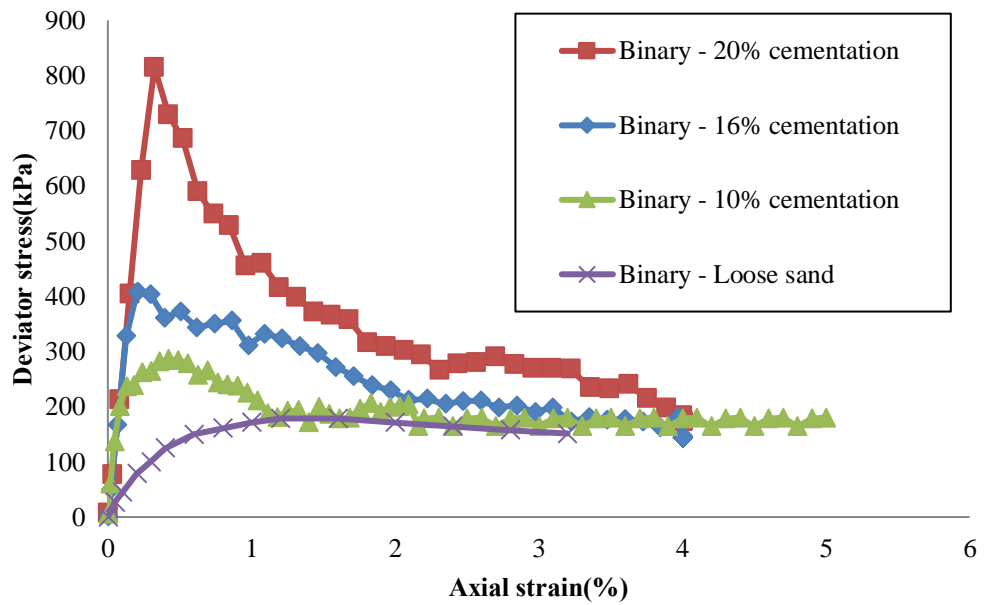
**Figure 4.17:** Stress-strain plots for loose and cemented sand columns at 150 kPa confining pressure

### iii. Sparsely cemented sand

Numerical simulations for sparsely cemented sand columns at 100 kPa triaxial compression as reported by Yang, O'Donnell et al. 2017, has been compared with the present method. Numerical parameters in the DEM model were adopted from Yang, O'Donnell et al. 2017, and experimental parameters are available in Feng and Montoya 2015. In this case, a binary model has been used. Fig. 4.18 presents the prior results and the present simulation. The variation in the percent of calcite is due to the method of calculation. Feng and Montoya 2015, proposed a numerical model for three different levels of cementations. The percentage of calcite in the samples was 0.9% to 4.3% (mass volume 0.37–1.76% by), (Fig. 4.18 (a)). It can be seen that the binary model is suitable for replicating the stress-strain behaviour (Fig. 4.18 (b)).



(a)



(b)

**Figure 4.18.** Stress-strain curves for sparsely cemented columns in 100 kPa triaxial compression (a) Yang, O'Donnell et al. 2017 (b) present binary model

The above examples demonstrate that the stress-strain curves of cemented columns under various triaxial compression can be replicated through trial and error parameter

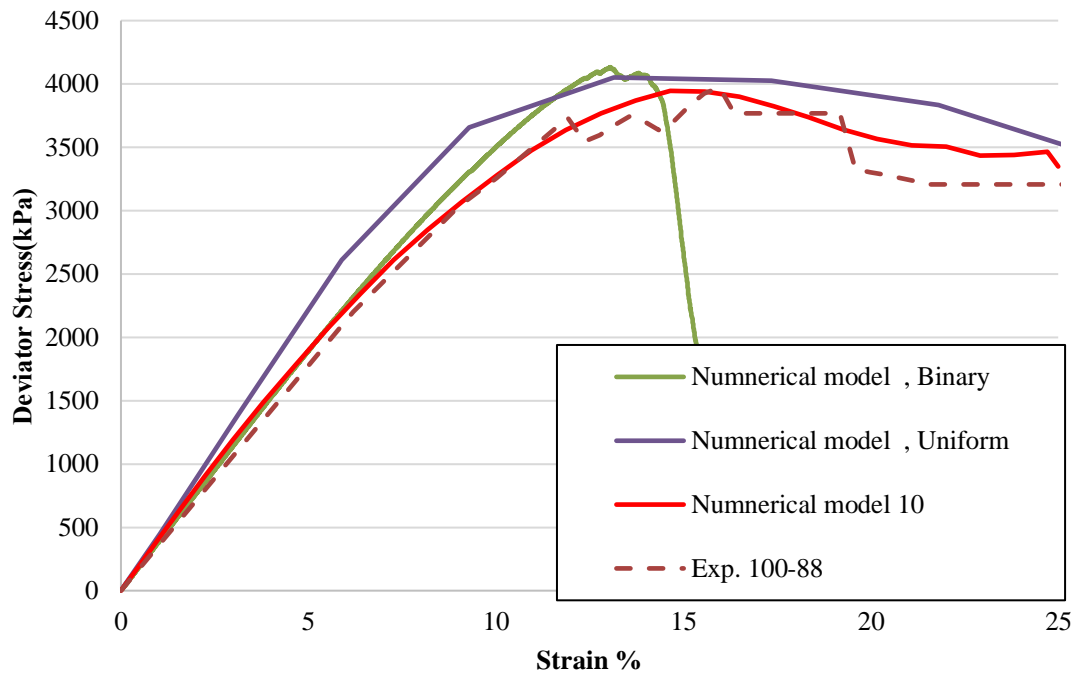
matching. However, in these investigations, no attempt has been made to capture the failure modes. A more sound basis of obtaining numerical parameters is imperative for prediction of failure modes along with the stress-strain curves.

#### **4.4. Present models**

In this Section, the present Spatio-temporal model has been tested with extensive experimental results. The homogeneous, binary and Spatio-temporal models, as described in Section 4.3.2, have been compared.

#### **4.1 Comparison of models**

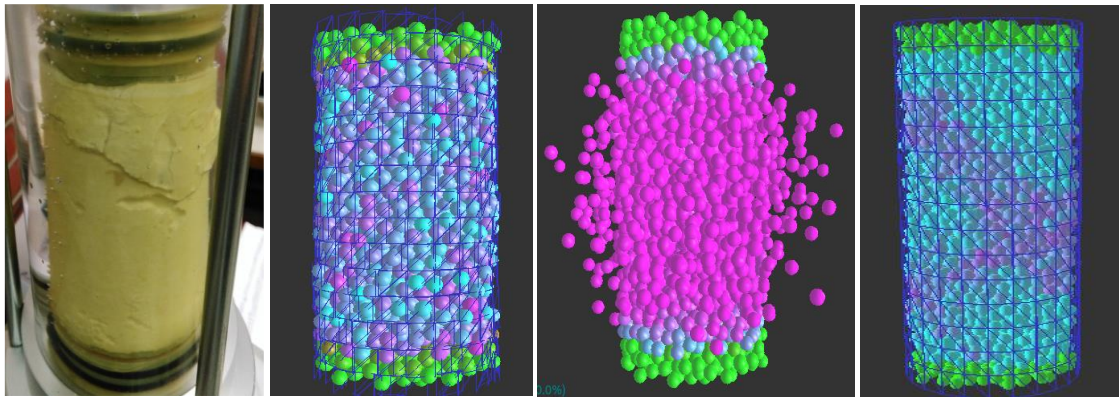
The result from experimental specimen 100-88 has been used to compare the three models. For the homogenous model, the inter-granular cohesive strength has been adjusted by trial and error to match the experimental curve closely. In the case of the binary model, the material parameters are kept the same as the homogenous model, but the percentage of cemented grains is varied. The Spatio-temporal model uses one of the cementation scenarios from the list presented in Table 4.6. Fig. 4.19 shows the stress-strain plots for the three models. It can be seen that all three models are able to predict the initial part of the curve. At this stage, the stress is too low to create any damage in the sample. The homogeneous model predicts over-stiff behaviour as damage initiates in the sample, and softening starts. The binary model follows the experimental curve more closely than the homogeneous model; however, as the peak stress is reached, the model unloads very rapidly. Thus, the binary model could predict the peak stress well. Still, the strain at peak load and the ultimate strain was under-predicted. However, the binary model can capture the trend of plasticity behaviour of the samples after peak stress; there are some opportunities to improve the accuracy. The Spatio-temporal model followed the experimental curve very closely all the way until failure. It may be recalled that the Spatio-temporal model relies on the unit cell model that obviates any trial and error selection of material properties which proves the suitability of the Spatio-temporal model.



**Figure 4.19.** Stress-strain plots for Homogenous, Binary and Spatio-temporal models

For examining the capability of the models to predict the damage mechanisms, two experimental samples that had undergone very different modes of failure were chosen. It may be recalled that two principal modes of deformation bulging (for the relatively lower level of cementation) and shear cracking (for higher levels of cementation) were observed. The triaxial compression tests for these two cases were simulated with homogeneous, binary and Spatio-temporal models and their deformations and inter-granular slips were observed. Fig. 4.20 shows the inter-granular slips at the instant of failure along with the image of the experimental sample that experienced bulging. It can be seen that in the case of the homogeneous model, the slip is seen everywhere in the sample. As the model is homogeneously cemented, it does not predict the localised effects. For the binary model, an uncontrolled slip happens at the instant of failure. In this model, a portion of the grains are cemented, but the others are loose. Thus, when the inter-granular separation force exceeds the cohesive strength, the specimen collapses catastrophically. The Spatio-temporal model predicts a shape closest to that of the experimental specimen, the bulging at the centre. Fig. 4.21 shows the case of shear cracking. In this case, too, the homogeneous model does not predict the localized crack, but an overall loss of cohesion. The binary model leads to catastrophic collapse. The Spatio-temporal model, on the other hand, predicts the shear banding. The Spatio-

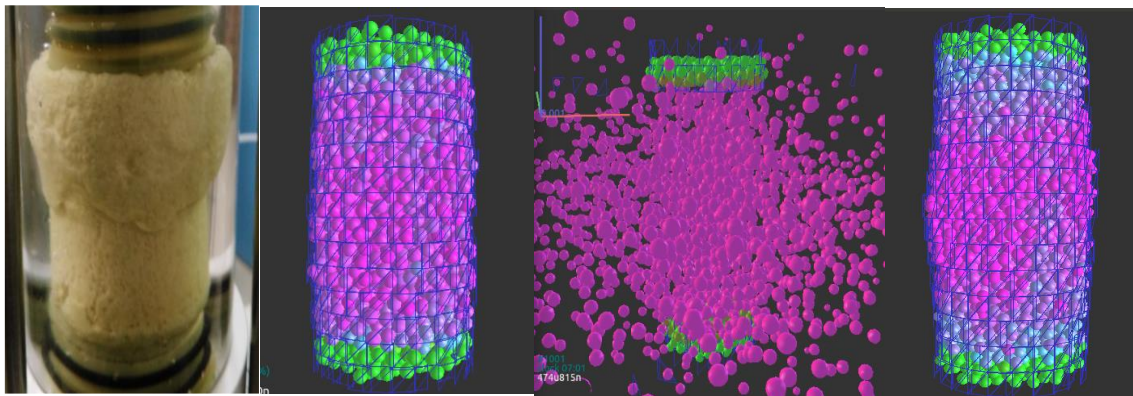
temporal model is capable of predicting not only the global stress-strain localize but also the localized effects.



(a) (b) (c) (d)

**Figure 4.20.** Numerical approach to predict the failure mode – Confining pressure 100kPa

For (a) Exp. 100-70, (b) Uniform, (c) Binary, (d) Spatio-temporal



(a) (b) (c) (d)

**Figure 4.21.** A numerical approach to predict the failure mode – Confining pressure 100kPa

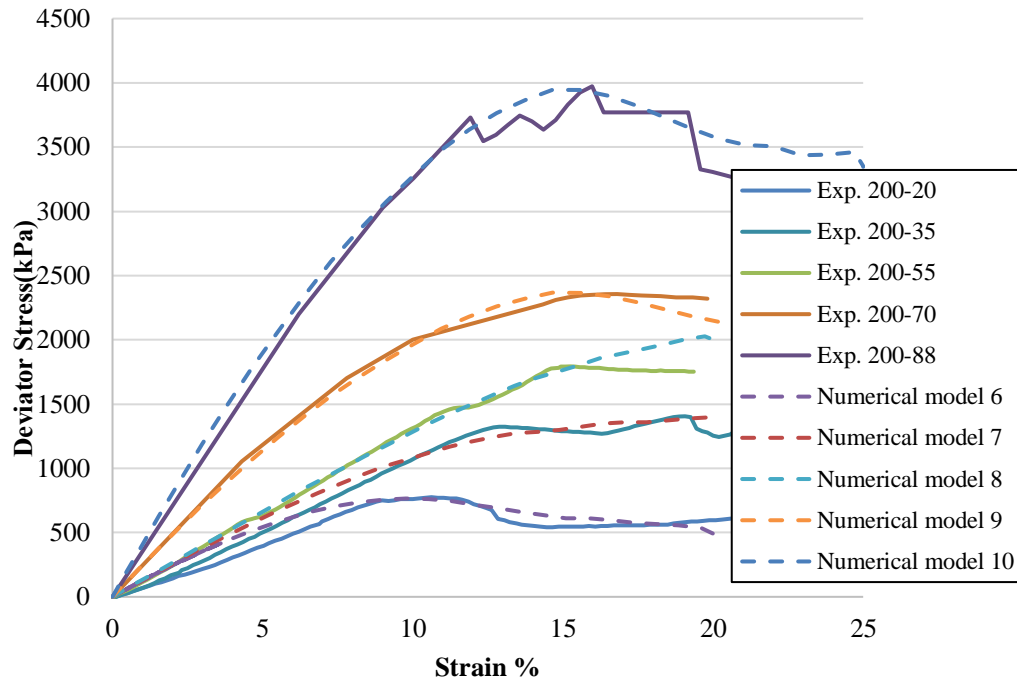
For (a) Exp. 100-35, (b) Uniform, (c) Binary, (d) Spatio-temporal

#### 4.4 Varying cementation and confining pressure

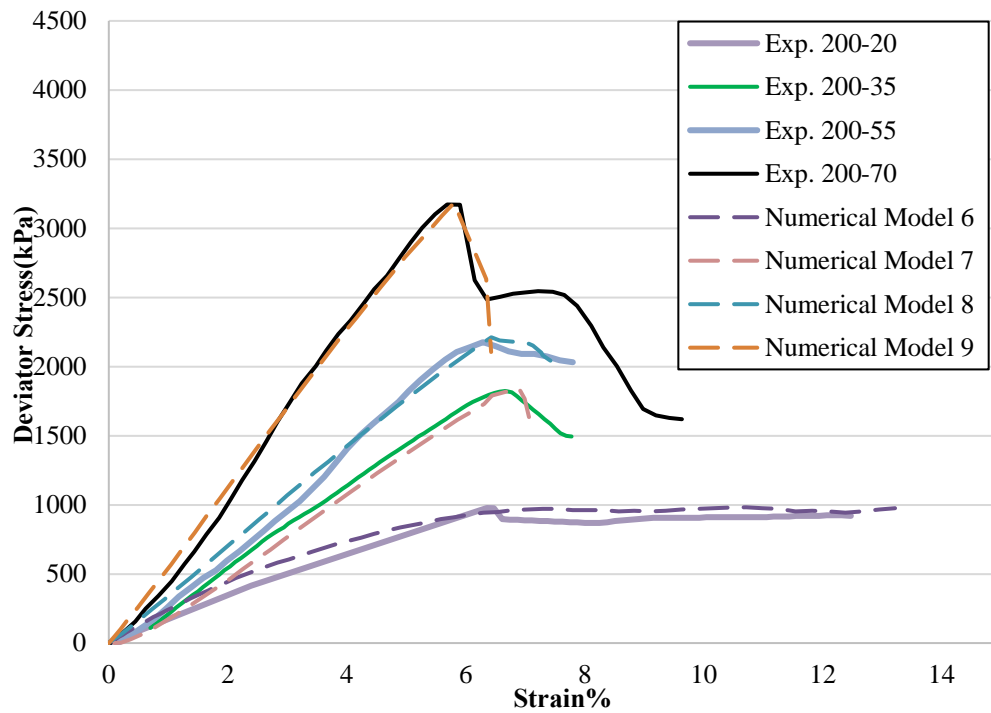
The Spatio-temporal model has been applied for varying cementation levels at two confining pressures. The results have been compared with the experimental plots obtained earlier. Fig. 4.22 presents the experimental and numerical stress-strain plots for 100 kPa confining pressure. The level of cementation varied from a low of 20% to a high of 88%. It can be seen that the prediction of the model is very close to the experimental observations. For 200 kPa confining pressure, the initial stiffness is



dramatically higher, and strain at maximum stress is significantly lower than that of the 100 kPa samples. Fig. 4.23 shows that the prediction of the model matched closely with the experimental ones in this case as well. This investigation demonstrates that the Spatio-temporal model is valid for the practical range of confining pressures and cementation.



**Figure 4.22.** Stress-strain plots for a confining pressure of 100kPa



**Figure 4.23.** Stress-strain plots for a confining pressure of 200kPa

#### 4.5. Concluding remarks

This paper presents numerical and experimental investigations for triaxial compression of sand columns. An extensive experimental project has been conducted to cover a wide range of cementation and confinement pressure. A numerical model has been developed to capture the entire range of behaviours. The novelty of the present numerical model is that it captures the Spatio-temporal variations of the biocementation process. A unit cell model has been developed to capture the inter-granular properties at different cementation levels. These properties have been plugged in the model to simulate the growing cementation levels. Gradual modelling of the cementation represents the Spatio-temporal nature of cementation. The numerical model has been validated with the existing experimental and numerical results. Then the model has been used on the range of experimental results generated in this investigation. Following conclusions can be made from this investigation:

- The micrographs in Fig. 5 illustrate the gradual growth of cementation that forms the basis of the present numerical model.

- The damage mechanics of cemented sand depends on two factors: level of cementation and confining pressure. At relatively low cementation, the samples bulge, while at higher cementation they fail by cracking.
- The Binary model was not successful post-stress pick.
- The Spatio-temporal behaviour of biocementation can be captured by randomly distributing the unit cells into the macro model. This process is a seminal improvement over the homogeneous cementation model used hitherto.
- The Spatio-temporal model also predicts the failure mode more accurately than conventional models.
- This investigation demonstrates that the Spatio-temporal model is valid for the entire practical range of confining pressures and cementation.

The models developed in the present investigation must be validated through further experiments, especially with field data. Research for the application of the current paradigm in the case of unconfined compression is ongoing and would be reported soon.

#### **4.6. Data Availability**

Some or all data, models, or code generated or used during the study are available from the corresponding author by request.

- Experimental data
- Numerical data

#### **4.7. References**

- Achal, V. and A. Mukherjee (2015). "A review of microbial precipitation for sustainable construction." Construction and Building Materials **93**: 1224-1235.
- Bardet, J. (1994). "Observations on the effects of particle rotations on the failure of idealized granular materials." Mechanics of Materials **18**(2): 159-182.
- Bardet, J. and J. Proubet (1991). "Numerical investigation of the structure of persistent shear bands in granular media." Géotechnique **41**(4): 599-613.
- Barkouki, T. H., B. C. Martinez, B. M. Mortensen, T. S. Weathers, J. D. De Jong, T. R. Ginn, N. F. Spycher, R. W. Smith and Y. Fujita (2011). "Forward and Inverse Bio-Geochemical Modeling of Microbially Induced Calcite Precipitation in Half-Meter Column Experiments." Transport in Porous Media **90**(1): 23.

- Belheine, N., J.-P. Plassiard, F.-V. Donzé, F. Darve and A. Seridi (2009). "Numerical simulation of drained triaxial test using 3D discrete element modeling." Computers and Geotechnics **36**(1-2): 320-331.
- Cheng, L., M. Shahin and R. Cord-Ruwisch (2014). "Bio-cementation of sandy soil using microbially induced carbonate precipitation for marine environments." Géotechnique **64**(12): 1010-1013.
- Chou, K.-C. (2011). "Some remarks on protein attribute prediction and pseudo amino acid composition." Journal of theoretical biology **273**(1): 236-247.
- DeJong, J. T., M. B. Fritzges and K. Nüsslein (2006). "Microbially induced cementation to control sand response to undrained shear." Journal of Geotechnical and Geoenvironmental Engineering **132**(11): 1381-1392.
- DeJong, J. T., B. M. Mortensen, B. C. Martinez and D. C. Nelson (2010). "Bio-mediated soil improvement." Ecological Engineering **36**(2): 197-210.
- DeJong, J. T., K. Soga, S. A. Banwart, W. R. Whalley, T. R. Ginn, D. C. Nelson, B. M. Mortensen, B. C. Martinez and T. Barkouki (2010). "Soil engineering in vivo: harnessing natural biogeochemical systems for sustainable, multi-functional engineering solutions." Journal of The Royal Society Interface **8**(54): 1-15.
- Díaz-Rodríguez, J. and J. López-Molina (2008). Strain thresholds in soil dynamics. Proceedings of the 14th World Conference on Earthquake Engineering.
- Dvorkin, J., A. Nur and H. Yin (1994). "Effective properties of cemented granular materials." Mechanics of Materials **18**(4): 351-366.
- Estrada, N., A. Lizcano and A. Taboada (2010). "Simulation of cemented granular materials. I. Macroscopic stress-strain response and strain localization." Physical Review E **82**(1): 011303.
- Evans, T., A. Khoubani and B. Montoya (2015). Simulating mechanical response in bio-cemented sands. Computer Methods and Recent Advances in Geomechanics: Proceedings of the 14th International Conference of International Association for Computer Methods and Recent Advances in Geomechanics, 2014 (IACMAG 2014), Taylor & Francis Books Ltd.
- Fauriel, S. and L. Laloui (2012). "A bio-chemo-hydro-mechanical model for microbially induced calcite precipitation in soils." Computers and Geotechnics **46**: 104-120.
- Feng, K. and B. Montoya (2015). "Influence of confinement and cementation level on the behavior of microbial-induced calcite precipitated sands under monotonic drained loading." Journal of Geotechnical and Geoenvironmental Engineering **142**(1): 04015057.
- Hannah Porter, N. K. D., Abhijit Mukherjee (2016). "Sustainable Road Bases with Microbial Carbonate Precipitation." SCMT4, Las Vegas, USA, August 7-11, 2016.
- Harkes, M. P., L. A. Van Paassen, J. L. Booster, V. S. Whiffin and M. C. van Loosdrecht (2010). "Fixation and distribution of bacterial activity in sand to induce carbonate precipitation for ground reinforcement." Ecological Engineering **36**(2): 112-117.
- Huang, J. and D. Airey (1998). "Properties of artificially cemented carbonate sand." Journal of Geotechnical and Geoenvironmental Engineering **124**(6): 492-499.
- Ismail, M. A., H. A. Joer, W. H. Sim and M. F. Randolph (2002). "Effect of cement type on shear behavior of cemented calcareous soil." Journal of Geotechnical and Geoenvironmental Engineering **128**(6): 520-529.

- Iwashita, K. and M. Oda (1998). "Rolling resistance at contacts in simulation of shear band development by DEM." Journal of engineering mechanics **124**(3): 285-292.
- Jiang, M., H.-S. Yu and D. Harris (2005). "A novel discrete model for granular material incorporating rolling resistance." Computers and Geotechnics **32**(5): 340-357.
- Jiang, M., F. Zhu and S. Utili (2015). "Investigation into the effect of backpressure on the mechanical behavior of methane-hydrate-bearing sediments via DEM analyses." Computers and Geotechnics **69**: 551-563.
- Karol, R. H. (2003). Chemical grouting and soil stabilization, revised and expanded, Crc Press.
- Kaur, N. P., J. K. Shah, S. Majhi and A. Mukherjee (2018). "Ultrasonic Monitoring of Healing of Concrete." Construction and Building Materials Communicated.
- Khoubani, A., T. M. Evans and B. M. Montoya, (2016). "Particulate Simulations of Triaxial Tests on Bio-Cemented Sand Using a New Cementation Model." Geo-Chicago 2016.
- Kozicki, J. and F. Donzé (2008). "A new open-source software developed for numerical simulations using discrete modeling methods." Computer Methods in Applied Mechanics and Engineering **197**(49): 4429-4443.
- Kozicki, J. and F. V. Donze (2008). "A new open-source software developed for numerical simulations using discrete modeling methods." Computer Methods in Applied Mechanics and Engineering **197**(49-50): 4429-4443.
- Li, G. (1985). "3D Constitutive Relationships for soils and experiment validation." Tsing Hua University.
- Martinez, B. C., J. T. DeJong and T. R. Ginn (2014). "Bio-geochemical reactive transport modeling of microbial induced calcite precipitation to predict the treatment of sand in one-dimensional flow." Computers and Geotechnics **58**: 1-13.
- Masson, S. and J. Martinez (2001). "Micromechanical analysis of the shear behavior of a granular material." Journal of engineering mechanics **127**(10): 1007-1016.
- Montoya, B., J. DeJong and R. Boulanger (2013). "Dynamic response of liquefiable sand improved by microbial-induced calcite precipitation." Géotechnique **63**(4): 302.
- Montoya, B., J. DeJong, R. W. Boulanger, D. W. Wilson, R. Gerhard, A. Ganchenko and J.-C. Chou (2012). Liquefaction mitigation using microbial induced calcite precipitation. GeoCongress 2012: State of the Art and Practice in Geotechnical Engineering: 1918-1927.
- Mortensen, B. and J. DeJong (2011). Strength and stiffness of MICP treated sand subjected to various stress paths. Geo-Frontiers 2011: Advances in Geotechnical Engineering: 4012-4020.
- O'Donnell, S. T., E. Kavazanjian Jr and B. E. Rittmann (2017). "MIDP: Liquefaction mitigation via microbial denitrification as a two-stage process. II: MICP." Journal of Geotechnical and Geoenvironmental Engineering **143**(12): 04017095.
- Oda, M., J. Konishi and S. Nemat-Nasser (1982). "Experimental micromechanical evaluation of strength of granular materials: effects of particle rolling." Mechanics of Materials **1**(4): 269-283.
- Porter, H., J. Blake, N. K. Dhami and A. Mukherjee (2018). "Rammed earth blocks with improved multifunctional performance." Cement & Concrete Composites **92**: 36-46.

- Porter, H., N. K. Dhimi and A. Mukherjee (2016). Sustainable Road Bases with Microbial Carbonate Precipitation. SCMT4, Las Vegas, USA, August 7-11, 2016.
- Porter, H., N. K. Dhimi and A. Mukherjee (2017). "Sustainable road bases with microbial precipitation." Proceedings of the Institution of Civil Engineers-Construction Materials: 1-14.
- Porter, H., N. K. Dhimi and A. Mukherjee (2017). "Synergistic chemical and microbial cementation for stabilization of aggregates." Cement and Concrete Composites.
- Saxena, S. K., A. S. Avramidis and K. R. Reddy (1988). "Dynamic moduli and damping ratios for cemented sands at low strains." Canadian Geotechnical Journal **25**(2): 353-368.
- Schnaid, F., D. M. Prietto Pedro and C. Consoli Nilo (2001). "Characterization of Cemented Sand in Triaxial Compression." Journal of Geotechnical and Geoenvironmental Engineering **127**(10): 857-868.
- Sitharam, T. and M. Nimbkar (1997). "Numerical modelling of the micromechanical behavior of granular media by discrete element method." Geotech. Eng. Bull **6**: 261-283.
- Van Paassen, L. A., C. M. Daza, M. Staal, D. Y. Sorokin, W. van der Zon and M. C. van Loosdrecht (2010). "Potential soil reinforcement by biological denitrification." Ecological Engineering **36**(2): 168-175.
- Wang, X. and J. Li (2014). "Simulation of triaxial response of granular materials by modified DEM." Science China Physics, Mechanics & Astronomy **57**(12): 2297-2308.
- Whiffin, V. S. (2004). Microbial CaCO<sub>3</sub> precipitation for the production of biocement, Murdoch University.
- Yang, P., S. O'Donnell, N. Hamdan, E. Kavazanjian and N. Neithalath (2017). "3D DEM Simulations of Drained Triaxial Compression of Sand Strengthened Using Microbially Induced Carbonate Precipitation." International Journal of Geomechanics **17**(6): 04016143.
- Zhao, X. and T. M. Evans (2009). "Discrete simulations of laboratory loading conditions." International Journal of Geomechanics **9**(4): 169-178.

# Chapter 5: A MICP Stabilised Unconfined Granular System

## Experimental Studies and Numerical Models for Granular Columns with Progressive Biocementation

Elaheh Kashizadeh <sup>1, a \*</sup> and Abhijit Mukherjee<sup>1, b</sup> Antoinette Tordesillas<sup>2, c</sup>

<sup>1</sup> Department of Civil Engineering, Curtin University, Bentley WA 6102 Australia

<sup>2</sup> Department of Mathematics & Statistics, The University of Melbourne, Victoria 3010 Australia

<sup>a</sup>[Elaheh.kashizadeh1@postgrad.curtin.edu.au](mailto:Elaheh.kashizadeh1@postgrad.curtin.edu.au),

<sup>b</sup>[Abhijit.mukherjee@curtin.edu.au](mailto:Abhijit.mukherjee@curtin.edu.au),

<sup>c</sup>[Atordes@unimelb.edu.au](mailto:Atordes@unimelb.edu.au)

### Abstract

This paper presents experimental and numerical investigations for modelling biocementation of granular columns. Sand columns have been biocemented at varying levels. Progress of cementation has been evidenced through scanning electron microscopy. Uniaxial compression test has been conducted on the cemented columns to obtain their stress-strain behaviour. Progressive damage until failure has been recorded using digital image correlation technique. A two-scale numerical model is proposed to capture both stress-strain behaviour and progressive damage. The unit grain properties at varying levels of cementation are estimated using a finite element model. The resulting properties have been used to develop a discrete element model of the sand columns that accounts for the Spatio-temporal progression of cementation. This model obviates the trial and error methods used hitherto. Results proof the capability of the model in simulating the stress-strain and damage mechanisms of bio-cemented columns under unconfined compression condition.

Keywords: granular materials; biocementation; unconfined compression; stress-strain plots; digital image correlation; failure mechanisms

## 5.1. Introduction

Cementation of granular materials is a fundamental requirement in construction technologies. Cementitious binders have evolved from mud to lime and industrial cement. The progression of cementation has improved the strength of cemented materials phenomenally. With the advent of cement, concrete has dominated as the preferred material for construction. More recently, the environmental penalty of industrial cement has been unravelled, and the need for a sustainable cementing material has been felt. Apart from concrete, cement is used in a large quantity in other applications such as soil stabilisation, mine backfills. Traditional soil improvement methods like cement or chemical treatment and soil replacement are not only costly and time-consuming, but they also affect the environment (DeJong et al., 2010a; Karol & Berardinelli, 2003). In the last decade, researchers have focused on finding an alternative method for improving the soil properties in a cost-effective and environmentally sustainable manner (DeJong et al., 2006; Van Paassen et al., 2010; Whiffin et al., 2007). Microbially Induced Calcium Carbonate Precipitation (MICP) that happens abundantly in nature. MICP process is considered a potential method of sustainable cementation of granular media (Madigan et al., 1997; Tiano et al., 2006; Whiffin, 2004). Biocement has been used in the restoration of stone monuments (Castanier et al., 2000; Rodriguez-Navarro et al., 2003), rammed earth construction (Porter et al., 2018a), soil improvement (Whiffin et al., 2007) as well as in concrete (Ramachandran et al., 2001a).

Different stages of sand grain cementation via MICP process have different use-cases. The shape of a heap of soil can be controlled by lightly cementing its grains to form clumping grains (Kashizadeh et al., 2020). Underground applications such as soil stabilisation, need an intermediate stage of cementation where the sand grains are subjected to confining stress (Kashizadeh et al., 2019), (Harkes., 2010)). Highly aggregated MICP samples are able to bear load without confinement. They have a number of overground applications improving engineering properties such as durability and strength (Achal et al., 2013a; Achal et al., 2013b; Qian et al., 2010; Reddy, 2013; Yang et al., 2011; Zhao et al., 2014). The unconfined compression strength of biocemented granular sand columns have been observed to have increased noticeably (Jiang et al., 2011; Oda et al., 1982; Porter et al., 2018b; Zhao et al., 2014).



To understand the mechanical behaviour of cemented sand, an insight into its inter-granular interactions is essential. Numerical models such as the discrete element method (DEM) have proved efficient in the modelling of loose sand columns within triaxial stress condition (Barkouki et al., 2011a; Gu et al., 2014; Kozicki & Donze, 2008; Martinez, 2012). Some studies on cemented sand are also reported. Stabilisation with biocement is fundamentally different from that with conventional cement. In biocementation, the aggregation builds up gradually with inherent variabilities in density and degree of cementation (Huang and Airey 1998). Thus, the numerical model becomes further complicated involving a coupled analysis of two phenomena: 1. a reactive transport process to determine the rate and distribution of cementation; 2. a load-resistance model to determine the mechanical properties of the cemented media. There are a few attempts to develop a coupled model. (Fauriel and Laloui 2012) have reported a coupled finite element model for this analysis where a homogenised property of the grains and the cement has been used, which ignores inter-grain interactions. A stand-alone reactive fluid transport model has been developed to determine the flow characteristics due to cementation (Martinez, DeJong et al. 2014); (Barkouki, Martinez et al. 2011). A number of load-resistance models following the traditional DEM techniques (Khoubani, Evans et al. 2016); (Jiang, Zhu et al. 2015) have also been reported. The degree of cementation has been included as inter-grain cohesive strength (Yang, O'Donnell et al. 2016). In general, an equivalent homogenised cohesive strength is assumed for the entire domain. In another variation, separate spheres as cement elements have been introduced (Khoubani, Evans et al. 2016). However, the increased computation does not improve the corresponding accuracy of the solution. In all these models, the stress-strain behaviour of columns as observed in experiments is matched in the computational model by adjusting the homogenised cohesive strength by trial and error (Evans, Khoubani et al. 2015).

This paper reports experimental and numerical investigations on mechanical properties of biocemented sand columns under unconfined compression condition. The novelty of this approach is 1) the inter-grain mechanical properties have been estimated for a range of cementation; 2) the prevailing trial and error approach for parameter matching is obviated through the introduction of the inter-grain properties; 3) an extensive experimental investigation has been performed to validate the numerical results, and 4) a comparison of the damage mechanism obtained through the experiments and that

predicted numerically has been presented. Bio-cemented samples were prepared at various level of aggregation from 0 to 88%. To assess the aggregation level of cemented grains Scanning Electron Microscopy (SEM) and Energy Dispersive X-ray Spectroscopy (EDS) have been performed. A finite element unit cell model has been developed to study the inter-granular behaviour at different levels of cementation. The unit cell results have been plugged into a global model of the sand column with statistically varying proportions of cementation. Both the stress-strain behaviour of the columns and their failure mechanisms has been estimated. The stress-strain behaviour is compared with that obtained experimentally. The failure paths have been compared with the experimental ones through Digital Image Correlation (DIC). The results show that the proposed numerical model is able to predict both stress-strain and the failure paths of aggregated granular systems.

## **5.2. Experimental Investigation**

This experimental investigation consists of three parts: preparation of samples with varying degree of cementation; performing unconfined compression tests with digital image correlation; and microscopic study for the degree of cementation.

### **5.2.1. Materials**

As it mentioned in the previous chapter, the material system is the combination of sand ( $D_{50} = 0.425$  mm) and cementation medium with 9% optimal moisture content. Details of cementation media have been explained in Chapter 4 (section 4.2.2)

### **5.2.2. Sample preparation**

The sand was compacted into a PVC mould of 50 mm diameter by 100 mm height with openings at top and bottom for injecting and discharging the fluids. The samples were treated for achieving varying levels of cementation. The samples were rinsed with 30mm calcium chloride solution to begin the treatment, in accordance with (Porter et al., 2017a). After an hour, one pore volume of bacterial solution was up flushed and retained for 12 hours. This was followed by periodic pumping of the cementation fluid containing urea and calcium chloride at an interval of 12 hours at 25°C. At the end of the treatment, all the samples were placed in a humidity-controlled chamber at 70°C over 7 days for drying. Samples were prepared in triplicate and treated with the

cementation solution for 0, 12, 21, 33, 42, 53 days. After 53 days, it became too difficult to feed and up flush the samples due to the high levels of aggregation.

### 5.2.3. Cementation levels

The estimate of calcium carbonate in each sample is presented in Table 3.2.

The relationship matrix between the levels of aggregation of the cement samples and the number of days treating the samples is presented in Table 5.1, Scanning Electron Micrograph (SEM) method is used to calculate the amount of participated calcium carbonate in each sample at a different stage of aggregation.

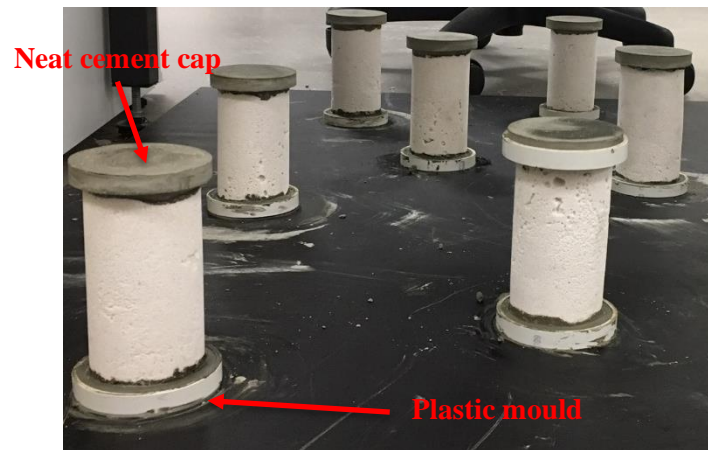
**Table 5.1:** Test matrix for the physical uniaxial test models

Treatment		CaCO <sub>3</sub> (g)	Number of samples
Days	%		
0	0	0	3
12	20	42	3
21	35	73.5	3
33	55	115.5	3
42	70	147	3
53	88	185.5	3

After demolding, the samples were capped on the top and bottom to avoid surface unevenness. A neat cement capping was used. The capping process was conducted per the AS 1012.9:2014 standard, as follow:

1. A stiff cement paste was prepared by mixing cement and water where the water/cement ratio was 0.35.
2. The cement pastes were put into the moulds then mount the samples from the bottom into the moulded cement paste. A measuring level was used for controlling the vertical and horizontal alignments of the samples.
3. Samples were left for 2 to 4 hours in this condition.
4. An amount of the stiff neat cement paste was placed on top of the cylindrical test specimen.

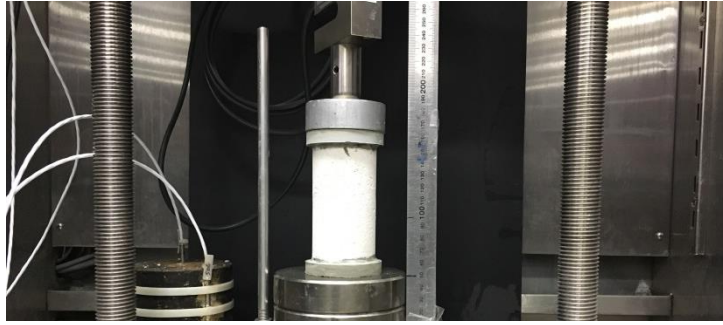
5. A glass plate having a thickness of not less than 6.5 mm and a diameter of at least 25 mm larger than the diameter of the test specimen was taken to level the samples.
6. The glass plate was pressed down the stiff cement paste by giving the container a rotary motion until it made complete contact with the rim of the mould. Before doing this, a thin layer of oil or grease on the glass plate applied to avoid adhesion of the paste with the glass plate.
7. After preparing the cap, it was left for some time to become hard.
8. Same procedure repeated to cap the other end of the cylindrical test specimen. The samples were demolded when they are dry (see Figure 5.1).



**Figure 5.1.** Cement Capped MICP samples for the UCS test

#### **5.2.4. Uniaxial Compressive Strength Test**

Uniaxial Compressive Strength tests were conducted in accordance with AS 5101.4 (AS5101.4, 2008). A universal testing machine (Shimadzu AGS – X) was used for the testing. The maximum load capacity was 10kN. The specimens were mounted on the bottom platen of the testing machine, and the top platen was lowered until it just touched the top of the specimen. The specimen was compressed at a constant displacement of 0.5 mm/min until failure. Force (N) and displacement (mm) were recorded electronically during the tests.



**Figure 5.2.** Experimental MICP samples under uniaxial compression test

The cylinder samples were tested to failure in simple compression at a constant rate of strain.

1. The length and diameter at three locations of samples were measured; the measurement was averaged to achieve the average length and diameter of each sample.
2. Flat stainless steel plates were placed at the top and bottom of the sample.
3. The travel rate was set 1 mm per minute. The value of both displacement and force before starting the compression device was set zero.

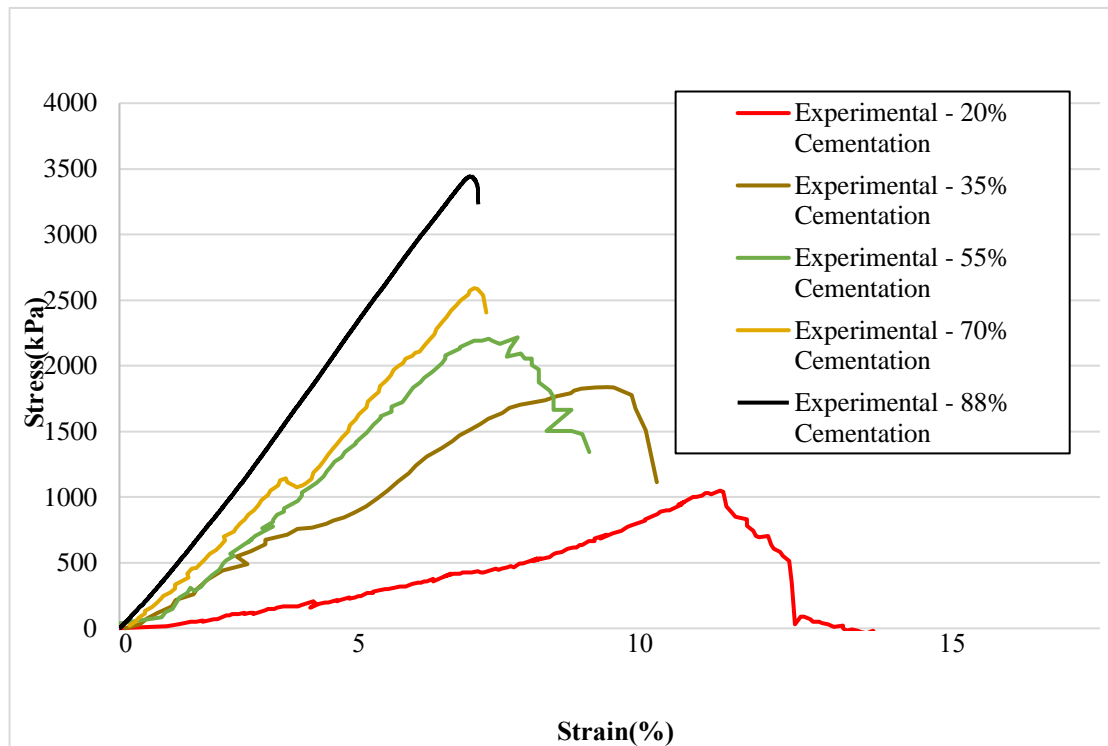
The load-deflection behaviour of each sample was recorded until failure.

The samples were photographed at defined load levels to observe the evolution of damage in them. The images were processed in a Digital Image Correlation (DIC) software to identify the strains, especially the horizontal strains, to track the cracks. MatLab software with a plugin NCORR, was used for this purpose.

### **5.2.5. Mechanical performance**

Figure 5.4 represents the stress-strain relationships for the different levels of aggregation. The graphs confirmed that the cementation had a noticeable effect on the strength of the samples. The maximum stress increased monotonically with the degree of cementation. It increased by around 3.5 times when the cementation went up from 20% to 88%. The stiffness of the samples too increased substantially, as evidenced by the increasing slope of the stress-strain curve. However, the strain at maximum stress reduced monotonically with the percentage of cementation. Thus, all the cementation makes the samples stronger; they become more brittle. Table 5.2. presents the stiffness,

maximum stress and the strain at maximum stress of each sample. These results are utilised in validating the numerical model.



**Figure 5.3.** Stress-stain curves with varying cementation

**Table 5.2.** The strength parameters with varying cementation

Cementation %	Initial stiffness (MPa)	Max stress (kPa)	Strain at maximum stress (%)
20%	6.1e7	1029.66	12
35%	1.9e8	1837.05	10
55%	3.2e8	2204.14	7.4
70%	3.3e8	2590.87	7.5
88%	3.7e8	3440.5	7.1

### 5.3. Numerical Modelling

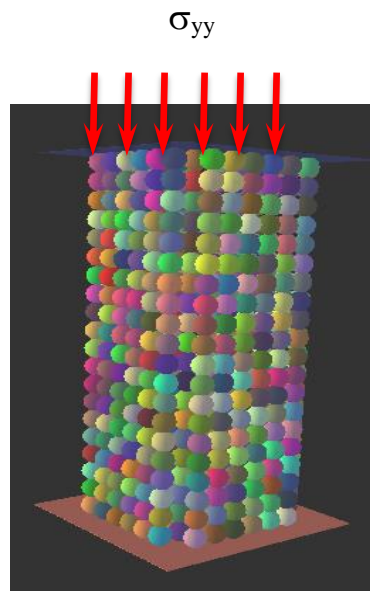
As discussed earlier to simulate the progressive cementation, a numerical model is proposed in this thesis to study the cemented cylindrical samples under uniaxial

compressive strength tests. For this purpose, a unit cell (section 4.3.1) designed to model the inter-grain behaviour of sand grains due to MICP treatment, the founding of the micro model is coupled to the DEM global model.

### 5.3.1. Global Model

A three-dimensional cylindrical model with spatial variation of cementation was developed using the YADE software based on DEM approach. The coding system was based on the soft-particle method (Belheine et al., 2009; Kozicki & Donzé, 2008). The linear contact model under compression was used., both stress-strain behaviour and the evolution of cracking are attempted by using the model.

A random pack of aggregated spheres was modelled in a cylindrical shape (Fig. 5.4). The diameter of the samples was 50mm, and the height was 100mm, they included around 10000 spheres, and the radii of the spheres varied between 0.15mm and 0.5mm. Using YADE, an equivalent network of interconnected cemented grains was created in the form of a cylinder. The bottom end of the cylinder was held fixed while a uniform downward displacement was applied on the top end. A nonlinear dynamic analysis calculated the ensuing deformation in the cylinder.

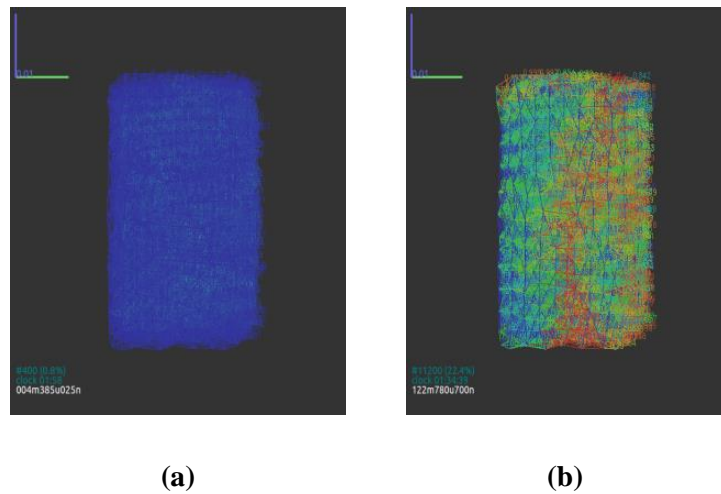


**Figure 5.4.** A numerical model for sand column

As discussed earlier, homogenous, non-homogenous binary and non-homogenous graded numerical models have been proposed in this thesis to simulate varying cementation. (Section 4.3.2).

It has been understood the non-homogenous graded numerical model not only is able to model the progression of cementation but also can model the cracks in cylindrical samples. Eleven types of material designed through the well-graded model are defined to model the samples for uniaxial compression test. (Section 4.3.2)

The samples were subjected to uniaxial compression at a constant rate until they collapsed. As the grains are tightly connected in the beginning, there was minimal inter-grain movement. As the load increased, the inter-grain stresses exceed the cohesive strength of the MICP at a few locations, resulting in grain separation or cracking. Cracking is signified by exaggerated inter-grain movement. With loading, the cracking grows, leading to the final collapse. By tracking the inter-grain movement, the damage evolution of the column can be obtained. Fig. 5.5 shows the initial and final maps of inter-grain movement for a typical column. The splitting failure of the sample is identified.

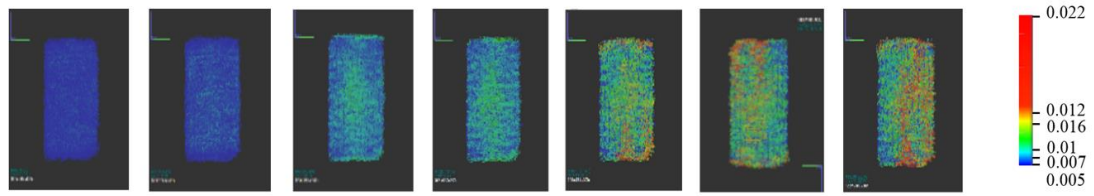


**Figure 5.5.** Initial and final states of a cylindrical sample under uniaxial compression

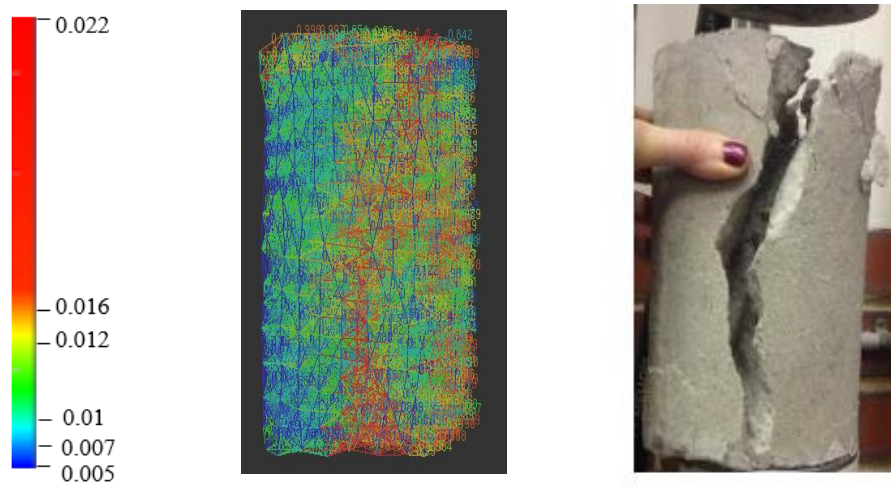
It can be noted that the DEM predicted a developing vertical crack as the loading progressed. The red areas representing the sand grains separations as in those areas, the distance between the grains had exceeded the average inter-grain distance at the beginning of the experiment. The DEM predicted a vertical split failure of the sample (Figure 5.6).



Figure 5.7 presents the failure predicted by the DEM and that obtained in the experiment. There is a striking similarity between the two. Thus, it can be concluded that the DEM was able to predict the failure mode of the aggregated MICP samples.



**Figure 5.6.** Inter-grain distances at different stages of the compression test – unit is mm



**Figure 5.7.** Comparison of the failure modes obtained through the experiment and the DEM simulation – unit is mm

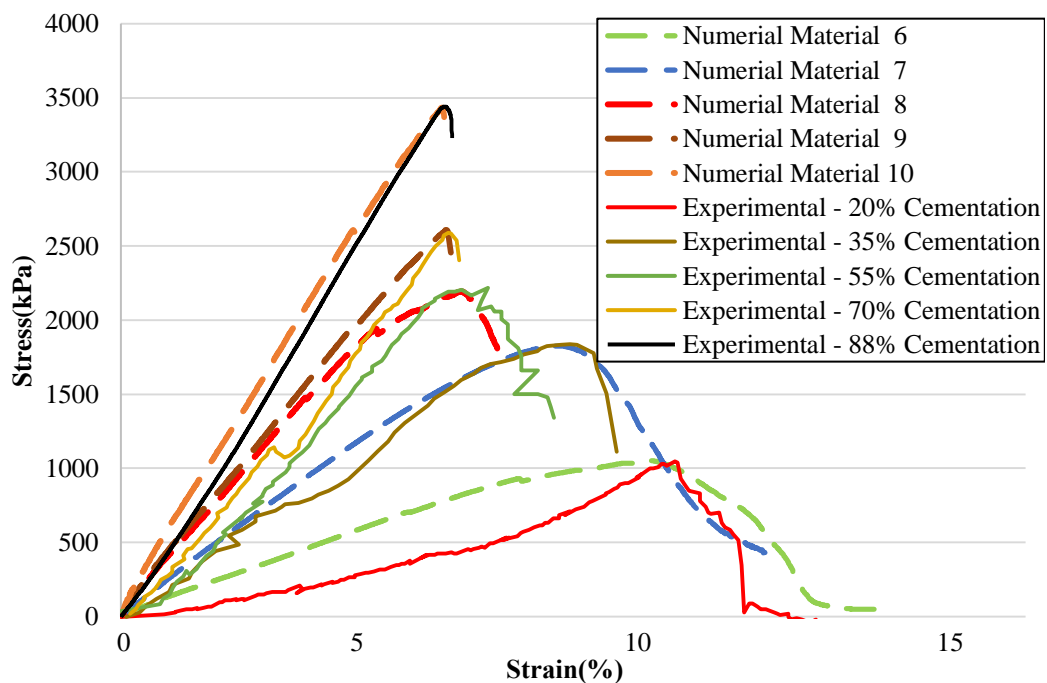
## 5.4. Numerical results and validation

The numerical model has been used for different cementation types as detailed in Table 4.6. Table 5.3 shows the parameters set for the numerical model. The stress-strain curves of all the cementation types have been plotted. They are compared with the experimentally obtained stress-strain graphs. An inherent difference between the numerical and the experimental results is that in case of numerical models, a detailed map of cementation levels could be generated, while in case of experiments only the total cement quantity could be estimated. Thus, the comparison is made based on the total amount of cement. Figure 5.8 illustrates the numerical and experimental stress-strain graphs. Cementation Types 6 to 10 agree well with cementation achieved from

20 to 88% experimentally. It can be seen that the experimental results and the numerical predictions agree well both in terms of maximum stress and strains. However, the undulations in the stress-strain path observed in the experiments are not found in the numerical models. The undulations in the experimental curves are due to local irregularities. The irregularities happen both in the contact between the sample and the platens as well as internal defects. These are not included in the numerical model.

**Table 5.3.** Parameters for the experimental models

Name of variable	Base value
Number of particles	10000
Time step	$5 \times 10^{-5}$ s
Particle size	0.15 - 1.0 mm
Density	2500 Kg/m <sup>3</sup>
Poisson ratio	0.4
Damping	0.4
Height of sample	100mm
Diameter of sample	50mm

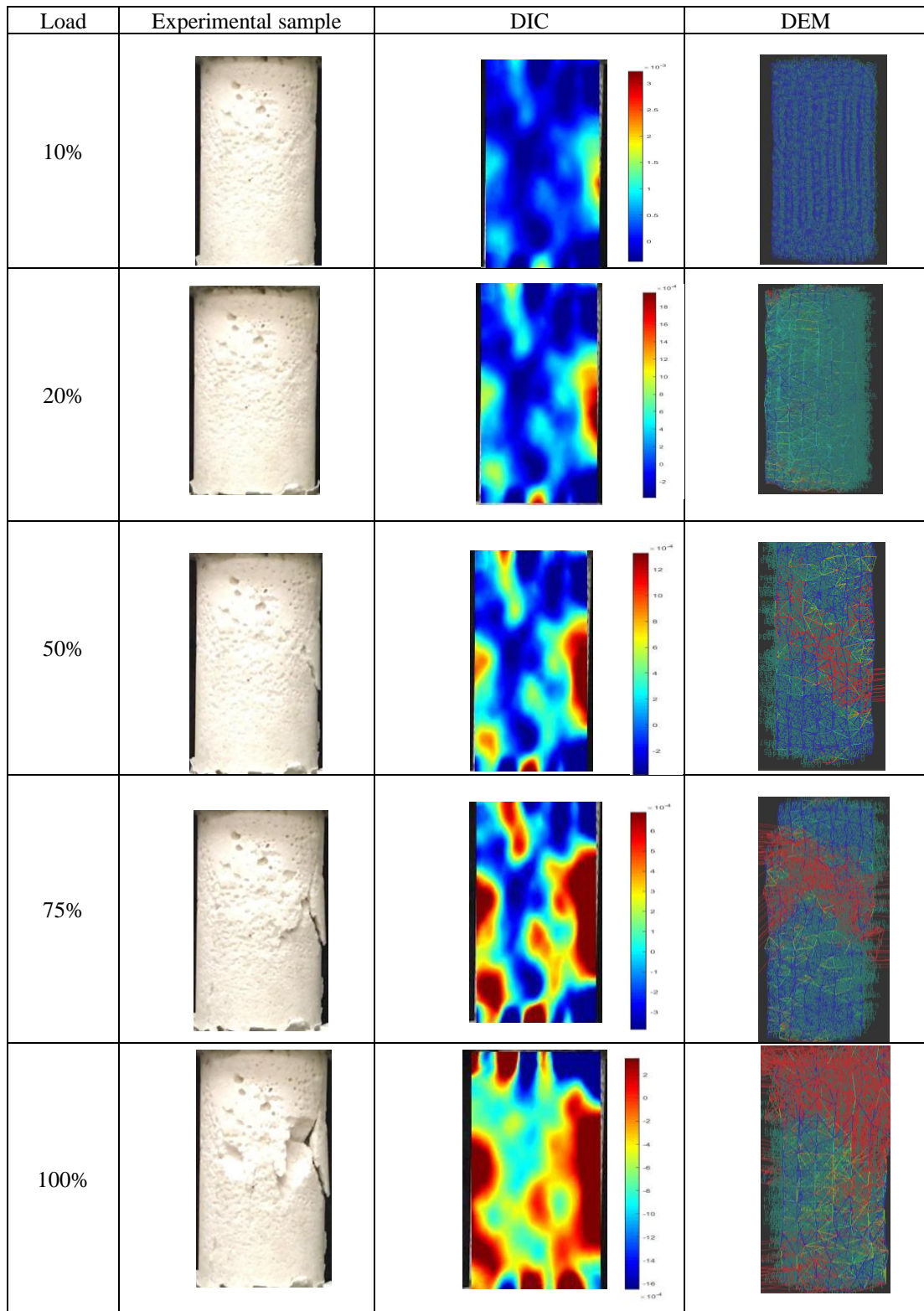


**Figure 5.8.** Comparison of experimental and numerical stress-strain plots

## 5.5. Evolution of Damage

Previous investigations included cementation as a uniform, cohesive bridge among all the grains. The cohesive strength parameters have been adjusted to match the numerical results with the experimental ones. However, such an approach would not capture the variations in the failure modes at different levels of cementation. This chapter studies the spatial variations of cementation through MICP process. This section compares the failure modes as observed in the experimental investigation and the numerical prediction. The evolution of damage is recorded in photographs of the specimens at the time of UCS testing (Fig. 5.9). It was observed that the cracks developed on the samples were not very clearly discerned. Therefore, a DIC analysis was performed to derive the strains from the observed grain movements. The areas of crack would have distinctly higher strains. It is noticed that the DIC images did identify the cracking zones very clearly. Finally, the DIC images have been compared with the inter-grain movement plots obtained from the DEM simulations.


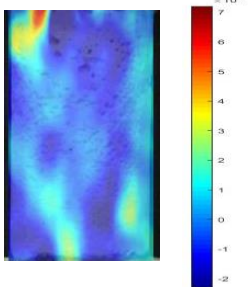
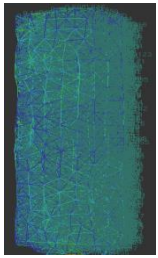

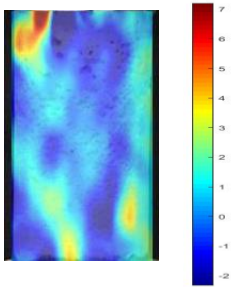
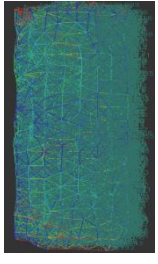
Fig. 5.9 shows the images at 35% cementation, which is a relatively low level of cementation. Even before loading, some voids are visible on the surface of the sample. At 50% load, spalling on the right side is noted that finally progresses to failure. As it is shown in DIC analysis, the damage happens on one side of the sample around 10% load. This damage gradually grew and coalesced with the crack from the left side, causing the failure. In the DEM no such early damage was seen. It is expected as the defects of the samples are not modelled in the DEM. However, by the time the load reached 50%, clear zones of damage were identified. This zone grew further, ultimately causing failure. Clearly, although the damage initiates at the locations of defect that is not modelled numerically, at an advanced stage, the correlation between the DIC and DEM is very good.

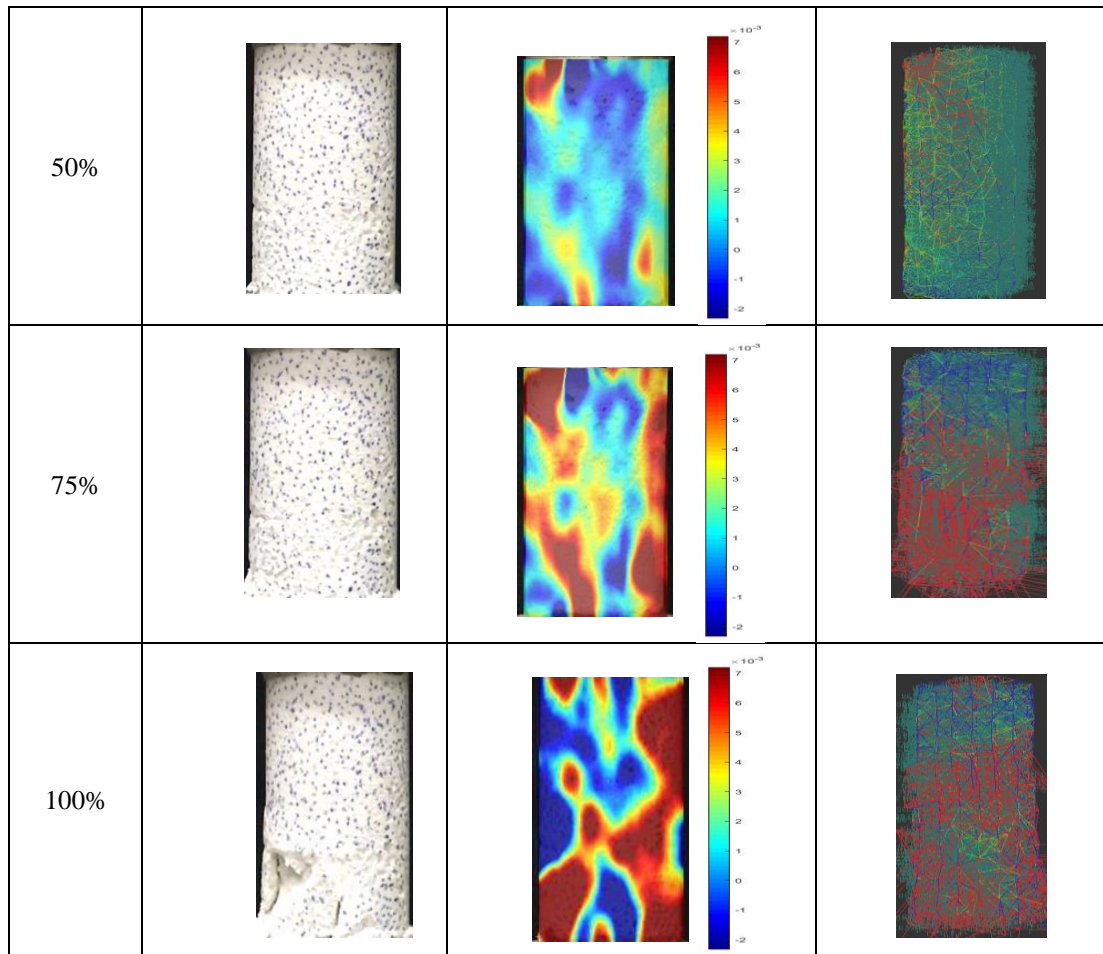


**Figure 5.9.** Damage evolution at 35% cementation

Fig. 5.10 presents the images for the sample with 55% cementation. At this level, no surface defect is observed in the sample. In the visual images, no sign of damage was observed until 75% loading. The sample failed suddenly with a spalling at the bottom of the sample. Compared to the sample with 35% cementation, this sample resisted damage until a considerably higher load level (75%). The damage progressed more rapidly from initiation to failure. It corroborates well with the stress-strain plots of the two samples. The sample with 35% cementation had a lower stiffness but higher strain at failure. Thus, its failure was gradual. The sample with 75% cementation had a considerably higher stiffness but a lower failure strain.

In the DIC, evident signs of strains at the top and bottom end of the sample was observed at 10% load. This is a classical mode of damage for a well-cemented sample. The strain zones extended with an increase in loading both from the top and bottom. At 75% loading, they coalesced and generated a bursting pressure on the exterior chunk of the sample. Finally, that chunk spalled out, causing failure of the sample. In DEM analysis, some signs of excessive grain movement in a small area at the top of the sample are noticed at 20% load. It grew gradually with the increase in load but remained relatively small until 75% load was reached. At the time of failure, excessive strain at the bottom of the sample is noticed. Thus, a stiff, brittle nature is seen in DEM as well at this level of cementation.

Load	Experimental sample	DIC	DEM
10%			
20%			



**Figure 5.10.** Damage evolution at 55% cementation


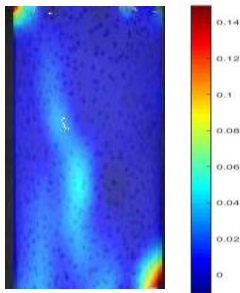
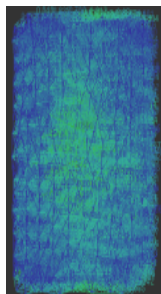

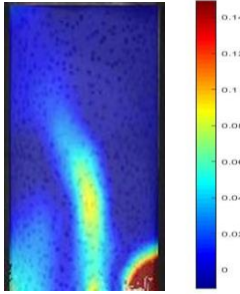
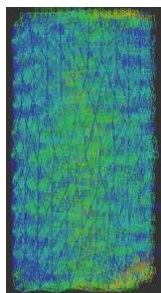
Fig. 5.11 shows Damage evolution at 70% loading. At this level, too no surface defect was observed on the sample. With the progression of loading, no visible damage could be noted until 75% load. The sample failed suddenly at 100% load. In this case, the failure mode was different from the samples with lower cementation. The sample split through the middle, as observed in heavily cemented concrete samples. DIC, however, shows that there are some excessive straining at the top and bottom corners even at 10% load.

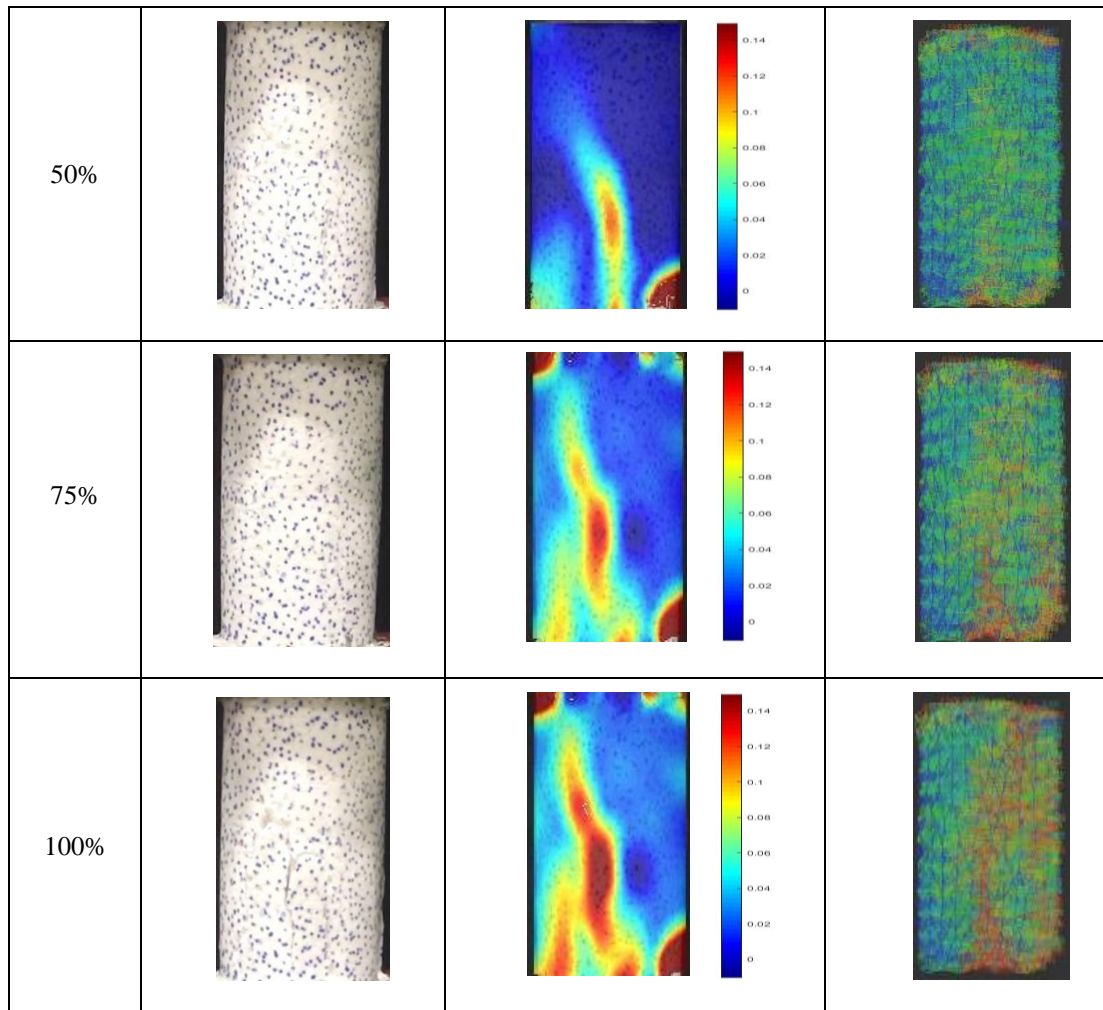
Along with that, another vertical line of strain in the middle of the sample is observed. At 20% load, the shear strain line has grown considerably, but the concentration at top has disappeared. The sample has adjusted the contact with the platen. The vertical line grows from the top to the bottom of the sample splitting it into two halves at failure. DEM shows high grain movement in a zone vertically oriented at the centre of the sample. However, the grain movements are much less than that observed in the



previous cases. This sample has the highest level of cementation, and therefore, it shows the most increased stiffness. A crack with a vertical orientation at the centre of the sample appears at 75% load. It rapidly expands, causing splitting of the specimen. This failure is similar to the one observed in DIC.

The present numerical technique is fundamentally different from the models presented hitherto in realistically modelling the spatial distribution of cementation in the column (refer to Table 4.1). Moreover, the trial and error method of parameter matching has been replaced with a detailed calculation of properties at various levels of cementation. The present model was accurate in the prediction of the stress-strain behaviour of the sand columns with a wide range of cementations. Developing this model is the first attempt to capture the local motions of the grains under load to capture the damage evolution. Through the experiments, it has been demonstrated that the damage evolution varies significantly with the level of cementation. The present numerical model is unique in capturing the local grain movements, and the damage evolution predicted by this model is close to that observed in the experiments.

Load	Experimental sample	Horizontal strain by DIC	Horizontal strain by DEM
10%			
20%			



**Figure 5.11.** Damage evolution at 70% cementation

## 5.6. Concluding remarks

This paper reports experimental and numerical investigations on biocemented sand columns with a widely varying level of cementation. A controlled laboratory experiment has been conducted to observe both stress-strain behaviour and damage evolution in the columns. A two-stage numerical model is proposed. At the first stage, finite element models for unit cells with varying cementation have been created. The properties obtained from the unit cell analysis have been plugged into a discrete element model of the column. The specialty of the model is that it realistically represents the distribution of different levels of cementation. The aim is to avoid the trial and error approach in selecting cementation parameters as well as to capture the damage evolution. Following major conclusions can be made from the present investigation:



- The cementation progresses with the cycles of treatment. However, at the initial stage, the cementation mainly covers the surface of the sand grains. Thus, a threshold level of cementation is necessary for the formation of cohesive bridges between the grains.
- When the level of cementation varied from 20% to 88%, the compressive strength went up from 1 MPa to nearly 3.5 MPa.
- Through cementation, the stiffness of the samples and the strain at failure are increased and dropped respectively. Thus, higher levels of cementation make the columns stronger but brittle.
- The finite element model of the unit cells with varying levels of cementation can capture the mechanical behaviour of the grains combined with the cementing element. They can be directly plugged into the global model of the column.
- The DEM with the spatial distribution of cementation as per its level realistically represents the mechanical system. The present model accurately predicted the stress-strain graph of the columns with a wide range of cementation.
- In the experiments, the damage evolution of the columns can be observed through the DIC images where the horizontal strain is plotted.
- A specialty of the present model is its ability to capture the grain movement of the sand column. Thus, the current model offers an opportunity to validate the damage evolution with the experimental results. This model has been successful in capturing the widely varying damage evolution patterns observed with different levels of cementation.

The present numerical model paves the way for a universal model for a wide range of biocemented systems. It should be possible to perform simulations at the field scale using the present paradigm. However, the computational time required by the model can be a challenge and may necessitate the use of massive computational facilities.

## 5.7. References

- Achal, V., A. Mukerjee, et al. (2013). "Biogenic treatment improves the durability and remediates the cracks of concrete structures." Construction and Building Materials **48**: 1-5.
- Achal, V., X. Pan, et al. (2013). "Remediation of Cr (VI) from chromium slag by biocementation." Chemosphere **93**(7): 1352-1358.
- Al Qabany, A., B. Mortensen, et al. (2011). "Microbial carbonate precipitation: correlation of S-wave velocity with calcite precipitation." Geo-Frontiers 2011: 3993-4001.
- AS5101.4 (2008). AS5101.4 - Methods for preparation and testing of stabilised materials. Method 4: Unconfined compressive strength of compacted materials. Sydney, NSW, Australia, Standards Australia.
- Barkouki, T., B. Martinez, et al. (2011). "Forward and inverse bio-geochemical modeling of microbially induced calcite precipitation in half-meter column experiments." Transport in Porous Media **90**(1): 23.
- Belheine, N., J.-P. Plassiard, et al. (2009). "Numerical simulation of drained triaxial test using 3D discrete element modeling." Computers and Geotechnics **36**(1-2): 320-331.
- Castanier, S., G. Le Metayer-Levrel, et al. (2000). Bacterial roles in the precipitation of carbonate minerals. Microbial sediments, Springer: 32-39.
- DeJong, J. T., M. B. Fritzges, et al. (2006). "Microbially induced cementation to control sand response to undrained shear." Journal of Geotechnical and Geoenvironmental Engineering **132**(11): 1381-1392.
- DeJong, J. T., B. M. Mortensen, et al. (2010). "Bio-mediated soil improvement." Ecological Engineering **36**(2): 197-210.
- DeJong, J. T., K. Soga, et al. (2010). "Soil engineering in vivo: harnessing natural biogeochemical systems for sustainable, multi-functional engineering solutions." Journal of The Royal Society Interface **8**(54): 1-15.
- Gu, X., M. Huang, et al. (2014). "DEM investigation on the evolution of microstructure in granular soils under shearing." Granular Matter **16**(1): 91-106.
- Hannah Porter, N. K. D., Abhijit Mukherjee (2016). "Sustainable Road Bases with Microbial Carbonate Precipitation." SCMT4, Las Vegas, USA, August 7-11, 2016.
- Harkes, M. P., L. A. Van Paassen, et al. (2010). "Fixation and distribution of bacterial activity in sand to induce carbonate precipitation for ground reinforcement." Ecological Engineering **36**(2): 112-117.
- Harkes., M. P., van Paassen., L. A.,Booster., J. L.,Whiffin., V. S.,van Loosdrecht., M. C. M. (2010). "Fixation and distribution of bacterial activity in sand to induce carbonate precipitation for ground reinforcement." Ecological Engineering **36**(2): 112-117.
- Jawad, F. and J.-J. Zheng (2016). "Improving Poorly Graded Fine Sand with Microbial Induced Calcite Precipitation."
- Jiang, M., H. Yan, et al. (2011). "Modeling shear behavior and strain localization in cemented sands by two-dimensional distinct element method analyses." Computers and Geotechnics **38**(1): 14-29.
- Karol, R. H. and C. Berardinelli (2003). "Chemical grouting and soil stabilization."
- Kashizadeh, E., A. Mukherjee, et al. "Numerical Model of Granular Materials Partially Cemented by Bacterial Calcite." ,V International conference on Particle-Based

- Methods -Fundamentals and Applications (PARTICLES 2017), 552-563, In Center Numerical Methods Engineering, 201.
- Kashizadeh, E., A. Mukherjee, et al. (2020). "Experimental and numerical investigation on heap formation of granular soil sparsely cemented by bacterial calcification." Powder Technology **360**: 253-263.
- Kashizadeh, E., A. Mukherjee, et al. (2019). "Experimental and Numerical Investigations on Confined Granular Systems Stabilised by Bacterial Cementation." Journal of Materials in Civil Engineering Communicated.
- Kozicki, J. and F. Donzé (2008). "A new open-source software developed for numerical simulations using discrete modeling methods." Computer Methods in Applied Mechanics and Engineering **197**(49): 4429-4443.
- Kuo, C.-Y., J. Frost, et al. (1996). "Three-dimensional image analysis of aggregate particles from orthogonal projections." Transportation Research Record: Journal of the Transportation Research Board(1526): 98-103.
- Madigan, M. T., J. M. Martinko, et al. (1997). Brock biology of microorganisms, Prentice hall Upper Saddle River, NJ.
- Martinez, B. C. (2012). Up-scaling of microbial induced calcite precipitation in sands for geotechnical ground improvement, University of California, Davis.
- Martinez, B. C. and J. T. DeJong (2009). Bio-mediated soil improvement: load transfer mechanisms at the micro-and macro-scales. Advances in Ground Improvement: Research to Practice in the United States and China: 242-251.
- Ng, T. T. and C. Wang (2001). "Comparison of a 3-D DEM simulation with MRI data." International Journal for Numerical and Analytical Methods in Geomechanics **25**(5): 497-507.
- Oda, M., J. Konishi, et al. (1982). "Experimental micromechanical evaluation of strength of granular materials: effects of particle rolling." Mechanics of Materials **1**(4): 269-283.
- Porter, H., J. Blake, et al. (2018). "Rammed earth blocks with improved multifunctional performance." Cement & Concrete Composites **92**: 36-46.
- Porter, H., N. K. Dhami, et al. (2017). "Sustainable road bases with microbial precipitation." Proceedings of the Institution of Civil Engineers-Construction Materials: 1-14.
- Porter, H., N. K. Dhami, et al. (2017). "Synergistic chemical and microbial cementation for stabilization of aggregates." Cement and Concrete Composites **83**: 160-170.
- Porter, H., N. K. Dhami, et al. (2018). "Sustainable road bases with microbial precipitation." Proceedings of the Institution of Civil Engineers - Construction Materials **171**(3): 95-108.
- Qian, C., R. Wang, et al. (2010). "Theory of Microbial Carbonate Precipitation and Its Application in Restoration of Cement-based Materials Defects." Chinese Journal of Chemistry **28**(5): 847-857.
- Ramachandran, S. K., V. Ramakrishnan, et al. (2001). "Remediation of concrete using micro-organisms." ACI Materials Journal-American Concrete Institute **98**(1): 3-9.
- Reddy, M. S. (2013). "Biomineralization of calcium carbonates and their engineered applications: a review." Frontiers in microbiology **4**: 314.
- Rodriguez-Navarro, C., M. Rodriguez-Gallego, et al. (2003). "Conservation of ornamental stone by *Myxococcus xanthus*-induced carbonate biomineralization." Appl. Environ. Microbiol. **69**(4): 2182-2193.
- Sarda, D., H. S. Choonia, et al. (2009). "Biocalcification by *Bacillus pasteurii* urease:

- a novel application." Journal of industrial microbiology & biotechnology **36**(8): 1111-1115.
- Tiano, P., E. Cantisani, et al. (2006). "Biomediated reinforcement of weathered calcareous stones." Journal of Cultural Heritage **7**(1): 49-55.
- Van Paassen, L. A. (2009). Biogrout, ground improvement by microbial induced carbonate precipitation, TU Delft, Delft University of Technology.
- Van Paassen, L. A., C. M. Daza, et al. (2010). "Potential soil reinforcement by biological denitrification." Ecological Engineering **36**(2): 168-175.
- Wang, Z., A. C. Bovik, et al. (2004). "Image quality assessment: from error visibility to structural similarity." IEEE transactions on image processing **13**(4): 600-612.
- Whiffin, V. S. (2004). Microbial CaCO<sub>3</sub> precipitation for the production of biocement, Murdoch University.
- Whiffin, V. S., L. A. van Paassen, et al. (2007). "Microbial carbonate precipitation as a soil improvement technique." Geomicrobiology Journal **24**(5): 417-423.
- Yang, Z., X. Cheng, et al. (2011). Engineering properties of MICP-bonded sandstones used for historical masonry building restoration. Geo-Frontiers 2011: Advances in Geotechnical Engineering: 4031-4040.
- Zhao, Q., L. Li, et al. (2014). "Factors affecting improvement of engineering properties of MICP-treated soil catalyzed by bacteria and urease." Journal of materials in civil engineering **26**(12): 04014094.

## **Chapter 6: Conclusions and Recommendations**

This research has studied different levels of cementation using the MICP process through a controlled physical approach (e.g., confined triaxial tests, unconfined compressive strength tests). The research investigates the mechanical behaviour of MICP samples in different stages of cementation. The experimental studies on the different phases of aggregation were modelled numerically through analytical and numerical approaches to design the granular systems under the effects of the MICP process; from very a low level of aggregation to the 88% MICP cemented materials.

A complete series of experimental and numerical studies have been conducted to investigate the essential parameters in this process. The numerical studies have been conducted in both the macro and micro scales.

The Discrete Element Method was employed to study the granular system and the effects of the MICP process at the macro level as a complex network. The approach was developed to simulate the impact of increasing the feeding cycles on the levels of aggregation between the sand grains. The Final Element approach was employed to define the cell characters in granular networks as the input to the DEM model at the macro scale to achieve more understanding with regards to the intergranular properties of the grains.

The most important conclusions are reviewed, and suggestions for future works are discussed in this chapter.

### **6.1 Conclusion**

In this research, the study of different levels of aggregation of the sand grains using the MICP process are categorised to three main stages:

- Loose and Semi-aggregated Sand Grains
- MICP stabilised confined granular system

- MICP stabilised unconfined granular system

The effect of the destabilising forces will be reported in the next step. This work is part of the modelling bio-cemented granular materials at three stages of cementation: 1) sparsely cemented and unconfined, where the grains form a heap; 2) cemented and confined, where the columns retain their shape as long as confinement has been applied; and 3) heavily cemented and unconfined, where the columns are able to withstand external loading without the necessity of confinement.

- Loose and Semi-aggregated Sand Grains

This thesis demonstrates the shapes of heaps of grains that are sparsely cemented by MICP. For this purpose, a controlled experiment has been performed to record the shapes of heaps with sparse cementation. The polynomial expression has been developed to define the shape of the heap. The expression is presented in two independent parameters: heap angle  $\theta$  and height-to-base ratio  $\eta$  (refer to equation 3.10). A discrete element model has been developed to model the cemented system, Present experimental results and published examples have been used to validate the DEM model. A parametric study for different material properties and level of cementation has been performed. Following conclusions can be made from the present study:

- The shape of a sand heap is significantly affected even at low levels of cementation.
- As it is shown in this research, the shape of the heap is defined by a 3rd degree polynomial. Limited experimental studies have conducted validation exercise. This expression may be refined when more results will be available in future.
- Heap angle  $\theta$  and height-to-base ratio  $\eta$  have been recognised as two independent parameters of the polynomial, which defined through an analytical model.
- It has been understood, both  $\theta$  and  $\eta$  rise with the degree of cementation.
- The proposed DEM model is capable of capturing the shapes of the heaps.
- By evaluating a series of micro parameters in the numerical model, it has been shown that damping has a marginal effect on the shape of the heap, while friction angle and grain size distribution influence the shape considerably.
- Sparse cementation can be modelled in DEM using clumping.

- The degree of clumping can be calibrated with the amount of calcium carbonate deposited due to biocementation.

The stage of study is limited to the prediction of the shape of a sparsely cemented sand heap only of a fixed mass.

- MICP stabilised confined granular system

In the next part of the thesis, numerical and experimental investigations have been done for triaxial compression of sand columns at widely varying levels of cementation and a range of confining pressure. An extensive experimental project has been conducted to cover a wide range of cementation and confinement pressure. A novel numerical model has been developed to capture the entire range of behaviours. The model captures the Spatio-temporal variation in the failure pattern as a function of the degree of biocementation To capture the inter-granular properties at different cementation levels; a unit cell model has been developed and introduced. Series of material properties are defined to simulate the Spatio-temporal nature of MICP cementation process. The existing experimental and numerical results have been used to validate the numerical model. Then the model has been used on the range of experimental results generated in this investigation. Following conclusions can be made from this investigation:

- The crystals grow to bridge the sand grains affecting cementation are shown in this research via the micrographs. They offer that cementation nucleates at several locations. The voids spaces between grains have been filled gradually due to cementation.
- The damage mechanics of cemented sand depends on two factors: level of cementation and confining pressure. At cementation levels up to 35%, the samples bulge considerably before failure. At higher cementation, vertical and diagonal cracking are the leading causes of failure.
- The samples with 200 kPa confinement generally show significantly higher stiffness and strength but lower ultimate strains than those at 100 kPa confinement.
- The mechanical behaviour of biocemented sand can be captured through a multi-scale model consisting of a unit cell and a macro model of the sand column. The unit cell model simulates two grains that are cemented with

varying width models. The inter-granular characteristics are varied at different levels of cementation. The sand column can be modelled through discrete elements consisting of the unit cells.

- The Spatio-temporal behaviour of biocementation can be captured by randomly distributing the unit cells into the macro model, this was simulated through the predefined numerical model engines in YADE software. This is a seminal improvement over the homogeneous cementation model used hitherto.
- The Spatio-temporal model does not need parameter matching by trial and error.
- Although it can model the undamaged state accurately, the homogeneous model predicts an over-stiff behaviour as damage initiates in the sample and softening starts. The binary model follows the experimental curve more closely than the homogeneous model; however, as the peak stress is reached, the model unloads very rapidly. The Spatio-temporal model followed the experimental curve very near all the way until failure. This demonstrates the suitability of the Spatio-temporal model.
- The Spatio-temporal model also predicts the failure mode more accurately than other models.
- This investigation demonstrates that the Spatio-temporal model is valid for the entire practical range of confining pressures and cementation.

The models developed in the present investigation must be validated through further experiments, especially with field data. Research on the application of the current paradigm in the case of unconfined compression is ongoing and would be reported soon.

- MICP stabilised unconfined granular system

In the last part of the thesis, experimental and numerical investigations on biocemented sand columns with a widely varying level of cementation are reported. A controlled laboratory experiment has been conducted to observe both stress-strain behaviour and damage evolution in the columns. A two-stage numerical model is proposed. At the first stage, finite element models for unit cells with varying cementation have been created. The properties obtained from the unit cell analysis have been plugged into a discrete element model of the column. The specialty of the model is that it realistically



represents the distribution of different levels of cementation. The aim is to avoid the trial and error approach in selecting cementation parameters as well as to capture the damage evolution. Following the significant conclusions can be made from the present research:

- The cementation progresses with the cycles of treatment. However, at the initial stage, the cementation mainly covers the surface of the sand grains. Thus, a threshold level of cementation is necessary for the formation of cohesive bridges between the grains.
- When the level of cementation varied from 20% to 88%, the compressive strength went up from 1 MPa to nearly 3.5 MPa.
- MICP cementation processes increase the stiffness of the samples dramatically. On the other hand, the strain at failure dropped with cementation. Thus, higher levels of cementation make the columns stronger but brittle.
- The finite element model of the unit cells with varying levels of cementation can capture the mechanical behaviour of the grains combined with the cementing element. They can be directly plugged into the global model of the column.
- The DEM with the spatial distribution of cementation as per its level realistically represents the mechanical system. The present model accurately predicted the stress-strain graph of the columns with a wide range of cementation.
- In the experiments, the damage evolution of the columns can be observed through the DIC images where the horizontal strain is plotted.
- A specialty of the present model is its ability to capture the grain movement of the sand column. Thus, the present model offers an opportunity to validate the damage evolution with the experimental results. This model has been successful in capturing the widely varying damage evolution patterns observed with different levels of cementation.

The present numerical model paves the way for a universal model for a wide range of biocemented systems. It should be possible to perform simulations at the field scale

using the present paradigm. However, the computational time required by the model can be a challenge and may necessitate the use of extensive computational facilities.

In conclusion, the proposed model in this study can model the inhomogeneous aggregation process of MICP and predict its effects on the engineering properties of aggregated sands.

Below are summarized the most critical conclusion points of this research:

- The DEM can model the aggregation of sand due to MICP at all of the stages. The overall stress-strain graphs matched well. However, understanding the DEM model's parameters plays a vital role in results.
- The open-source Yade software was able to model the failure modes of the MICP samples.
- The FEM can model the micro intergranular parameters between each of two grains connected through the calcium carbonate precipitation process.
- The main recognised physical parameter to control the MICP aggregation process is cohesion.
- The proposed DEM model can simulate the MICP process using a well-graded model by defining the different types of cohesion between the sand grains. The model can represent the inhomogeneity of the cementation.
- The shape of a semi-aggregated heap can be modelled by the clumping of grains to triads form.
- The stress-strain graphs of the aggregated cylinders, as obtained in the confined and unconfined experiment tests, can be emulated using the DEM. However, the limit strength parameters, such as the cohesion and plastic moment limit, have to be appropriately set.
- The inter-grain distance is a good measure for tracking the cracks in aggregated cylinders. The failure mode predicted by the DEM was very close to that obtained in the experiment.
- The failure modes and crack development behaviours captured using the DEM model had a good agreement with the digital image correlation approaches.

- Increasing the feeding cycles in the MICP process had a direct effect on increasing the strength of the granular materials.
- Considering the size and type of material and the porosity, the optimum number of days to achieve 100% aggregation could be achieved by 60 days feeding (120 cycles of feeding). A 40 ml cementation or bacterial solution was used in each process.
- The results confirmed the proposed numerical and experimental frameworks can design the MICP samples with optimum levels of aggregation.
- The effects of the MICP phenomenon on the mechanical behaviours of aggregated sand grains are investigated.
- The results of this investigation provide encouragement to explore the DEM modelling further for capturing the MICP process for a wide range of applications. A reliable numerical model would undoubtedly expand the understanding of this exciting new technology for a wide range of applications.

## **6.2 Recommendations**

Some of the recommendations and suggestions for futures work are as follows:

- Considering the price of calcium chloride, urea and the bacterial media, the current MICP process sounds costly. Although on an industrial scale, through mass production, the costs will be decreased; it is suggested that methods need to be developed for reducing the urea in the MICP process or extracting calcium from waste.
- Most of the MICP experiments have been conducted on the sand. It is recommended to study the effects of the MICP process on clayey soil as well.
- Although the results achieved in this study are promising, in the proposed numerical model, only the solid phase of the MICP process is modelled. It is suggested to model the fluid phase of the MICP process, which can be coupled with the current model to simulate the full picture of the MICP process through a numerical approach.

## Chapter 7: References

- (2006) *Year Book Australia, 2004, 2006*. Available online: <http://www.abs.gov.au/ausstats/abs@.nsf/Previousproducts/1301.0Feature%20Article32004> [Accessed].  
(!!! INVALID CITATION !!! ).
- Achal, V., Mukherjee, A. & Reddy, M. S. (2013a) Biogenic treatment improves the durability and remediates the cracks of concrete structures. *Construction and Building Materials*, 48, 1-5.
- Achal, V. & Mukherjee, A. (2015) A review of microbial precipitation for sustainable construction. *Construction and Building Materials*, 93, 1224-1235.
- Achal, V., Mukherjee, A., Goyal, S. & Reddy, M. S. (2012a) Corrosion prevention of reinforced concrete with microbial calcite precipitation. *ACI Materials journal*, 109(2).
- Achal, V., Mukherjee, A., Kumari, D. & Zhang, Q. (2015) Biomineralization for sustainable construction - A review of processes and applications. *Earth-Science Reviews*, 148, 1-17.
- Achal, V., Mukherjee, A. & Reddy, M. (2011) Effect of calcifying bacteria on permeation properties of concrete structures. *Journal of industrial microbiology & biotechnology*, 38(9), 1229-1234.
- Achal, V., Mukherjee, A. & Reddy, M. S. (2010) ORIGINAL RESEARCH: Biocalcification by *Sporosarcina pasteurii* using corn steep liquor as the nutrient source. *Industrial Biotechnology*, 6(3), 170-174.
- Achal, V., Pan, X., Lee, D.-J., Kumari, D. & Zhang, D. (2013b) Remediation of Cr (VI) from chromium slag by biocementation. *Chemosphere*, 93(7), 1352-1358.
- Achal, V., Pan, X. & Zhang, D. (2012b) Bioremediation of strontium (Sr) contaminated aquifer quartz sand based on carbonate precipitation induced by Sr resistant *Halomonas* sp. *Chemosphere*, 89(6), 764-768.
- Al Qabany, A., Mortensen, B., Martinez, B., Soga, K. & DeJong, J. (2011) Microbial carbonate precipitation: correlation of S-wave velocity with calcite precipitation. *Geo-Frontiers 2011*, 3993-4001.
- AS5101.4 (2008) *2008: AS5101.4 - Methods for preparation and testing of stabilised materials*. Sydney, NSW, Australia: Standards Australia.
- Bang, S. C. & Bang, S. S. (2011) KGS Awards Lectures: application of microbiologically induced soil stabilization technique for dust suppression. *International Journal of Geo-Engineering*, 3(2), 27-37.
- Bardet, J. (1994) Observations on the effects of particle rotations on the failure of idealized granular materials. *Mechanics of Materials*, 18(2), 159-182.
- Bardet, J. & Proubet, J. (1991) Numerical investigation of the structure of persistent shear bands in granular media. *Géotechnique*, 41(4), 599-613.
- Barkouki, T., Martinez, B., Mortensen, B., Weathers, T., De Jong, J., Ginn, T., Spycher, N., Smith, R. & Fujita, Y. (2011a) Forward and inverse bio-geochemical modeling of microbially induced calcite precipitation in half-meter column experiments. *Transport in Porous Media*, 90(1), 23.
- Barkouki, T. H., Martinez, B. C., Mortensen, B. M., Weathers, T. S., De Jong, J. D., Ginn, T. R., Spycher, N. F., Smith, R. W. & Fujita, Y. (2011b) Forward and Inverse Bio-Geochemical

Modeling of Microbially Induced Calcite Precipitation in Half-Meter Column Experiments. *Transport in Porous Media*, 90(1), 23-39.

Belheine, N., Plassiard, J.-P., Donzé, F.-V., Darve, F. & Seridi, A. (2009) Numerical simulation of drained triaxial test using 3D discrete element modeling. *Computers and Geotechnics*, 36(1-2), 320-331.

Benini, S., Gessa, C. & Ciurli, S. (1996) Bacillus pasteurii urease: a heteropolymeric enzyme with a binuclear nickel active site. *Soil Biology and Biochemistry*, 28(6), 819-821.

Bolander, P. & Yamada, A. (1999) *Dust palliative selection and application guide*.

Braissant, O., Cailleau, G., Dupraz, C. & Verrecchia, E. P. (2003) Bacterially induced mineralization of calcium carbonate in terrestrial environments: the role of exopolysaccharides and amino acids. *Journal of Sedimentary Research*, 73(3), 485-490.

Carstensen, J. T. & Chan, P.-C. (1976) Relation between particle size and repose angles of powders. *Powder Technology*, 15(1), 129-131.

Castanier, S., Le Metayer-Levrel, G. & Perthuisot, J.-P. (2000) Bacterial roles in the precipitation of carbonate minerals, *Microbial sediments* Springer, 32-39.

Cheng, L., Cord-Ruwisch, R. & Shahin, M. A. (2013) Cementation of sand soil by microbially induced calcite precipitation at various degrees of saturation. *Canadian Geotechnical Journal*, 50(1), 81-90.

Cheng, L., Shahin, M. & Cord-Ruwisch, R. (2014) Bio-cementation of sandy soil using microbially induced carbonate precipitation for marine environments. *Géotechnique*, 64(12), 1010-1013.

Cho, G.-C., Dodds, J. & Santamarina, J. C. (2006) Particle Shape Effects on Packing Density, Stiffness, and Strength: Natural and Crushed Sands. *Journal of Geotechnical and Geoenvironmental Engineering*, 132(5), 591-602.

Chou, K.-C. (2011) Some remarks on protein attribute prediction and pseudo amino acid composition. *Journal of theoretical biology*, 273(1), 236-247.

Chu, J., Stabnikov, V. & Ivanov, V. (2012) Microbially induced calcium carbonate precipitation on surface or in the bulk of soil. *Geomicrobiology Journal*, 29(6), 544-549.

Cundall, P. A. (1971) *The measurement and analysis of accelerations in rock slopes* University of London.

Cundall, P. A. & Strack, O. D. (1979) A discrete numerical model for granular assemblies. *Géotechnique*, 29(1), 47-65.

De Jong, J., Soga, K., Kavazanjian, E., Burns, S., Van Paassen, L., Al Quabany, A., Aydilek, A., Bang, S., Burbank, M. & Caslake, L. F. (2013) Biogeochemical processes and geotechnical applications: progress, opportunities and challenges. *Geotechnique*, 63 (4), 2013.

De Muynck, W., Debrouwer, D., De Belie, N. & Verstraete, W. (2008) Bacterial carbonate precipitation improves the durability of cementitious materials. *Cement and concrete research*, 38(7), 1005-1014.

DeJong, J. T., Fritzges, M. B. & Nüsslein, K. (2006) Microbially induced cementation to control sand response to undrained shear. *Journal of Geotechnical and Geoenvironmental Engineering*, 132(11), 1381-1392.

DeJong, J. T., Mortensen, B. M., Martinez, B. C. & Nelson, D. C. (2010a) Bio-mediated soil improvement. *Ecological Engineering*, 36(2), 197-210.

DeJong, J. T., Soga, K., Banwart, S. A., Whalley, W. R., Ginn, T. R., Nelson, D. C., Mortensen, B. M., Martinez, B. C. & Barkouki, T. (2010b) Soil engineering in vivo: harnessing natural biogeochemical systems for sustainable, multi-functional engineering solutions. *Journal of The Royal Society Interface*, 8(54), 1-15.

Derakhshani, S. M., Schott, D. L. & Lodewijks, G. (2015) Micro–macro properties of quartz sand: experimental investigation and DEM simulation. *Powder Technology*, 269, 127-138.

Dhami, N. K., Mukherjee, A. & Reddy, M. S. (2013) Viability of calcifying bacterial formulations in fly ash for applications in building materials. *Journal of Industrial Microbiology & Biotechnology*, 40(12), 1403-1413.

Dhami, N. K., Mukherjee, A. & Reddy, M. S. (2016a) Micrographical, mineralogical and nano-mechanical characterisation of microbial carbonates from urease and carbonic anhydrase producing bacteria. *Ecological Engineering*, 94, 443-454.

Dhami, N. K., Reddy, M. S. & Mukherjee, A. (2012) Improvement in strength properties of ash bricks by bacterial calcite. *Ecological Engineering*, 39, 31-35.

Dhami, N. K., Reddy, M. S. & Mukherjee, A. (2016b) Significant indicators for biomineralisation in sand of varying grain sizes. *Construction and Building Materials*, 104, 198-207.

Díaz-Rodríguez, J. & López-Molina, J. (2008) Strain thresholds in soil dynamics, *Proceedings of the 14th World Conference on Earthquake Engineering*.

Dimoudi, A. & Tompa, C. (2008) Energy and environmental indicators related to construction of office buildings. *Resources, Conservation and Recycling*, 53(1-2), 86-95.

Dvorkin, J., Nur, A. & Yin, H. (1994) Effective properties of cemented granular materials. *Mechanics of Materials*, 18(4), 351-366.

Eric, B. & Nick, L. (2015) *Beach Renourishment*.

Estrada, N., Lizcano, A. & Taboada, A. (2010) Simulation of cemented granular materials. I. Macroscopic stress-strain response and strain localization. *Physical Review E*, 82(1), 011303.

Evans, T., Khoubani, A. & Montoya, B. (2015) Simulating mechanical response in bio-cemented sands, *Computer Methods and Recent Advances in Geomechanics: Proceedings of the 14th International Conference of International Association for Computer Methods and Recent Advances in Geomechanics, 2014 (IACMAG 2014)*. Taylor & Francis Books Ltd.

Fauriel, S. & Laloui, L. (2012) A bio-chemo-hydro-mechanical model for microbially induced calcite precipitation in soils. *Computers and Geotechnics*, 46, 104-120.

Feng, K. & Montoya, B. (2015) Influence of confinement and cementation level on the behavior of microbial-induced calcite precipitated sands under monotonic drained loading. *Journal of Geotechnical and Geoenvironmental Engineering*, 142(1), 04015057.

Ferris, F., Stehmeier, L., Kantzas, A. & Mourits, F. (1996) Bacteriogenic mineral plugging. *Journal of Canadian Petroleum Technology*, 35(08).

Friedman, S. P. & Robinson, D. A. (2002) Particle shape characterization using angle of repose measurements for predicting the effective permittivity and electrical conductivity of saturated granular media. *Water Resources Research*, 38(11).

Gielen, D., Newman, J. & Patel, M. K. (2008) Reducing industrial energy use and CO<sub>2</sub> emissions: the role of materials science. *MRS bulletin*, 33(4), 471-477.

Gu, X., Huang, M. & Qian, J. (2014) DEM investigation on the evolution of microstructure in granular soils under shearing. *Granular Matter*, 16(1), 91-106.

Hannah Porter, N. K. D., Abhijit Mukherjee (2016) Sustainable Road Bases with Microbial Carbonate Precipitation. *SCMT4, Las Vegas, USA, August 7-11, 2016*.

Harkes, M. P., Van Paassen, L. A., Booster, J. L., Whiffin, V. S. & van Loosdrecht, M. C. (2010) Fixation and distribution of bacterial activity in sand to induce carbonate precipitation for ground reinforcement. *Ecological Engineering*, 36(2), 112-117.

Harkes, M. P., van Paassen, L. A., Booster, J. L., Whiffin, V. S., van Loosdrecht, M. C. M. (2010) Fixation and distribution of bacterial activity in sand to induce carbonate precipitation for ground reinforcement. *Ecological Engineering*, 36(2), 112-117.

Herrmann, H. J. (1998) On the Shape of a Sandpile, in H.J., H., JP, H. & S., L. (eds), *Physics of Dry Granular Media* NATO ASI Series (Series E: Applied Sciences) . Springer, Dordrecht.

Huang, J. & Airey, D. (1998) Properties of artificially cemented carbonate sand. *Journal of Geotechnical and Geoenvironmental Engineering*, 124(6), 492-499.

Imbabi, M. S., Carrigan, C. & McKenna, S. (2012) Trends and developments in green cement and concrete technology. *International Journal of Sustainable Built Environment*, 1(2), 194-216.

Ismail, M. A., Joer, H. A., Sim, W. H. & Randolph, M. F. (2002) Effect of cement type on shear behavior of cemented calcareous soil. *Journal of Geotechnical and Geoenvironmental Engineering*, 128(6), 520-529.

Iwashita, K. & Oda, M. (1998) Rolling resistance at contacts in simulation of shear band development by DEM. *Journal of engineering mechanics*, 124(3), 285-292.

Jacobson, D. E., Valdes, J. R. & Evans, T. M. (2007) A numerical view into direct shear specimen size effects. *Geotechnical Testing Journal*, 30(6), 512-516.

Jiang, M., Yan, H., Zhu, H. & Utili, S. (2011) Modeling shear behavior and strain localization in cemented sands by two-dimensional distinct element method analyses. *Computers and Geotechnics*, 38(1), 14-29.

Jiang, M., Yu, H.-S. & Harris, D. (2005) A novel discrete model for granular material incorporating rolling resistance. *Computers and Geotechnics*, 32(5), 340-357.

Jiang, M., Zhu, F. & Utili, S. (2015) Investigation into the effect of backpressure on the mechanical behavior of methane-hydrate-bearing sediments via DEM analyses. *Computers and Geotechnics*, 69, 551-563.

Jonkers, H. M. & Schlangen, E. (2008) Development of a bacteria-based self healing concrete, *Proc. int. FIB symposium*.

Karol, R. H. (2003) *Chemical grouting and soil stabilization, revised and expanded*, 12Crc Press.

Karol, R. H. & Berardinelli, C. (2003) Chemical grouting and soil stabilization.

Kashizadeh, E., Mukherjee, A. & Tordesillas, A. (2020) Experimental and numerical investigation on heap formation of granular soil sparsely cemented by bacterial calcification. *Powder Technology*, 360, 253-263.

Kashizadeh, E., Mukherjee, A. & Tordesillas, A. (2019) Experimental and Numerical Investigations on Confined Granular Systems Stabilised by Bacterial Cementation. *Journal of Materials in Civil Engineering*, Communicated.

Kaur, N. P., Shah, J. K., Majhi, S. & Mukherjee, A. (2018) Ultrasonic Monitoring of Healing of Concrete. *Construction and Building Materials*, Communicated.

Khoubani, A., Evans, T. & Montoya, B. (2016) Particulate simulations of triaxial tests on bio-cemented sand using a new cementation model, *Geo-Chicago 2016*, 84-93.

Khoubani, A. & Evans, T. M. (2018) An efficient flexible membrane boundary condition for DEM simulation of axisymmetric element tests. *International Journal for Numerical and Analytical Methods in Geomechanics*, 42(4), 694-715.

Kozicki, J. & Donzé, F. (2008) A new open-source software developed for numerical simulations using discrete modeling methods. *Computer Methods in Applied Mechanics and Engineering*, 197(49), 4429-4443.

Kozicki, J. & Donze, F. V. (2008) A new open-source software developed for numerical simulations using discrete modeling methods. *Computer Methods in Applied Mechanics and Engineering*, 197(49-50), 4429-4443.

Kozicki, J. & Tejchman, J. (2011) Numerical simulations of sand behaviour using DEM with two different descriptions of grain roughness, *II International Conference on Particle-based Methods—Fundamentals and Applications. Particles*.

Kuo, C.-Y., Frost, J., Lai, J. & Wang, L. (1996) Three-dimensional image analysis of aggregate particles from orthogonal projections. *Transportation Research Record: Journal of the Transportation Research Board*(1526), 98-103.

Le Metayer-Levrel, G., Castanier, S., Oriol, G., Loubiere, J.-F. & Perthuisot, J.-P. (1999) Applications of bacterial carbonatogenesis to the protection and regeneration of limestones in buildings and historic patrimony. *Sedimentary geology*, 126(1-4), 25-34.

Lohnes, R. A. & Coree, B. (2002) *Determination and evaluation of alternate methods for managing and controlling highway-related dust*.

Madigan, M. T., Martinko, J. M. & Parker, J. (1997) *Brock biology of microorganisms*, 11Prentice hall Upper Saddle River, NJ.

Martinez, B. C. (2012) *Up-scaling of microbial induced calcite precipitation in sands for geotechnical ground improvement* University of California, Davis.

Martinez, B. C. & DeJong, J. T. (2009) Bio-mediated soil improvement: load transfer mechanisms at the micro-and macro-scales, *Advances in Ground Improvement: Research to Practice in the United States and China*, 242-251.

Martinez, B. C., DeJong, J. T. & Ginn, T. R. (2014) Bio-geochemical reactive transport modeling of microbial induced calcite precipitation to predict the treatment of sand in one-dimensional flow. *Computers and Geotechnics*, 58, 1-13.

Masson, S. & Martinez, J. (2001) Micromechanical analysis of the shear behavior of a granular material. *Journal of engineering mechanics*, 127(10), 1007-1016.

Matuttis, H.-G. (1998) Simulation of the pressure distribution under a two-dimensional heap of polygonal particles. *Granular Matter*, 1(2), 83-91.

Mehta, P. K. (2004) High-performance, high-volume fly ash concrete for sustainable development, *Proceedings of the international workshop on sustainable development and concrete technology*. Iowa State University Ames, IA, USA.

Miller, R. L. & Byrne, R. J. (1966) The angle of repose for a single grain on a fixed rough bed. *Sedimentology*, 6(4), 303-314.

Montoya, B., DeJong, J. & Boulanger, R. (2013) Dynamic response of liquefiable sand improved by microbial-induced calcite precipitation. *Géotechnique*, 63(4), 302.

Montoya, B., DeJong, J., Boulanger, R. W., Wilson, D. W., Gerhard, R., Ganchenko, A. & Chou, J.-C. (2012) Liquefaction mitigation using microbial induced calcite precipitation, *GeoCongress 2012: State of the Art and Practice in Geotechnical Engineering*, 1918-1927.

Mortensen, B. & DeJong, J. (2011) Strength and stiffness of MICP treated sand subjected to various stress paths, *Geo-Frontiers 2011: Advances in Geotechnical Engineering*, 4012-4020.

Mortensen, B., Haber, M., DeJong, J., Caslake, L. & Nelson, D. (2011) Effects of environmental factors on microbial induced calcium carbonate precipitation. *Journal of applied microbiology*, 111(2), 338-349.

Mujah, D., Shahin, M. A. & Cheng, L. (2017) State-of-the-Art Review of Biocementation by Microbially Induced Calcite Precipitation (MICP) for Soil Stabilization. *Geomicrobiology Journal*, 34(6), 524-537.

Nemati, M. & Voordouw, G. (2003) Modification of porous media permeability, using calcium carbonate produced enzymatically in situ. *Enzyme and Microbial Technology*, 33(5), 635-642.

Ng, T. T. & Wang, C. (2001) Comparison of a 3-D DEM simulation with MRI data. *International Journal for Numerical and Analytical Methods in Geomechanics*, 25(5), 497-507.

Ng, W.-S., Lee, M.-L. & Hii, S.-L. (2012) An overview of the factors affecting microbial-induced calcite precipitation and its potential application in soil improvement. *World Academy of Science, Engineering and Technology*, 62, 723-729.

O'Donnell, S. T., Kavazanjian Jr, E. & Rittmann, B. E. (2017) MIDP: Liquefaction mitigation via microbial denitrification as a two-stage process. II: MICP. *Journal of Geotechnical and Geoenvironmental Engineering*, 143(12), 04017095.

Oda, M., Konishi, J. & Nemat-Nasser, S. (1982) Experimental micromechanical evaluation of strength of granular materials: effects of particle rolling. *Mechanics of Materials*, 1(4), 269-283.

Okwadha, G. D. & Li, J. (2010) Optimum conditions for microbial carbonate precipitation. *Chemosphere*, 81(9), 1143-1148.

Pilpel, N. (1970) Cohesive pharmaceutical powders. *Advances in pharmaceutical sciences*, 3, 173-219.

Polat Pelin, Asha Latha Ramachandran, Abhijit Mukherjee & Dhama, N. K. (2018) Characterisation of beach rock biocementation in natural and in vitro conditions. *Frontiers of Microbiology*, Communicated.



- Porter, H., Blake, J., Dhami, N. K. & Mukherjee, A. (2018a) Rammed earth blocks with improved multifunctional performance. *Cement & Concrete Composites*, 92, 36-46.
- Porter, H., Dhami, N. & Mukherjee, A. (2016a) Sustainable road bases with Microbial carbonate precipitation, *Fourth International conference on Sustainable Construction Materials and Technologies*. Las Vegas, USA, 7-11 August 2016.
- Porter, H., Dhami, N. K. & Mukherjee, A. (2016b) Sustainable Road Bases with Microbial Carbonate Precipitation, *SCMT4, Las Vegas, USA, August 7-11, 2016*.
- Porter, H., Dhami, N. K. & Mukherjee, A. (2017a) Sustainable road bases with microbial precipitation. *Proceedings of the Institution of Civil Engineers-Construction Materials*, 1-14.
- Porter, H., Dhami, N. K. & Mukherjee, A. (2017b) Synergistic chemical and microbial cementation for stabilization of aggregates. *Cement and Concrete Composites*.
- Porter, H., Dhami, N. K. & Mukherjee, A. (2018b) Sustainable road bases with microbial precipitation. *Proceedings of the Institution of Civil Engineers - Construction Materials*, 171(3), 95-108.
- Qian, C., Wang, R., Cheng, L. & Wang, J. (2010) Theory of Microbial Carbonate Precipitation and Its Application in Restoration of Cement-based Materials Defects. *Chinese Journal of Chemistry*, 28(5), 847-857.
- Ramachandran, S. K., Ramakrishnan, V. & Bang, S. S. (2001a) Remediation of concrete using micro-organisms. *ACI Materials Journal-American Concrete Institute*, 98(1), 3-9.
- Ramachandran, S. K., Ramakrishnan, V. & Bang, S. S. (2001b) Remediation of concrete using microorganisms. *ACI Materials journal*, 98(1).
- Reddy, M. S. (2013) Biomineralization of calcium carbonates and their engineered applications: a review. *Frontiers in microbiology*, 4, 314.
- Robinson, D. & Friedman, S. (2002) Observations of the effects of particle shape and particle size distribution on avalanching of granular media. *Physica A: Statistical Mechanics and its Applications*, 311(1), 97-110.
- Rodriguez-Navarro, C., Rodriguez-Gallego, M., Chekroun, K. B. & Gonzalez-Munoz, M. T. (2003) Conservation of ornamental stone by *Myxococcus xanthus*-induced carbonate biomineralization. *Appl. Environ. Microbiol.*, 69(4), 2182-2193.
- Rushing, J. F., Moore, V. M. & Tingle, J. S. (2006) *Evaluation of chemical dust palliatives for helipads*.
- Saxena, S. K., Avramidis, A. S. & Reddy, K. R. (1988) Dynamic moduli and damping ratios for cemented sands at low strains. *Canadian Geotechnical Journal*, 25(2), 353-368.
- Schnaid, F., Prietto Pedro, D. M. & Consoli Nilo, C. (2001) Characterization of Cemented Sand in Triaxial Compression. *Journal of Geotechnical and Geoenvironmental Engineering*, 127(10), 857-868.
- Shaffer, G. (2010) Long-term effectiveness and consequences of carbon dioxide sequestration. *Nature Geoscience*, 3(7), 464-467.
- Sharma, A. & Bhattacharya, A. (2010) Enhanced biomimetic sequestration of CO<sub>2</sub> into CaCO<sub>3</sub> using purified carbonic anhydrase from indigenous bacterial strains. *Journal of molecular catalysis B: Enzymatic*, 67(1), 122-128.
- Sitharam, T. & Nimbkar, M. (1997) Numerical modelling of the micromechanical behavior of granular media by discrete element method. *Geotech. Eng. Bull.*, 6, 261-283.
- Steffen, W., Hunter, J. & Hughes, I. (2014) *Counting the Costs: Climate Change and Coastal Flooding*.
- Stocks-Fischer, S., Galinat, J. K. & Bang, S. S. (1999) Microbiological precipitation of CaCO<sub>3</sub>. *Soil Biology and Biochemistry*, 31(11), 1563-1571.
- Suiker, A. S. & Fleck, N. A. (2004) Frictional collapse of granular assemblies. *Journal of Applied Mechanics*, 71(3), 350-358.
- Thomas, P. A. & Bray, J. D. (1999) Capturing Nonspherical Shape of Granular Media with Disk Clusters. *Journal of Geotechnical and Geoenvironmental Engineering*, 125(3), 169-178.

- Tiano, P., Cantisani, E., Sutherland, I. & Paget, J. (2006) Biomediated reinforcement of weathered calcareous stones. *Journal of Cultural Heritage*, 7(1), 49-55.
- Ting, J. M., Meachum, L. & Rowell, J. D. (1995) Effect of particle shape on the strength and deformation mechanisms of ellipse-shaped granular assemblages. *Engineering computations*, 12(2), 99-108.
- Train, D. (1958) Some aspects of the property of angle of repose of powders. *Journal of Pharmacy and Pharmacology*, 10(S1), 127T-135T.
- Umar, M., Kassim, K. A. & Chiet, K. T. P. (2016a) Biological process of soil improvement in civil engineering: A review. *Journal of Rock Mechanics and Geotechnical Engineering*, 8(5), 767-774.
- Umar, M., Kassim, K. A. & Ping Chiet, K. T. (2016b) Biological process of soil improvement in civil engineering: A review. *Journal of Rock Mechanics and Geotechnical Engineering*, 8(5), 767-774.
- Utili, S. & Nova, R. (2008) DEM analysis of bonded granular geomaterials. *International Journal for Numerical and Analytical Methods in Geomechanics*, 32(17), 1997-2031.
- Van Paassen, L., Harkes, M., Van Zwieten, G., Van der Zon, W., Van der Star, W. & Van Loosdrecht, M. (2009) Scale up of BioGrout: a biological ground reinforcement method, *Proceedings of the 17th international conference on soil mechanics and geotechnical engineering*. Lansdale IOS Press.
- van Paassen, L., Isimite, J., Picioreanu, C. & van Loosdrecht, M. (2008) Computational model to study microbial carbonate precipitation in porous media at micro-scale. *Proc. 1st Int. Conf. on Bio-Geo-Civil Engineering, 23–25 June, The Netherlands*, 45-50.
- Van Paassen, L. A., Daza, C. M., Staal, M., Sorokin, D. Y., van der Zon, W. & van Loosdrecht, M. C. (2010) Potential soil reinforcement by biological denitrification. *Ecological Engineering*, 36(2), 168-175.
- Wang, X. & Li, J. (2014) Simulation of triaxial response of granular materials by modified DEM. *Science China Physics, Mechanics & Astronomy*, 57(12), 2297-2308.
- Wang, Z., Bovik, A. C., Sheikh, H. R. & Simoncelli, E. P. (2004) Image quality assessment: from error visibility to structural similarity. *IEEE transactions on image processing*, 13(4), 600-612.
- Warren, L. A., Maurice, P. A., Parmar, N. & Ferris, F. G. (2001) Microbially mediated calcium carbonate precipitation: implications for interpreting calcite precipitation and for solid-phase capture of inorganic contaminants. *Geomicrobiology Journal*, 18(1), 93-115.
- Wensrich, C. & Katterfeld, A. (2012) Rolling friction as a technique for modelling particle shape in DEM. *Powder Technology*, 217, 409-417.
- Whiffin, V. S. (2004) *Microbial CaCO<sub>3</sub> precipitation for the production of biocement* Murdoch University.
- Whiffin, V. S., van Paassen, L. A. & Harkes, M. P. (2007) Microbial carbonate precipitation as a soil improvement technique. *Geomicrobiology Journal*, 24(5), 417-423.
- Williams, A. T., Rangel-Buitrago, N., Pranzini, E. & Anfuso, G. (2018) The management of coastal erosion. *Ocean & Coastal Management*, 156, 4-20.
- Yan, H., Shen, Q., Fan, L. C., Wang, Y. & Zhang, L. (2010) Greenhouse gas emissions in building construction: A case study of One Peking in Hong Kong. *Building and Environment*, 45(4), 949-955.
- Yang, P., Kavazanjian, E. & Neithalath, N. (2019) Particle-scale mechanisms in undrained triaxial compression of biocemented sands: insights from 3D DEM simulations with flexible boundary. *International Journal of Geomechanics*, 19(4), 04019009.
- Yang, P., O'Donnell, S., Hamdan, N., Kavazanjian, E. & Neithalath, N. (2016) 3D DEM Simulations of Drained Triaxial Compression of Sand Strengthened Using Microbially Induced Carbonate Precipitation. *International Journal of Geomechanics*, 04016143.

- Yang, Z., Cheng, X. & Li, M. (2011) Engineering properties of MICP-bonded sandstones used for historical masonry building restoration, *Geo-Frontiers 2011: Advances in Geotechnical Engineering*, 4031-4040.
- Zhao, Q., Li, L., Li, C., Li, M., Amini, F. & Zhang, H. (2014) Factors affecting improvement of engineering properties of MICP-treated soil catalyzed by bacteria and urease. *Journal of materials in civil engineering*, 26(12), 04014094.
- Zhao, X. & Evans, T. M. (2009) Discrete simulations of laboratory loading conditions. *International Journal of Geomechanics*, 9(4), 169-178.
- Zhou, C. & Ooi, J. Y. (2009) Numerical investigation of progressive development of granular pile with spherical and non-spherical particles. *Mechanics of Materials*, 41(6), 707-714.
- Zhou, Y., Xu, B., Yu, A. & Zulli, P. (2001) Numerical investigation of the angle of repose of monosized spheres. *Physical Review E*, 64(2), 021301.
- Zhou, Y., Xu, B. H., Yu, A.-B. & Zulli, P. (2002) An experimental and numerical study of the angle of repose of coarse spheres. *Powder Technology*, 125(1), 45-54.

## Chapter 8: Appendix - Conference paper

V International Conference on Particle-based Methods – Fundamentals and Applications  
PARTICLES 2017  
P. Wriggers, M. Bischoff, E. Oñate, D.R.J. Owen, & T. Zohdi (Eds)

### A Model of Granular Materials Partially Cemented by Bacterial Calcite

ELAHEH KASHIZADEH <sup>1</sup>, ABHIJIT MUKHERJEE <sup>2</sup> AND  
ANTOINETTE TORDESILLAS <sup>3</sup>

<sup>1</sup>Department of Civil Engineering, Curtin University  
Bentley WA 6102, Australia  
E-mail address: [Elahesh.kashizadeh1@postgrad.curtin.edu.au](mailto:Elahesh.kashizadeh1@postgrad.curtin.edu.au), URL:  
<http://www.curtin.edu.au/>

<sup>2</sup>Department of Civil Engineering, Curtin University  
Bentley WA 6102, Australia  
E-mail address: [Abhijit.mukherjee@curtin.edu.au](mailto:Abhijit.mukherjee@curtin.edu.au), URL: <http://www.curtin.edu.au/>

<sup>3</sup>School of Mathematics and Statistics, University of Melbourne  
Victoria 3010, Australia  
E-mail address: [atordes@unimelb.edu.au](mailto:atordes@unimelb.edu.au), URL: <http://www.unimelb.edu.au/>

#### Abstract

Nature aggregates granular materials such as sand, silt and clay into form beach rocks, anthills and other forms of microbialites. Microbial Induced Calcium Carbonate Precipitation (MICP) is a standard bio-geo-chemical cementation process. (MICP), occurs due to the mineralization of calcium through bacterial enzymatic action. Unlike engineered cement, which consumes very high amounts of energy and emits large quantities of CO<sub>2</sub>, this natural cementation occurs in ambient conditions, with negligible energy consumption. Hence, it is a sustainable construction method. Natural cementation is a gradual process, where grains are initially bonded to form clumps. The clumps grow in size to form aggregates, finally creating free-standing

columns. Numerical models of the mechanical behaviours of cemented grains at the various stages of aggregation offer a way to explore and understand this process. In this paper, we propose a discrete element method (DEM) of aggregated granular materials formed due to MICP. The model is applied to study different levels of aggregation of sand, from sand heaps involving unbonded and bonded grains to free-standing columns. The results are compared against experiments, and the most important parameters are discussed.

**Keywords:** MICP, Loose, Dense, Soil, Mechanical properties, DEM

## 8.1. Introduction

Granular materials such as sand, silt and clay are primary resources for construction. They are used in their natural unbonded forms such as earth embankments, and in bonded states as in concrete. A binder, typical cement, is used to bond the grains together. The mechanism of resistance for loading in the loose and the bonded forms is fundamentally different. The loose material depends on the inter-granular friction for resistance against an applied force while the bonded material that behaves as a solid block has considerable inter-granular cohesion. A numerical model that can capture all the stages of sand aggregation is challenging.

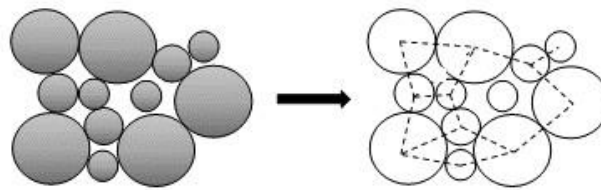
Presently, 3.6 billion tonnes per annum of Portland Cement is produced, contributing approximately 6% of all anthropogenic greenhouse gases [1]. Technologies that effectively reduce or possibly eliminate Portland cement must be explored to improve the sustainability quotient of civil infrastructure. Recently, new natural cementation, MICP, has been introduced as an alternative to cement binder [2]. In this process, bacterial enzymes are utilized to nucleate calcium carbonate as the cementing material [3]. Several critical applications of the process are reported [4-6]. It is essential to complement the experiments with a reliable numerical model to optimize the process. The model should be able to capture all phases of aggregation: from an assembly of loose grains to a free-standing assembly of fully aggregated (bonded) grains. In this paper, we propose a model of aggregated granular materials formed due to MICP using the discrete element method (DEM).

MICP is a bio-geo-chemical process that is performed to bond granular materials for a designed mechanical performance. Different aspects of the process, such as mass transport, biochemical reactions and consequent alteration in the mechanical response of the material have been modelled. Reactive transport models have been introduced to model biogrouting of soil [7, 8]. There have been attempts to simulate the biochemical process involved in MICP by solving transport and thermodynamic equations [9]. However, combining it with mechanical models is not reported hitherto. The mechanical property of sand columns resulting from MICP has been predicted using DEM [10, 11]. In these models, MICP has been simulated as a homogenised cohesive system. However, the process can be highly localised, at least in the early stages. Moreover, no model exists to simulate the mechanical behaviour of different stages of granular mode cementation through MICP process

The use of DEM for modelling granular materials dates back to Cundall & Strack [12]. The effect of non-idealized particle shapes on strength and deformation has extensively studied, and one approach is by clustering idealized shape grains (e.g., circular disks and spheres) [13]. With the significant increase of computing power, discrete element models have been used to study the deformation of granular materials under a wide range of conditions in various fields including geomechanics, pharmaceuticals, petroleum engineering, to name a few examples [14]. The present work is a first step towards the development of a DEM framework for modelling the mechanical behaviour of granular materials under MICP at all stages of aggregation. The model is applied to study the different levels of aggregation of sand, from sand heaps involving unbonded and bonded grains to free-standing columns. The results are compared against simulations, and experiments and the most important parameters are discussed.

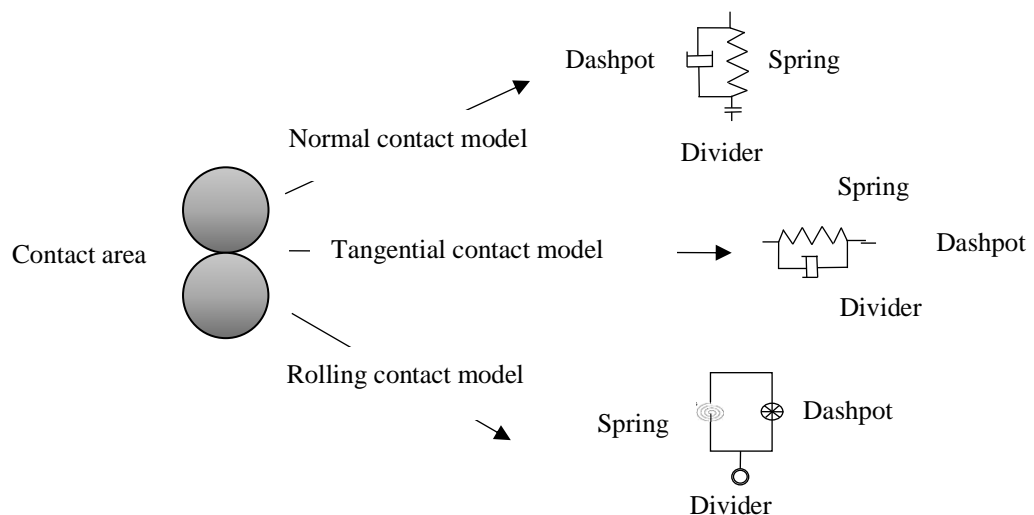
## 8.2. DEM Modelling

In this study, a large complex granular system is considered as an n-body structure of interconnected spheres where the mechanical model hitherto to simulate cementation of granular materials in deferent stages. The centre of each sphere is connected to the centre of the nearest contracted sphere(s). The connected lines create an intricate network (Figure 8.1). Material constitutive properties are assigned to each connection.



**Figure 8.1.** The relation between a granular material and a highly complex structural frame [15]

A spring–dashpot system is used for assigning the constitutive properties [11]. To simulate the contact forces between connected spheres; the spring, the divider and the dashpot model the contact force, the separation and damping. Figure 8.2 illustrates different spring-dashpot systems that are designed in the numerical model to address normal, shear and rolling contacts.



**Figure 8.2.** The contact models for grains with rolling resistance by Cundall [11]

A constitutive model with a combination of Hooke's and Coulomb's laws defines the interaction between the contacting particles:

A constitutive model with a combination of Hooke's and Coulomb's laws defines the interaction between the contacting particles:

$$f^n = k^n \Delta u^n + b^n \dot{\Delta u}^n \quad (1)$$

$$f^t = k^t \Delta u^t + b^t \dot{\Delta u}^t, \text{ for } |\Delta u^t| < \mu |f^n| / k^t \quad (2)$$

Where:

$f_n$	Normal force component
$f_t$	Tangential force component
$k^n$ & $k^t$	Spring stiffness coefficients
$b^t$ & $b^n$	Viscous damping coefficients
$\mu$	Coulomb friction coefficient
$\Delta u^t$ & $\Delta u^n$	Relative normal and tangential displacement
$\Delta \dot{u}^t$ & $\Delta \dot{u}^n$	Relative normal and tangential translational velocities

The normal stiffness,  $k^n$ , shear stiffness,  $k^s$  and rolling stiffness,  $k^r$  parameters were calculated, as follows (Figure 8.2)

$$k^n = E_c \frac{2R_1 R_2}{R_1 + R_2} \quad (3)$$

$$k^s = E_c \nu_c \frac{2R_1 R_2}{R_1 + R_2} \quad (4)$$

$$k^r = \beta K^s R_1 R_2 \quad (5)$$

Where  $E_c$  is the Young modulus,  $\nu_c$  is the Poisson ratio,  $R_1$  and  $R_2$  are the radii of the two connected spheres, and  $\beta$  is the rolling stiffness coefficient.

The rolling resistance,  $I^c$ , the moments are introduced. The rolling resistance or contact moment, defined in an analogous fashion to Coulomb's law, is expressed as:

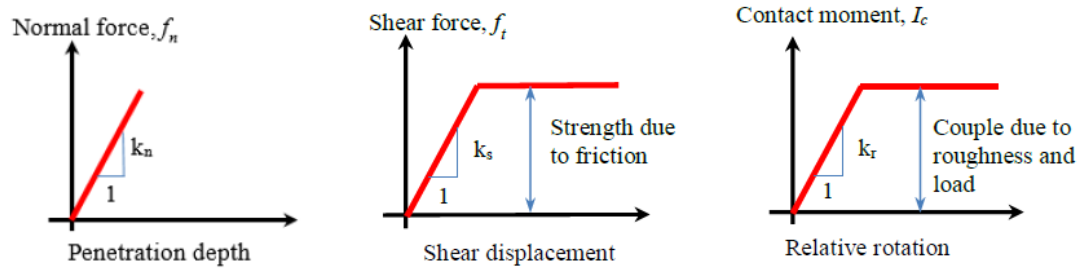


$$I^c = k^r \Delta\alpha + b^r \Delta\dot{\alpha}, \text{ for } |\Delta\alpha| < \mu^r R_{\min} |f^n| / k^r \quad (6)$$

$$I^c = \mu^r R_{\min} |f^n|, \text{ for } |\Delta\alpha| \geq \mu^r R_{\min} |f^n| / k^r$$

Where:

- $R_{\min}$  Minimum radii of the two interacting particles
- $k^r$  Rolling stiffness coefficients
- $\mu^r$  Friction coefficient
- $\Delta\alpha$  Relative rotation
- $\Delta\dot{\alpha}$  Relative rotational velocities



**Figure 8.3.** Mechanical stiffness of normal, tangential and rolling contact models [16]

Based on Mohr-Coulomb rupture criterion equation Figure 8.3 represents the mechanical response of normal, tangential and rolling contact model [17].

A numerical approach should be adopted to solve the complex granular mechanism [15]. In this paper, an explicit finite difference, time-stepping algorithm, based on a Newton integration equation, has been developed. The present numerical model is validated with experimental studies.

### 8.3. Methodology

To understand the mechanical behaviour of granular materials a discrete element model

(DEM) has been developed by using open source discrete element software (YADE).

To illustrate the capability of our numerical approach for modelling loose, semi-

aggregated and fully aggregated samples, a series of investigations are carried out. Numbers of spheres are created with specific grain size distribution in defined cubic format. Then the property of the material is assigned to spheres by defining the micro parameters. By controlling the number of grains and the size of the sample are the desired porosity is defined. The DEM models are closely calibrated to the initial configurations and packing densities of the experimental, as well as the contact and size distributions of the constituent particles.

### **8.3.1. Loose and Semi-aggregated Grains**

In a loose or semi-aggregated state, the grains do not form a solid mass. Thus, they deform

under the action of gravity and form a heap. When they are packed in a container, and then the walls are removed, the grains move to form a heap. In the loose state, the grains are free to slide or roll over other grains once the intergranular friction is overcome. There is no cohesion between the grains. Partial aggregation is considered as a state when grains formed clumps due to the MICP process. Although the grains' movement is restricted due to the formation of clumps, the bonding is not widespread enough to stop grains moving due to gravity. The shape of the heap is dependent on the degree of aggregation. The semi aggregated state is modelled by rigidly connecting three grains to create triads. The fraction of triads is proportional to the degree of aggregation. The shape of the heap is altered due to the formation of triads.

A model has been developed in YADE to illustrate the capability of our numerical approach to model this effect. A cubic granular sample surrounded by walls is generated. All walls are removed simultaneously, and the grains fall under the action of gravity. The released grains roll and slip on each other until their motion is below a set threshold. The threshold is placed on the mean force magnitude of inter-particle interactions. Initially, there are a lot of movements, and the time progresses, the particles stabilize into a shape resulting in negligible interaction forces. The tolerance value for this study for mean forces is  $1e-2$  Pa. In other words, the heap obtained when the mean interaction force drops below this threshold, all grains are considered static, and the heap is considered to be the final configuration. A common assumption is that the shape of the heap will be conical, and just the angle of repose can represent it.

However, for semi-aggregated grains, the shape of the heap is more complex, and more parameters may be necessary to define the shape.

### **8.3.2. Aggregated Grains**

In the case of aggregated samples, the specimen retains its shape under the action of gravity. In addition to the frictional resistance between the grains, deposition of calcium carbonate causes inter-granular cohesion between grains. The cohesive strength is dependent on the degree of MICP. As the samples are able to retain their shapes under the action of gravity, it is not necessary to contain them with the walls. Cylindrical samples have been developed with the specified grain size distribution. The samples have been subjected to uniaxial compression at a constant rate until they collapse. In contrast to the previous case, in the case of aggregated samples, the grains are tightly connected in the beginning. As a result, there is very little inter-granular movement, but as the load increases the inter-granular stress exceed the cohesive strength of MICP at a few locations resulting in cracking. As the cracking in the sample increases, the inter-granular movement also becomes more pronounced. As a result, the mean force magnitude of inter-particle interactions rises exponentially at the end of the numerical process indicating large inter-granular motions leading to collapse.

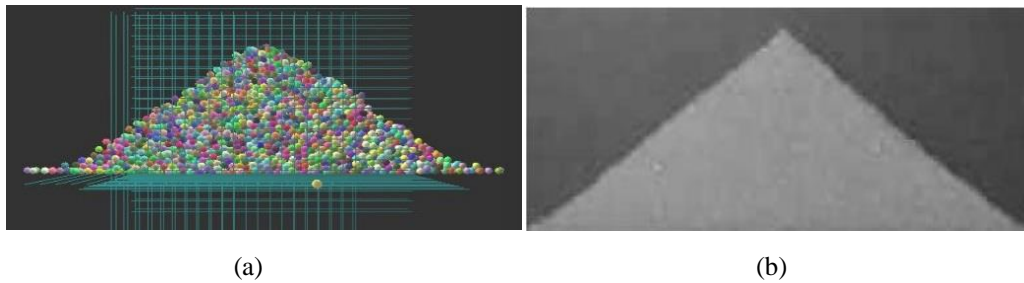
## **8.4. Results**

Results of simulation of grains aggregated in varying degrees by MICP using YADE is presented here. The aim is to validate the numerical observations with experimental results. The DEM simulation is controlled by the parameters described in (eqs. 1-6) that determine the inter-granular interaction (micro-parameters). It is not possible to have all these parameters measured experimentally. Thus, some of the parameters are adjusted to obtain the desired macro-parameters, e.g. the angle of repose, the compressive strength.

### **8.4.1. Loose spherical glass beads**

Zhou et al. [18] studied the angle of repose for mono-sized coarse spheres with 2mm

diameter glass beads constrained by two glass walls separated by 40mm. The numerical model was developed by developing a container consisting of four glass walls with 80×8mm in a pan and 40mm in height. The box was filled with 2mm diameter glass beads. Then two smaller walls have been removed to allow the flow of beads under the action of gravity. Flow-through the shorter sides were allowed while the longer sides were rigidly constrained. The micro - parameters for the simulation are presented in Table 1. The shape of the heap after 10e6-time steps is illustrated in Fig. 8.4. The angle of repose measured from the simulation and the experimentally observed angle is around 37°. The present DEM model was able to model the stable configuration of the heap of glass beads.



**Figure 8.4.** (a) The proposed numerical model in this study, (b) The experimental study by Zhou *et al.* [18], the angle of repose in both studies are 37 degree

**Table 8.1.** The variables which have been considered for validation

Name of variable	Base value	Name of variable	Base value
Number of particles	2000	Density	2500 Kg/m <sup>3</sup>
Time step	10000000	Poisson ratio	0.3
Particle size	2 mm	Young's	2.16e6 Pa
Rolling friction	0.05	Damping	0.4
Sliding friction	0.5	Friction angle	22°
Container thickness	40 mm		

### 8.4.2. Semi-aggregated granules

To assess the intermediate situation, when a few grains have aggregated, but it is not enough to prevent the flow under the action of gravity, an experiment with a box of popcorns was conducted. The popcorns can approximate the shape of a triad where three spheres are clumped together signifying partial aggregation. A plastic container

was filled with popcorns. The box was placed face down on a firm table (Fig. 8.5a). Then the container was lifted suddenly. The popcorn takes the shape of a heap (Fig. 8.5b). The shape of the heap is noted by fitting a smooth curve to the contour of the heap.

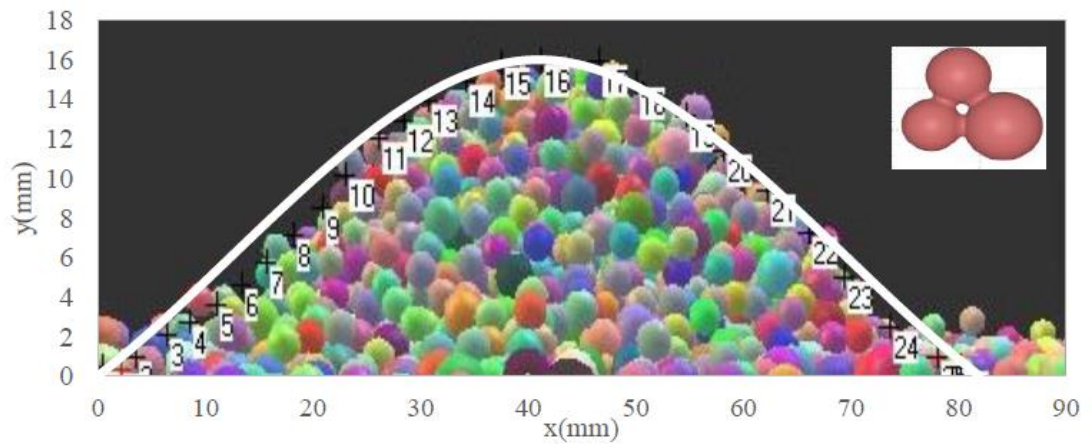


(a)

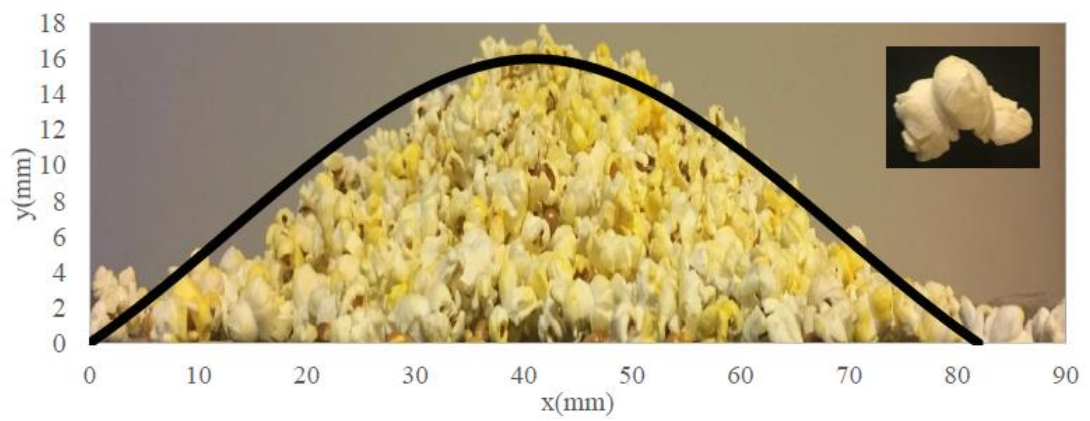
(b)

**Figure 8.5.** The angle of repose study with popcorn (a) pop-cons in the box (b) accumulated shape of popcorns after removing the container

Physical models are created by using popcorn because of the triad shape of grains to be aligned with the numerical model has been approximated as three spheres joined as a triad. The shape of the heap after  $1e7$  time steps is illustrated in (Fig. 8.6a) where the numbers of grains are 5000. A confined space of the same shape and size of the container is created by introducing four rigid walls. The confined space has been filled with the triads. Then the walls have been removed to allow triads moving until a stable configuration is reached (Fig. 8.6a). The shapes obtained from the experiment and the numerical model have been found to agree very well.



(a)



(b)

**Figure 8.6.** Comparison of Numerical model – the coloured grains have been used to make clumps distinguishable (a) and Experimental study (b) for semi-aggregated heaps, where the shape of the pop-corn grain is simulated as three spheres clumped

### 8.4.3. Aggregated cylinders

Simulations of aggregated particles are validated with two experimental results at different extents of aggregation and particle size distribution. Jawad et al. [19] reported the results of unconfined compression tests of sand of single-particle size (Fig. 8.7a) aggregated with MICP. At the same time, Porter et al. [20] reported MICP in well-graded sand samples (Fig. 8.7b). Both models were simulated in DEM and subjected to a displacement controlled unconfined compression test and the stress-strain curve for the sample has been plotted. It is essential to set the micro-parameters for DEM to obtain a close fit with the experiments. The initial part of the curve is closely related to the elastic modulus of the grains. When the inter-granular stress exceeds the strength of the cementation, the grains start separating, sliding and rolling. Under these conditions, the cohesion parameters play the most crucial role. Post-peak part of the stress-strain curve is dominated by the rolling stiffness and plastic moment limit strain.

Table 8.2 shows the values of parameters that are studied in the numerical approach to model the experimental of Jawad et al. [19]. Figure 8.8 illustrates the stress-strain curves from the numerical and experimental results. It can be seen that the two curves agreed overall. However, there are local differences between them. The initial slope of the numerical curve was considerably higher than that of the experiment. However, the slope reduced significantly between 2 and 4% of the strain rate. A good agreement at the peak of the stress-strain graph is recorded. It is known that the samples created through MICP often have unevenness at their end surfaces. As a result, the initial slope is lower than expected as during the initial loading, the uneven areas get gradually flattened, resulting in a more uniform distribution of stresses within the sample. The post-peak behaviour of the models was similar.

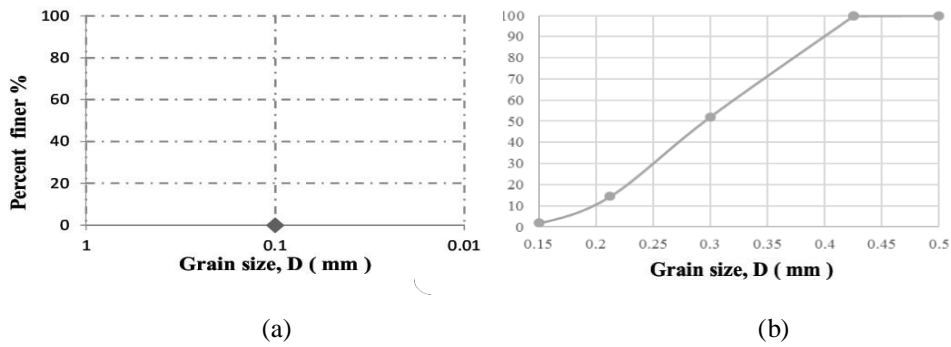


Figure 8.7. Sand grain distribution to study Jawad *et al.* [19], Porter *et al.* [20]

Table 8.2. Optimum values of micro parameters to model Jawad [19] experimental results

Name of variable	Base value	Name of variable	Base value
Number of particles	10000	Height of the sample	80mm
Time step	1e7	Diameter of sample	37mm
Particle size	0.1 mm	Porosity	37.67%
Friction angle	36.5°	Young modulus	17e6 Pa
Sliding friction coefficient	0.4	Normal cohesion	30e4 Pa
Density	2500 Kg/m <sup>3</sup>	Shear cohesion	9e6 Pa
Poisson ratio	0.4	Rolling stiffness coefficient	0.5
Damping	0.4	Plastic moment limit coefficient	0.15

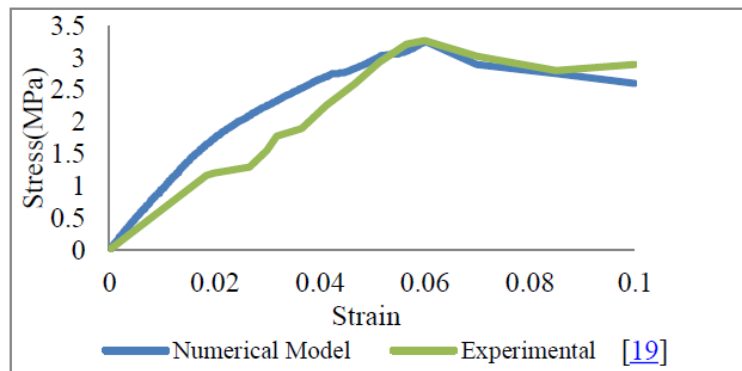


Figure 8.8. The stress-strain of the proposed numerical and experimental study [19]

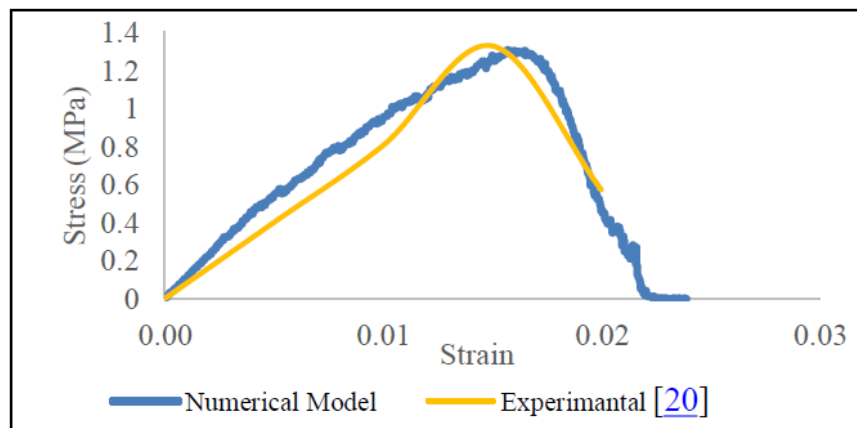
The experiment reported by Porter *et al.* [20] has well-graded grains. The samples have been given a lower level of MICP treatment resulting in the intermediate level of aggregation, enough to have a cylinder but of lower strength than the previous example. The sphere packing technique is used to model the experimental samples to reach the porosity of the sample around 36%. The parameters set in the DEM for this example are presented in Table 8.3. The stress-strain plots of the experimental and the numerical results are shown in Fig. 8.9. In this case, also, there was a good



overall match between the experiment and numerical simulation. The initial apparent softness in the sample due to the unevenness of the loading surfaces is discernible in this experiment as well. The peak stress in the simulation occurred slightly later than that observed in the experimental model. The post-peak behaviour was captured well by the DEM. These examples demonstrate the capability of DEM in capturing the stress-strain behaviour of granular samples aggregated by MICP for a range of grain size distribution and exact of aggregation.

**Table 8.3.** Optimum values of micro parameters to model Porter *et al.* [20] experimental results

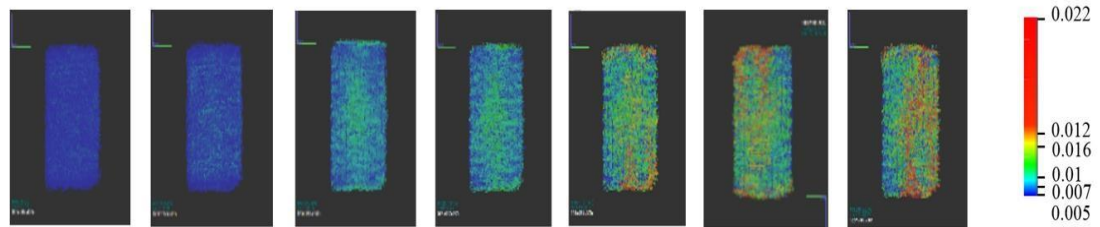
Name of variable	Base value	Name of variable	Base value
Number of particles	10000	Height of the sample	60mm
Time step	1e7	Diameter of sample	30mm
Particle size	0.45 mm and 0.07	Porosity	37.67
Friction angle	36.5°	Young modulus	17e6
Sliding friction coefficient	0.4	Normal cohesion	25e6
Density	2500 Kg/m3	Shear cohesion	6e3
Poisson ratio	0.4	Rolling stiffness coefficient	0.15
Damping	0.4	Plastic moment limit coefficient	0.15



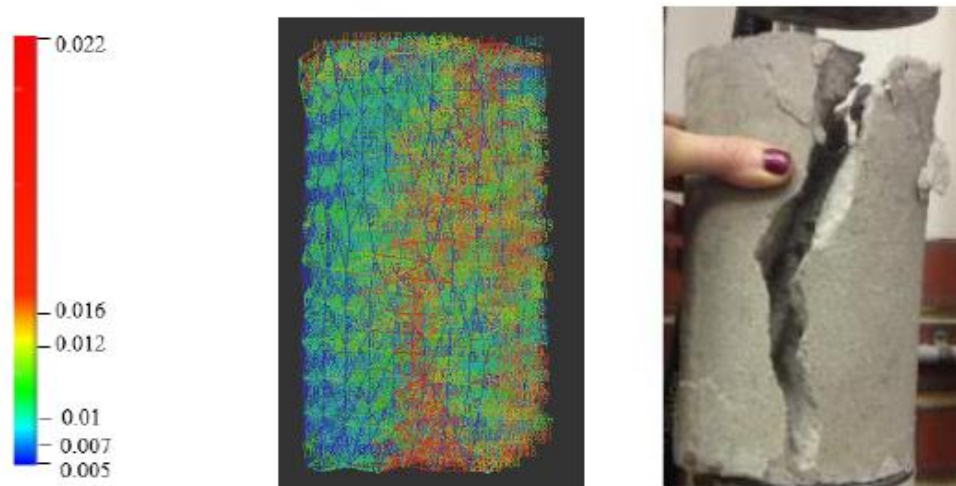
**Figure 8.9.** The stress-strain of the proposed numerical in the current study and experimental study by Porter *et al.* [20]

We further explore the ability of DEM to identify cracks as they develop in the sample with the increasing load. Figure 8.10 shows the network of inter-granular distance for the grains on the surface of the cylinder as cracks appear the grains that were initially cemented together separate when the stress in the cementation exceeds the cohesive strength. It can be noted that DEM predicts a developing vertical crack as the

loading progresses. The red areas can be considered as separation. In red areas, the distance between the grains has exceeded the average inter-grain length at the beginning of the experimental model. Fig. 8.11 compares the DEM simulation with the experimental vertical split failure. Thus, it can be concluded that DEM can predict the failure mode of the Aggregated MICP samples.



**Figure 8.10.** Inter-grain distances at different stages of the compression test on a highly complex structural frame where different colors are representing distance between grains; the blue is the smallest and red is largest distance– unit is mm



**Figure 8.11.** Comparison of failure modes obtained through the experiment and DEM simulation –unit is mm

## 8.5. Conclusion

This investigation explores the capability of DEM simulation for aggregation of grains by MICP to different extents. The following conclusions can be made comparing the series of simulation results with experiments:

- Dem can model the aggregation of sand due to MICP at all the stages. The overall stress-strain graphs match well. However, the parameters of DEM must be appropriately set to get the best results.

The clumping of grains can model-The shape of the semi-aggregated heap to form triads.

- The stress-strain graphs of aggregated cylinders as obtained in the experiments can be emulated through DEM. However, the limit strength parameters such as cohesion and plastic moment limit must be set, appropriately.

- The inter-grain distance is a good measure for tracking cracks in aggregated cylinders. The failure mode predicted by the DEM was very close to that obtained in the experiment.

- The results of this investigation encourage us to explore the DEM modelling further for capturing MICP for a wide range of applications. A reliable numerical model would undoubtedly expand the understanding of this exciting new technology for a wide range of applications.

## 8.6. References

- [1] Imbabi, M.S., C. Carrigan, and S. McKenna, Trends and developments in green cement and concrete technology. *International Journal of Sustainable Built Environment*, 2012. 1(2): p. 194-216.
- [2] Achal, V., et al., Biomineralization for sustainable construction - A review of processes and applications. *Earth-Science Reviews*, 2015. 148: p. 1-17.
- [3] Achal, V. and A. Mukherjee, A review of microbial precipitation for sustainable construction. *Construction and Building Materials*, 2015. 93: p. 1224-1235.
- [4] Achal, V., A. Mukherjee, and M.S. Reddy, Microbial Concrete: Way to Enhance the Durability of Building Structures. *Journal of Materials in Civil Engineering*, 2011. 23(6): p. 730-734

- [5] Achal, V., et al., Corrosion Prevention of Reinforced Concrete with Microbial Calcite Precipitation. *Aci Materials Journal*, 2012. 109(2): p. 157-163.
- [6] Achal, V., A. Mukherjee, and M.S. Reddy, ORIGINAL RESEARCH: Biocalcification by *Sporosarcina pasteurii* using corn steep liquor as the nutrient source. *Industrial Biotechnology*, 2010. 6(3): p. 170-174.
- [7] Laloui, L. and S. Fauriel, Birout propagation in soils.pdf. *Multiscale and Multiphysics Processes in Geomechanics*, 2011(SSGG): p. 77–80.
- [8] Van Wijngaarden, W., et al., Modelling Biogrout: a new ground improvement method based on microbial-induced carbonate precipitation. *Transport in Porous Media*, 2011. 87(2): p. 397-420.
- [9] Bouchelaghem, F. and L. Vulliet, Mathematical and numerical filtration-advection- dispersion model of miscible grout propagation in saturated porous media. *International Journal for Numerical and Analytical Methods in Geomechanics*, 2001. 25(12): p. 1195-1227.
- [10] Yang, P., et al., 3D DEM Simulations of Drained Triaxial Compression of Sand Strengthened Using Microbially Induced Carbonate Precipitation. *International Journal of Geomechanics*, 2016: p. 04016143.
- [11] Cundall, P.A., The measurement and analysis of accelerations in rock slopes. 1971, University of London.
- [12] Cundall, P.A. and O.D. Strack, A discrete numerical model for granular assemblies. *Géotechnique*, 1979. 29(1): p. 47-65.
- [13] Steefel, C.I., D.J. DePaolo, and P.C. Lichtner, Reactive transport modeling: An essential tool and a new research approach for the Earth sciences. *Earth and Planetary Science Letters*, 2005. 240(3): p. 539-558.
- [14] Yeh, G.-T. and V.S. Tripathi, A critical evaluation of recent developments in hydrogeochemical transport models of reactive multichemical components. *Water Resources Research*, 1989. 25(1): p. 93-108.
- [15] O'Sullivan, C., *Particulate discrete element modelling*. 2011: Taylor & Francis.
- [16] Kozicki, J. and J. Tejchman. Numerical simulations of sand behaviour using DEM with two different descriptions of grain roughness. in *II International Conference on Particle- based Methods–Fundamentals and Applications*. Particles. 2011.
- [17] Kozicki, J. and F. Donzé, A new open-source software developed for numerical simulations using discrete modeling methods. *Computer Methods in Applied Mechanics and Engineering*, 2008. 197(49): p. 4429-4443.
- [18] Zhou, Y., et al., An experimental and numerical study of the angle of repose of coarse spheres. *Powder Technology*, 2002. 125(1): p. 45-54.
- [19] Jawad, F. and J.-J. Zheng, Improving Poorly Graded Fine Sand with Microbial Induced Calcite Precipitation. 2016.
- [20] Hannah Porter, N.K.D., Abhijit Mukherjee, Sustainable Road Bases with Microbial Carbonate Precipitation. SCMT4, Las Vegas, USA, August 7-11, 2016

